INSTITUTO POLITÉCNICO NACIONAL (IPN)

CENTRO MEXICANO PARA LA PRODUCCIÓN MÁS LIMPIA (CMP+L)

DEVELOPMENT OF A FUNCIONALIZED MESOPOROUS CATALYST FOR THE HYDROPROCESSING OF A GAS OIL AND VEGETABLE OIL BLEND

T H E S I S

In partial Fulfillment to obtain the degree of:

Doctor in Energy (PhD)

PRESENTED BY:

Jonatan Ricardo Restrepo Garcia

MSc. in Chemical Engineering

ADVISORS:

Ignacio Elizalde Martínez, PhD. (IPN)

León Pablo Torres Mancera, PhD. (IMP)

December 4th of 2023

SIP-13
REP 2017

INSTITUTO POLITÉCNICO NACIONAL

SECRETARIA DE INVESTIGACIÓN Y POSGRADO

Dirección de Posgrado

ACTA DE REGISTRO DE TEMA DE TESIS
Y DESIGNACIÓN DE DIRECTOR DE TESIS

Ciudad de México, 29 de Septiembre del 2023.

El Colegio de Profesores de Posgrado de Centro Mexicano para la Producción más Limpia (Unidad Académica) en su Sesión ordinaria No. 8 celebrada el día 19 del mes de septiembre de 2023 conoció la solicitud presentada por el (la) alumno (a):

Apellido Paterno:	Restrepo	Apellido Materno:	Garcia	Nombre (s):	Jonatan Ricardo

Número de boleta: A 2 0 1 0 7 6

del Programa Académico de Posgrado: Doctorado en Energía

Referente al registro de su tema de tesis

1.- Se acordó aprobar el tema de tesis:

"Development of a functionalized mesoporous catalyst for the hydroprocessing of a gas oil and vegetable oil blend"

Objetivo general del trabajo de tesis:

To establish the influence on the catalytic activity of Ni-W type sulfided active phases, and the acid and textural properties of the Al-SBA-15 material for the development of a catalyst with a higher yield to cleaner liquid fuels in hydro-co-processing of a mixture of gas oil and vegetable oil.

2.- Se designa como Directores de Tesis a los profesores:

Director: Dr. Ignacio Elizalde Martínez 2° Director: Dr. León Pablo Torres Mancera

No aplica: ☐

3.- El Trabajo de investigación base para el desarrollo de la tesis será elaborado por el alumno en:

En el laboratorio ambiental del Centro Mexicano para la Producción más Limpia (CMP+L) del Instituto Politécnico Nacional.

que cuenta con los recursos e infraestructura necesarios.

4.- El interesado deberá asistir a los seminarios desarrollados en el área de adscripción del trabajo desde la fecha en que se suscribe la presente, hasta la aprobación de la versión completa de la tesis por parte de la Comisión Revisora correspondiente.

Director(a) de Tesis

Ignacio Elizalde
Dr. Ignacio Elizalde Martínez

2° Director de Tesis (en su caso)

Dr. León Pablo Torres Mancera

Alumno

M. en C. Jonatan R. Restrepo García

Presidente del Colegio

Dr. Raúl Hernández Altamirano

CENTRO MEXICANO PARA LA PRODUCCIÓN MÁS LIMPIA

INSTITUTO POLITÉCNICO NACIONAL

SECRETARÍA DE INVESTIGACIÓN Y POSGRADO

Dirección de Posgrado

ACTA DE REVISIÓN DE TESIS

En la Ciudad de México siendo las 17:00 horas del día 5 del mes diciembre del 2023 se reunieron los miembros de la Comisión Revisora de la Tesis, designada por el Colegio de Profesores de Posgrado de: Centro Mexicano para la Producción más Limpia para examinar la tesis titulada:

"Development of a functionalized mesoporous catalyst for the hydroprocessing of a gas oil and vegetable oil blend"

del (la) alumno (a):

Apellido Paterno:	Restrepo	Apellido Materno:	Garcia	Nombre (s):	Jonatan Ricardo

Número de boleta: A 2 0 1 0 7 6

Alumno del Programa Académico de Posgrado: Doctorado en Energía

Una vez que se realizó un análisis de similitud de texto, utilizando el software antiplagio, se encontró que el trabajo de tesis tiene 0 % de similitud. **Se adjunta reporte de software utilizado.**

Después que esta Comisión revisó exhaustivamente el contenido, estructura, intención y ubicación de los textos de la tesis identificados como coincidentes con otros documentos, concluyó que en el presente trabajo **SI** ☐ **NO** ■ **SE CONSTITUYE UN POSIBLE PLAGIO.**

JUSTIFICACIÓN DE LA CONCLUSIÓN: *(Por ejemplo, el % de similitud o fuentes en metodología adecuadamente referidas o fuente original)*

El porcentaje de similitud indica que el documento de tesis doctoral no constituye un posible plagio ya que es inferior al 5%. En este caso 0% de similitud con trabajos de otros autores.

****Es responsabilidad del alumno como autor de la tesis la verificación antiplagio, y del Director o Directores de tesis el análisis del % de similitud para establecer el riesgo o la existencia de un posible plagio.**

Finalmente y posterior a la lectura, revisión individual, así como el análisis e intercambio de opiniones, los miembros de la Comisión manifestaron **APROBAR** ■ **SUSPENDER** ☐ **NO APROBAR** ☐ la tesis por **UNANIMIDAD** ■ o **MAYORÍA** ☐ en virtud de los motivos siguientes:

El documento de tesis doctoral cumple con los requisitos establecidos en el REP2017, no constituye plagio y demuestra el cumplimiento de los objetivos de investigación planteados.

COMISIÓN REVISORA DE TESIS

Ignacio Elizalde

Director de Tesis
Dr. Ignacio Elizalde Martínez

Issis C Romero

Dra. Isais Claudette Romero Ibarra

2° Director de Tesis (en su caso)
Dr. León Pablo Torres Mancera

Dr. Víctor Gabriel Baldovino Medrano

Dr. Fabián Salvador Medeiros Pinto

Dr. Raúl Hernández Altamirano
PRESIDENTE DEL COLEGIO DE PROFESORES

CENTRO MEXICANO PARA LA PRODUCCIÓN MÁS LIMPIA

INSTITUTO POLITÉCNICO NACIONAL

SECRETARÍA DE INVESTIGACIÓN Y POSGRADO

CARTA DE AUTORIZACIÓN DE USO DE OBRA PARA DIFUSIÓN

En la Ciudad de México el día 5 del mes de diciembre del año 2023, el (la) que suscribe Jonatan Ricardo Restrepo Garcia alumno(a) del programa Doctorado en Energía con número de registro A201076, adscrito(a) a Centro Mexicano para la Producción más Limpia manifiesta que es autor(a) intelectual del presente trabajo de tesis bajo la dirección del Dr. Ignacio Elizalde Martínez y el Dr. León Pablo Torres Mancera y cede los derechos del trabajo intitulado "Development of a functionalized mesoporous catalyst for the hydroprocessing of a gas oil and vegetable oil blend", al Instituto Politécnico Nacional, para su difusión con fines académicos y de investigación.

Los usuarios de la información no deben reproducir el contenido textual, gráficas o datos del trabajo sin el permiso expresado del autor y/o director(es). Este puede ser obtenido escribiendo a las siguiente(s) dirección(es) de correo. ielizaldem@ipn.mx; jonatan.restrepo@outlook.com. Si el permiso se otorga, al usuario deberá dar agradecimiento correspondiente y citar la fuente de este.

JONATAN RICARDO RESTREPO GARCIA
Estudiante

ACKNOWLEDMENTS

Firstly, I would like to dedicate this research work and achievement to God the "All Mighty", the only responsible for supporting me in times of need, secondly, to my parents: Martha Lucía García Moreno and Ricardo Restrepo Reyes for their sacrifice, love, and support. Finally, to my sisters: Gineth Vivian Restrepo Garcia and Mariana Ivette Restrepo García for their lovely company, support and encouragement, giving me the motivation and strength to overcome adversity. Holding a PhD degree is a more a duty than an honor with the society.

On the other hand, I would like to acknowledge to my research advisors: Dr. Ignacio Elizalde-Martínez, and Dr. León Pablo Torres Mancera for giving the opportunity to be part of their researching team and their patience and teachings. I also acknowledge to my evaluators: Dra. Issis Claudette Moreno Ibarra (UPIITA-IPN), Dr. Fabián Salvador Mederos-Nieto (CMP+L-IPN), and Dr. Víctor Gabriel Baldovino-Medrano (CICAT-UIS Colombia) for all the lessons given and their priceless advice for conducting this research. I'm deeply grateful for being part of the "Mexican Centre for Cleaner Production (CMP+L from Spanish) of the National Polytechnique Institute (IPN from Spanish).

Finally, I also acknowledge to the Mexico Government, specifically to the National Council of Humanities, Science, and Technology (CONAHCYT), the BEIFI PIFI program in IPN, for the research grants given to me to carry out this thesis. In addition, I acknowledge to the Centre of Nanosciences and Micro and Nanotechnologies (CNMN) of the IPN for experimental support in data acquisition for the following characterization techniques: FTIR, RAMAN, TEM, SEM, ^{1}H-NMR, ^{27}Al-MAS-NMR, and ESI-MS, to the ICAT-UNAM, for the N_2 @ 77 K physisorption measurements and ^{1}H-NMR spectroscopy, and the CFATA-UNAM for LA-XRD, and WA-XRD data acquisition.

CONTENT

RESUMEN 13
ABSTRACT 14
ORGANIZATION OF THIS WORK 15
1. CONTEXT OF THE RESEARCH 17
1.1 PROBLEM STATEMENT 17
1.2 HYPOTHESIS 18
1.3 OBJECTIVES AND GOALS 19
1.3.1 General objective 19
1.3.2 Specific objectives 19
1.3.3 Goals 19
1.4 JUSTIFICATION 21
1.5 SCOPE 22
1.6 CONTRIBUTION 22
2. LITERATURE REVIEW 23
3. EFFECT OF THE Al/Si MOLAR RATIO IN THE HYDRO-COPROCESSING OF A MIXTURE OF VEGETABLE AND GAS OIL WITH A Ni-W/Al(X)-SBA-15 SULFIDED CATALYST 26
3.1. EXPERIMENTAL 26
3.1.1. Synthesis of Al (x)-SBA-15 catalytic supports 26
3.1.2. Catalysts preparation 27
3.1.3. Characterization 28
3.1.3.1. Textural Properties 28
3.1.3.2. Materials Crystallinity by XRD 28
3.1.3.3. Porous Structure by HR-TEM 29
3.1.3.4. Materials Acid Sites Distribution (Brønsted/Lewis) by Pyridine-FTIR 29
3.1.3.5. Molecular Structure of Aluminum Species by ^{27}Al-MAS-NMR Measurements 29
3.1.3.6. Chemical functional groups by RAMAN spectroscopy 29
3.1.3.7. FTIR spectra of liquid products during the hydro-coprocessing 29
3.1.3.8. Electrospray ionization (ESI) mass spectrometry 29
3.1.3.9. Analysis of liquid products by ^{1}H-NMR 29
3.1.4. Catalytic Evaluation 30
3.1.5. Catalytic Activity 31
3.1.5.1. Hydrodesulfurization (HDS) percentage (sulfur removal) 31
3.1.5.2. Hydrodeoxygenation (HDO) percentage (oxygen removal) 31
3.1.5.3. ASTM D2887 boiling point distributions and fraction compositions 33
3.2. RESULTS AND DISCUSSION 33
3.2.1. Characterization of catalytic supports and catalysts 33
3.2.1.1. Effect of the synthesis conditions in the textural properties of the materials 33
3.2.1.2. Effect of the synthesis conditions in materials crystallinity and mesoporosity 35
3.2.1.3. Textural Properties of final catalysts and catalytic supports 37
3.2.1.4. Mesoporous structure of Al(x)-SBA-15 mix1 catalytic supports and Ni-W/Al(x)-SBA-15 mix1 catalysts crystallinity 41
3.2.1.5. Porous structure of catalytic supports and catalysts 43
3.2.1.6. Materials Acid Sites Distribution (Brønsted/Lewis) by *Py*-FTIR 44

3.2.1.7. Molecular Structure of Aluminum Species by ^{27}Al-MAS-NMR Measurements 46
3.2.1.8. Chemical functional groups by RAMAN spectroscopy 47
3.2.1.9. FTIR spectra of liquid products obtained from the hydro-coprocessing of the vegetable oil and gas oil 48
3.2.1.10. Qualitative hydrocarbon distribution by ESI mass spectrometry 49
3.2.1.11. ^{1}H-NMR spectra for liquid products and vegetable oil 50
3.2.2. Catalytic evaluation of NiO(2.5%)-WO_3(15%)/Al(x)-SBA-15 mix1 sulfided catalysts... 51
3.2.2.1. Effect of the Al content in the hydrodesulfurization properties of NiO(2.5%)-WO_3(15%)/Al(x)-SBA-15 sulfided catalysts 51
3.2.2.2. Effect of the Al content in the Hydrodeoxygenation (HDO) properties of Ni-W/Al(x)-SBA-15 mix1 sulfided catalysts 52
3.2.2.3. Effect of the Al content in the Hydrocracking (HCK) properties of Ni-W/Al(x)-SBA-15 sulfided catalysts 54
3.3. Conclusions 55
4. EFFECT OF THE NiO AND WO_3 COMPOSITION IN THE HYDRO-COPROCESSING OF A MIXTURE OF GAS OIL AND VEGETABLE OIL WITH A NiO(y)- WO_3(z)/Al(0.05)-SBA-15 SULFIDED CATALYST 57
4.1. EXPERIMENTAL 57
4.1.1. Synthesis of Al(0.05)-SBA-15 catalytic support 57
4.1.2. Catalyst preparation 57
4.1.3. Characterization 57
4.1.4. Catalytic Evaluation 57
4.1.5. Catalytic Activity 58
4.2. RESULTS AND DISCUSSION 58
4.2.1. Characterization of catalytic supports and catalysts 58
4.2.1.1. Mesoporous structure and crystallinity of Al(0.05)-SBA-15 materials and NiO(y)-WO_3(z)/Al(0.05)-SBA-15 oxide phase catalysts 58
4.2.1.2. Textural properties of NiO(y)-WO_3(z)/Al(0.05)-SBA-15 mix2 oxide phase catalysts . 60
4.2.1.3. Chemical functional groups by RAMAN spectroscopy 61
4.2.1.4. Molecular Structure of Aluminum Species by ^{27}Al-MAS-NMR Measurements 62
4.2.1.5. FTIR spectra of liquid products during the hydro-coprocessing of the vegetable oil and gas oil 63
4.2.1.6. ^{1}H-NMR spectra for liquid products and vegetable oil 64
4.2.1.7. Qualitative hydrocarbon distribution by ESI mass spectrometry 65
4.2.2. Catalytic evaluation of NiO(y)-WO_3(z)/Al(0.05)-SBA-15 sulfided catalysts 66
4.2.2.1. Effect of metallic load in the hydrodesulfurization properties of NiO(y)-WO_3(z)/Al(0.05)-SBA-15 sulfided catalysts 66
4.2.2.2. Effect of metallic load in the hydrodeoxygenation (HDO) properties of NiO(y)-WO_3(z)/Al(0.05)-SBA-15 sulfided catalysts 67
4.2.2.3. Effect of metallic load in the hydrocracking properties of NiO(y)-WO_3(z)/Al(0.05)-SBA-15 sulfided catalysts 68
4.3. CONCLUSIONS 69
5. EFFECT OF THE OPERATING TEMPERATURE IN THE HYDRO-COPROCESSING OF A MIXTURE OF GAS OIL AND VEGETABLE OIL WITH A Ni-W/Al(X)-SBA-15 SULFIDED CATALYST 70

5.1. EXPERIMENTAL 70
5.1.1. Catalyst preparation 70
5.1.2. Characterization 70
5.1.3. Catalytic Evaluation 70
5.1.4. Catalytic Activity 70
5.2. RESULTS AND DISCUSSION 71
5.2.1. Characterization of the catalyst 71
5.2.1.1. Mesoporous structure and crystallinity of NiO(5.5%)-WO_3(25%)/Al(0.05)-SBA-15 oxide phase catalyst 71
5.2.1.2. Textural properties of NiO(5.5%)-WO_3(25%)/Al(0.05)-SBA-15 oxide phase catalyst 72
5.2.1.3. Chemical functional groups by RAMAN spectroscopy 73
5.2.1.4. Molecular Structure of Aluminum Species by ^{27}Al-MAS-NMR Measurements 74
5.2.1.5. FTIR spectra of liquid products during the hydro-coprocessing of the vegetable oil and gas oil 75
5.2.1.6. ^{1}H-NMR spectra for liquid products during the hydro-coprocessing of the reaction mixture 76
5.2.1.7. Qualitative hydrocarbon distribution by ESI mass spectrometry 77
5.2.2. Catalytic evaluation of NiO(5.5%)-WO_3(25%)/Al(0.05)-SBA-15 sulfided catalyst 78
5.2.2.1. Effect of temperature in the hydrodesulfurization properties of NiO(5.5%)-WO_3(25%)/Al(0.05)-SBA-15 sulfided catalyst 78
5.2.2.2. Effect of temperature in the hydrodeoxygenation (HDO) properties of NiO(5.5%)-WO_3(25%)/Al(0.05)-SBA-15 sulfided catalyst 78
5.2.2.3. Effect of temperature in the hydrocracking properties of NiO(5.5%)-WO_3(25%)/Al(0.05)-SBA-15 sulfided catalyst 79
5.3. CONCLUSIONS 80
6. KINETICS OF THE HYDRO-COPROCESSING OF THE MIXTURE OF VEGETABLE OIL AND GAS OIL WITH A SULFIDED NiO(5.5%)-WO_3(15%)/Al(0.05)-SBA-15 CATALYST 81
6.1. EXPERIMENTAL 81
6.1.1. Experimental data and reaction conditions for kinetic analysis 81
6.1.2. Kinetic parameter estimation procedure 83
6.2. RESULTS AND DISCUSSION 84
6.2.1. Kinetics and parameter estimation for HDS reactions 84
6.2.2. Kinetics and parameter estimation for HDO reactions 87
6.2.3. Kinetics and parameter estimation for HCK reactions 89
6.3. CONCLUSIONS 92
OVERALL CONCLUSIONS AND PERSPECTIVES 93
REFERENCES 95
APPENDIX 1- Results of kinetic parameters estimation for a five-lumped HCK model 102

LIST OF FIGURES

Fig. 1. Schematic procedure for Al(x)-SBA-15 synthesis. x: Al/Si molar ratio..... 26
Fig. 2. Schematic procedure for NiO(2.5%)-WO_3(15%)/Al(x)-SBA-15 synthesis. x: Al/Si molar ratio. 27
Fig. 3. Schematic procedure for catalytic evaluation of sulfided catalysts. 30
Fig. 4. Schematic procedure for sulfidation of oxide phase catalysts. 31
Fig. 5. Determination curve for vegetable oil composition at ~1750 cm^{-1} FTIR band. 32
Fig. 6. Determination curve for free fatty acids composition at ~1750 cm^{-1} FTIR band. 32
Fig. 7. Nitrogen @77 K physisorption isotherms for SBA-15, Al(x)-SBA-15-*n*, *x*: Al/Si molar ratio; *n*: synthesis number. 34
Fig. 8. Low Angle X-ray diffraction profiles for SBA-15, and Al(x)-SBA-15-*n* materials, *x*: Al/Si molar ratio; *n*: synthesis number 35
Fig. 9. Wide Angle X-ray diffraction profiles for NiO(2.5%)-WO_3(15%)/Al(x)-SBA-15-*n* catalysts, x: Al/Si molar ratio; *n*: synthesis number..... 36
Fig. 10. N_2@-196.15 °C adsorption-desorption isotherms for a) Al(x)-SBA-15 materials b) NiO(2.5%)-WO_3(15%)/Al(x)-SBA-15 oxide phase catalysts; x: Al/Si molar ratio..... 39
Fig. 11. XRD patterns for a) Al(x)-SBA-15 mix1 materials (LA, low angle), b) NiO(2.5%)-WO_3(15%)/Al(x)-SBA-15 oxide phase catalysts (WA, wide angle); x: Al/Si molar ratio. 41
Fig. 12. HR-TEM micrographs for Al(x)-SBA-15 mix1 supports and catalyst, a) Al(0.0)-SBA-15 mix1, b) Al(0.1)-SBA-15 mix1, c)Al(0.05)-SBA-15 mix1, d) Al(0.033)-SBA-15 mix1, e) Al(0.025)-SBA-15 mix1, f) NiO(2.5%)-WO_3(15%)/Al(0.1)-SBA-15 mix1. x: Al/Si molar ratio. 43
Fig. 13. *py*-FTIR spectra at 50 °C a) Al(x)-SBA-15 mix1 catalytic supports, b) NiO(2.5%)-WO_3(15%)/Al(x)-SBA-15 mix1 oxide phase catalysts. x: Al/Si molar ratio. 44
Fig. 14. ^{27}Al-MAS-NMR spectra a) Al(x)-SBA-15 catalytic supports, b) NiO(2.5%)-WO_3(15%)/Al(x)-SBA-15 oxide phase catalysts. x: Al/Si molar ratio. 46
Fig. 15. RAMAN spectra for NiO(2.5%)-WO_3(15%)/Al(x)-SBA-15 oxide phase catalysts. x: Al/Si molar ratio. 47
Fig. 16. FTIR spectra for liquid products using NiO(2.5%)-WO_3(15%)/Al(x)-SBA-15 oxide phase catalysts. x: Al/Si molar ratio 48
Fig. 17. ESI-MS spectra for the liquid product of NiO(2.5%)-WO_3(15%)/Al(x)-SBA-15 mix1 sulfided phase catalysts and the feedstock. x: Al/Si molar ratio. 49
Fig. 18. ^{1}H-NMR spectra for the liquid product of NiO(2.5%)-WO_3(15%)/Al(x)-SBA-15 mix1 sulfided phase catalysts and the feedstock. x: Al/Si molar ratio. 50
Fig. 19. HDS expressed as sulfur removal percentage for NiO(2.5%)-WO_3(15%)/Al(x)-SBA-15 mix1 oxide phase catalysts. x: Al/Si molar ratio. 51
Fig. 20. HDO conversion as the reduction of absorbance at FTIR band of about 1710 cm^{-1} for NiO(2.5%)-WO_3(15%)/Al(x)-SBA-15 mix1 oxide phase catalysts. x: Al/Si molar ratio..... 52
Fig. 21. Lumps mass fraction percentage distribution for NiO(2.5%)-WO_3(15%)/Al(x)-SBA-15 mix1 oxide phase catalysts. x: Al/Si molar ratio. 54
Fig. 22. Low Angle X-ray diffraction profiles for : a) Al(0.05)-SBA-15-n materials, b) Al(0.05)-SBA-15 mix2, n: synthesis number..... 58
Fig. 23. Wide Angle X-ray diffraction profiles for NiO(y)-WO_3(z)/ Al(0.05)-SBA-15 mix2 oxide phase catalysts. y: NiO weight percentage, z: WO_3 weight percentage. 59
Fig. 24. N_2@-196.15 °C adsorption-desorption isotherms NiO(y)-WO_3(z)/Al(0.05)-SBA-15 mix2 and Al(0.05)-SBA-15 mix2 catalytic support. Y: NiO weight percentage, z: WO_3 weight percentage. 60

Fig. 25. RAMAN spectra for NiO(y)-WO_3(z) /Al(0.05)-SBA-15 mix2 oxide phase catalysts. y: NiO weight percentage, z: WO_3 weight percentage. 61
Fig. 26. 27Al-MAS-NMR spectra for NiO(y)-WO3(z) /Al(0.05)-SBA-15 mix2 oxide phase catalysts. y: NiO weight percentage, z: WO3 weight percentage. 62
Fig .27. FTIR spectra for liquid products using NiO(y)-WO_3(z) /Al(0.05)-SBA-15 mix2 oxide phase catalysts. y: NiO weight percentage, z: WO_3 weight percentage. 63
Fig. 28. ^{1}H-NMR spectra for the liquid product of NiO(y)-WO_3(z) /Al(0.05)-SBA-15 mix2 sulfided phase catalysts. y: NiO weight percentage, z: WO_3 weight percentage. 64
Fig. 29. ESI-MS spectra for the liquid product of NiO(y)-WO_3(z) /Al(0.05)-SBA-15 mix2 oxide phase catalysts. y: NiO weight percentage, z: WO_3 weight percentage. 65
Fig. 30. HDS expressed as sulfur removal percentage for NiO(y)-WO_3(z) /Al(0.05)-SBA-15 mix2 oxide phase catalysts. y: NiO weight percentage, z: WO_3 weight percentage. 66
Fig. 31. HDO expressed as the reduction of absorbance at FTIR band of about 1710 cm^{-1} for NiO(y)-WO_3(z) /Al(0.05)-SBA-15 mix2 oxide phase catalysts. y: NiO weight percentage, z: WO_3 weight percentage. 67
Fig.32. Lumps mass fraction percentage distribution for NiO(y)-WO_3(z)/Al(0.05)-SBA-15 mix2 oxide phase catalysts. y: NiO weight percentage, z: WO_3 weight percentage. 68
Fig. 33. XRD patterns for NiO(5.5%)-WO_3(25%)/Al(0.05)-SBA-15 mix2 oxide phase catalyst a) Low Angle (LA), b) Wide Angle (WA). 71
Fig. 34. N_2@-196.15 °C adsorption-desorption isotherms NiO(5.5%)-WO_3(25%)/Al(0.05)-SBA-15 mix2 and Al(0.05)-SBA-15 mix2 catalytic support. 72
Fig. 35. RAMAN spectrum for NiO(5.5%)-WO_3(25%) /Al(0.05)-SBA-15 mix2 oxide phase catalyst. 73
Fig. 36. ^{27}Al-MAS-NMR spectra for NiO(5.5%)-WO_3(25%) /Al(0.05)-SBA-15 mix2 oxide phase catalyst 74
Fig. 37. FTIR spectra for liquid products using NiO(5.5%)-WO_3(25%) /Al(0.05)-SBA-15 mix2 oxide phase catalyst. 75
Fig. 38 ^{1}H-NMR spectra for the liquid product of NiO (5.5%)-WO_3(25%)/Al(0.05)-SBA-15 mix2 sulfided catalyst at different reaction temperature (T): 380 °C, 400 °C, and 420 °C. 76
Fig. 39. ESI-MS spectra for the liquid product of NiO(5.5%)-WO_3(25%) /Al(0.05)-SBA-15 mix2 oxide phase catalyst. 77
Fig. 40. HDS expressed as sulfur removal percentage for NiO(5.5%)-WO_3(25%) /Al(0.05)-SBA-15 mix2 oxide phase catalyst. 78
Fig. 41. HDO expressed as the reduction of absorbance at FTIR band of about 1710 cm^{-1} for NiO(5.5%)-WO_3(25%)/Al(0.05)-SBA-15 mix2 oxide phase catalyst. 78
Fig. 42. Lumps mass fraction percentage distribution for NiO(5.5%)-WO_3(25%)/Al(0.05)-SBA-15 mix2 oxide phase catalyst. 79
Fig. 43. Kinetics and parity chart for HDS reactions using the NiO(5.5%)-WO_3(25%)/Al(0.05)-SBA-15 mix2 sulfided catalyst at different reaction temperatures (T) and time (h). 84
Fig. 44. Kinetics and parity chart for HDO reactions using the NiO(5.5%)-WO_3(25%)/Al(0.05)-SBA-15 mix2 sulfided catalyst at different reaction temperatures (T) and time (h). 88
Fig. 45. Kinetics a parity chart for HCK reactions using the NiO(5.5%)-WO_3(25%)/Al(0.05)-SBA-15 mix2 sulfided catalyst at different reaction temperatures (T) and time (h). 89
Fig.46. Five-lumped kinetic model for the HCK reaction using the NiO(5.5%)-WO_3(25%)/Al(0.05)-SBA-15 mix2 sulfided catalyst, R=Residue, G=Gasoil, D= Diesel, K=Kerosene, and N= Naphtha. 102

Fig.47. Kinetics and parity chart for the five-lumped HCK model using the NiO(5.5%)-WO_3(25%)/Al(0.05)-SBA-15 mix2 sulfided catalyst at different reaction temperatures (T) and time (h). 103

LIST OF TABLES

Table 1. Textural Properties for SBA-15 and Al(x)-SBA-15 synthesized materials 33
Table 2. Wall thickness estimation for Al(x)-SBA-15 type synthesized materials. 36
Table 3. Average W nanoparticle size for catalysts as computed by Debye-Scherrer equation. 37
Table 4. Textural Properties for Al(x)-SBA-15 supports and Ni-W/Al(x)-SBA-15 catalysts; x: Al/Si molar ratio. 38
Table 5. Crystallite size [nm] for WO_3 in NiO(2.5%)-WO_3(18%)/Al(x)-SBA-15 catalysts, x: Al/Si molar ratio. 42
Table 6. Brønsted acid sites concentration for NiO(2.5%)-WO_3(18%)/Al(x)-SBA-15 catalysts, x: Al/Si molar ratio. 45
Table 7. Lewis' acid sites concentration for NiO(2.5%)-WO_3(18%)/Al(x)-SBA-15 catalysts, x: Al/Si molar ratio. 45
Table 8. Crystallite size [nm] for WO_3(y) in NiO(y)-WO_3(z)/Al(0.05)-SBA-15 catalysts. y: NiO weight percentage, z: WO_3 weight percentage. 59
Table 9. Textural Properties for NiO(y)-WO_3(z)/Al(0.05)-SBA-15 mix2 oxide phase catalysts and support. *y*: NiO weight percentage, z: WO_3 weight percentage. 61
Table 10. Experimental data of concentration (wt.%) for the feedstock and the liquid products of hydro-coprocessing a vegetable oil and gas oil blend with a sulfided NiO(5.5%)-WO_3(25%)/Al(0.05)-SBA-15 mix2 catalyst. 82
Table 11. Kinetic parameters for HDS during the hydro-coprocessing a vegetable oil and gas oil blend with a sulfided NiO(5.5%)-WO_3(25%)/Al(0.05)-SBA-15 mix2 catalyst 86
Table 12. Initial reaction rates for HDS during the hydro-coprocessing a vegetable oil and gas oil blend with a sulfided NiO(5.5%)-WO_3(25%)/Al(0.05)-SBA-15 mix2 catalyst. 87
Table 13. Kinetic parameters for HDO during the hydro-coprocessing a vegetable oil and gas oil blend with a sulfided NiO(5.5%)-WO_3(25%)/Al(0.05)-SBA-15 mix2 catalyst. 88
Table 14. Initial reaction rated for HDO during the hydro-coprocessing a vegetable oil and gas oil blend with a sulfided NiO(5.5%)-WO_3(25%)/Al(0.05)-SBA-15 mix2 catalyst. 88
Table 15. Kinetic parameters for HCK during the hydro-coprocessing a vegetable oil and gas oil blend with a sulfided NiO(5.5%)-WO_3(25%)/Al(0.05)-SBA-15 mix2 catalyst 92
Table 16. Kinetic parameters for a five-lumped kinetic model for HCK during the hydro-coprocessing a vegetable oil and gas oil blend with a sulfided NiO(5.5%)-WO_3(25%)/Al(0.05)-SBA-15 mix2 catalyst 103

RESUMEN

Esta investigación doctoral se centró en desarrollar un catalizador mesoporoso mejorado tipo NiO-WO_3/Al(x)-SBA-15 para las reacciones de hidro-co-procesamiento de una mezcla de aceite vegetal (*Jatropha curcas* L.) con una mezcla de gasóleos (ligero y pesado). Lo anterior, con el propósito de reducir la emisión de contaminantes (S, N, V, etc.) y favorecer la obtención de destilados medios (MD), como el diésel, más limpios, haciendo el proceso de refinación más "verde". Así, se evalúo de manera secuencial y sistemática el efecto de las propiedades intrínsecas del catalizador (acidez y carácter metálico) en reacciones en discontinúo a 360 °C, 6 MPa de presión inicial de hidrógeno y 4 h de reacción con una mezcla de aceite vegetal. Inicialmente se determinó la mejor relación molar Al/Si(x) variando está en: 0.1, 0.05, 0.033, y 0.025, pero, fijando el contenido de NiO(y) y WO_3(z) en 2.5% y 15%, respectivamente. El efecto del *Al* fue promover las reacciones de HDS (hidrodesulfuración) y HDO (hidrodesoxigenación), en lugar de la HDC (hidrodesintegración catalítica) en función de la concentración de sitios ácidos de Brønsted (0.05 mmol g^{-1} para el Al(0.05)-SBA-15). La mejor carga metálica (*y*+*z*) se determinó variando el contenido de NiO en: 3.5%, 4.5%, y 5.5% y el de WO_3 en: 18%, 20% y 25%, usando como soporte catalítico el material Al(0.05)-SBA-15. A mayor carga metálica mayor rendimiento para las reacciones de hidrotratamiento (25% HDS y 87.1% HDO), y un incremento del 4.5% en el rendimiento a la fracción tipo diésel. Finalmente, empleando el catalizador mejorado NiO(5.5%)-WO_3(25%)/Al(0.05)-SBA-15 se evaluó el efecto de la temperatura (T) en tres niveles adicionales: 380 °C, 400 °C y 420 °C. Elevar la máxima temperatura (420 °C) maximiza la HDS (53.5%) y la HDO (96%), pero reduce el rendimiento a la fracción tipo diésel (35%) por efectos térmicos. Por lo tanto, el máximo rendimiento a una fracción tipo diésel más limpia se obtuvo a 360 °C (49.3%). El análisis cinético del hidro-coprocesamiento de la mezcla demostró que la HDO fue la reacción más favorecida, seguida de la HDC y de la HDS, siendo, las dos últimas limitadas por la presencia de compuestos más pesados y azufrados recalcitrantes, respectivamente. El orden de reacción para la HDO fue 1.4, mientras que para la HDS y la HDC las reacciones fueron de primer orden, siendo la actividad para HDO 2 veces mayor que la HDS y la HDC.

ABSTRACT

This doctoral research was focused on developing an enhanced NiO-WO_3/Al-SBA-15 type mesoporous catalyst for the hydro-coprocessing reactions of a vegetable oil (*Jatropha curcas* L.) with a gas oil mix (light and heavy) blend. The latter aiming to reduce the contaminants (S, N, V, etc.) emissions and favoring getting cleaner middle distillates (MD), like diesel, making the refining process greener. Accordingly, sequential, and systematically the effect of intrinsic catalytic properties (acidity and metallic character) was assessed in batch reactions at 360 °C, 6 MPa of hydrogen initial pressure, and 4 h of reaction time with a vegetable oil blend. Initially, the best Al/Si molar ratio (x) was determined varying it in 0.1, 0.05, 0.033, and 0.023, but, fixing NiO(y) and WO_3(z) content in 2.5 wt.% and 15 wt.%, respectively. The effect of *Al* was promoting HDS (hydrodesulfurization) and HDO (hydrodeoxygenation) reactions rather than HCK (hydrocracking) on function of Brønsted acid sites concentration (0.05 mmol g^{-1} for the Al(0.05)-SBA-15). The best metallic load (y+z) was determined varying the NiO content in 3.5, 4.5, and 5.5 wt.% and the WO_3 content in 18, 20, and 25 wt.%, using as catalytic support Al(0.05)-SBA-15. The more metallic load, the higher yield for hydrotreating reactions (25% HDS and 87.1% HDO), and an increase of 4.5% in the diesel-like fraction yield. Finally, by using the enhanced catalyst, NiO(5.5 wt.%)-WO_3(25 wt.%)/Al(0.05)-SBA-15, the effect of reaction temperature (T) at three levels: 380 °C, 400 °C, and 420 ° was evaluated. Increasing T to the highest point (420 °C) maximized HDS (53.5%) and HDO (96%) reactions at expenses of reducing the diesel-like fraction yield by thermal effects. Therefore, the highest diesel-like fraction yield was obtained at 360 °C. The kinetic analysis for the hydro-coprocessing reactions demonstrated that HDO was the most promoted reaction, followed by HCK and HDS, being, those reactions limited by the occurrence of heavier compounds and recalcitrant sulfur compounds, respectively. The reaction order for HDO was 1.5, while for HDS and HCK the reaction order was 1.0, being HDO activity 2 times higher than HDS and HCK.

ORGANIZATION OF THIS WORK

This research work consists of three (3) stages of experimental work to elucidate the effect of the intrinsic properties (porosity, acidity, and metallic charge) of the catalysts to be synthesized and evaluated in the hydro-coprocessing of a mixture of gas oil and vegetable oil. Thus, the first stage consists of the study of the effect of the acidity of the catalysts on the yield or selectivity to a diesel-like fraction during the hydro-coprocessing of the mixture. The second stage corresponds to the study of the effect of the metal oxide composition of the catalysts on the selective removal of sulfur (S) and oxygen (O) present in the mixture during hydro-coprocessing. Third, the study of the effect of the operating temperature on the yielding for the diesel-like fraction, and the removal of S and O when hydro-coprocessing the components of the gas oil and vegetable oil mixture. Finally, a kinetic assessment for the three main hydro-coprocessing reactions: HDS, HDO, and HCK. As a result, an enhanced catalyst with a better distribution of acid sites and metallic active phases was tested and developed in terms of promoting the hydro-coprocessing of the reaction mixture.

Based on the foregoing, this doctoral thesis document was developed in six (6) chapters as listed below:

Chapter 1: It corresponds to the description of the research context regarding the research topic. This chapter contains: problem statement, hypotheses, objectives, goals, expected results, scope, and contribution of the research.

Chapter 2: It corresponds to a literature review highlighting the problem to solve as a border problem. This review made it available some of the relevant technical, operational, and scientific knowledge for the execution of this work of research.

Chapter 3: It corresponds to the description of the experimental procedure to determine the effect of the distribution of acid sites and/or type of acid sites in hydro-coprocessing the gas oil and vegetable oil mixture. The results of modifying the Al/Si molar ratio in the series of catalysts to be synthesized are presented and discussed. The effect of Al on the yield to a diesel-like fraction during hydro-coprocessing is also presented and discussed.

Chapter 4: It corresponds to the description of the experimental procedure for determining the effect of the metallic load (metallic oxides) in hydro-coprocessing of the mixture of gas oil and vegetable oil with a fixed Al/Si molar ratio catalyst. The results of systematically varying the content of nickel oxide (NiO) and tungsten oxide (WO_3) in the performance to hydrodesulfurization (HDS) and hydrodeoxygenation (HDO) of the components of the diesel-oil mixture are presented and discussed.

Chapter 5: based on the results of the previous experiments (effect of the Al/Si ratio and the metallic load), hydro-coprocessing a gas oil and vegetable oil mixture was caried out with the enhanced catalyst, varying operating temperature (380-420 °C). The effect of temperature on yielding to a diesel-like fraction, sulfur removal, and the selective removal of O in vegetable oil is analyzed and discussed.

Chapter 6: This chapter describes a kinetic analysis procedure for the hydro-coprocessing reactions: HDS, HDO, and HCK (hydrocracking), the kinetic parameter estimation for the proposed kinetic models, and the discussion derived thereof to correlate catalytic activity results.

Conclusions: It corresponds to the general conclusions of the research work. This chapter aims to clarify the analysis of global results presented in each of the previous chapters to demonstrate the contribution of new knowledge of this thesis in research topic that was addressed.

1. CONTEXT OF THE RESEARCH

1.1 PROBLEM STATEMENT

Conventional processes to obtain liquid fuels (i.e., lower molecular weight and higher added value fractions) are based on the processing non-renewable sources such as petroleum and its derivatives. These sources constitute a serious problem, due to the difficulty in their processing and the emission of pollutants into the environment during their extraction and transformation into a refinery(1). In this sense, there is currently the need to implement scientific and technological improvements to the processes and their transition to cleaner and more sustainable technologies (2, 3). Such technologies must be focused on obtaining oil fractions or cuts with lower molecular weight, eliminating contaminating heteroatoms (S, N, V, etc.), and incorporating renewable sources (e.g., animal fat and vegetable oil), thus, further reducing the existing dependence on fossil fuels (4). Thus, seen the fuel sources separately, from the heavy oil fractions it is necessary to obtain middle distillates (MD) with lower content of sulfur (S), nitrogen (N), and other pollutants(5). Therefore, answering the question: How to treat larger molecules and eliminate contaminating impurities selectively and simultaneously? Likewise, to treat liquid derivatives from vegetable oil it is required selectively removing oxygen (carbonyl and carboxyl groups) from its oligomeric constituents. The latter with the sole purpose of producing biofuels that can replace the traditional sources in internal combustion engines(4). Consequently, how can these reactions occur? And under what conditions when treating mixtures of petroleum fractions and vegetable oils? In this regard, in recent years hydroprocessing of mixtures of vegetable oil and petroleum derivatives, and hydrotreating (HDT) reactions have been studied to obtain cleaner fuels. Among these reactions, the following stand out: HDS (hydrodesulfurization), HDN (hydrodenitrogenation), HDA (hydrodearomatization), HCK (Hydrocracking), and others (6-9).

Hydroprocessing reactions occur on active sites of heterogeneous catalysts in an environment rich in hydrogen gas (H_2) at high pressure (2.5 MPa-5.5 MPa) and temperature (350-420 °C). Depending on the application, the research has been extensive, and the use of bifunctional catalysts has been highlighted (hydrogenolysis/hydrogenation and type of acidity) (10-12). The type of sulfided active phases is known for the desired reaction, for example, Co-Mo for HDS, Ni-Mo for HDN, and Ni-W for both hydrotreating reactions (HDS, and HDN), and HCK (13, 14). On the other hand, catalytic supports (solids in which the precursor metals of the active phases are deposited, fixed, or impregnated) have also been studied. These supports vary depending on its porosity, its distribution of acidic sites (Brønsted-Lowry and Lewis) and the size of the molecules to be treated with. The following stand out: ɤ-Al_2O_3, SiO_2-Al_2O_3, ASA (Amorphous Aluminosilicates), and mesostructured

silica type MCM-41 (Mobil Composition of Matter N° 41), SBA-15 (Santa Barbara Amorphous N° 5) and MCF (Mesocellular Silica Foam). All these previous materials have the advantage of tailoring their textural properties (specific surface area S_{BET}, volume, and pore size) during their synthesis process (15-18). Hence, those materials are particularly attractive for processes such as hydroprocessing of larger molecules and for contaminants removal. In addition, those catalytic supports can be functionalized with various elements (Al, Ti. Zr, etc.) and acid-base molecules to generate a stronger distribution and strength of acid sites on their catalyst surface compared to the traditional ɤ-Al_2O_3 support, whose porosity and acid strength is limited (Lewis-type acid sites)(1, 19-22).

At present times, research with such materials (conventional and modified ones) and active phases in hydroprocessing to obtain biofuels has made it possible to elucidate that the catalysts that have been conventionally used to treat fractions of heavy and light crude oils can be used to treat mixtures of these crude oils with vegetable oil. Various studies have been reported, varying both the type of catalyst depending on the nature of the load (composition and concentration of the vegetable oil) (23-25). However, what are the optimal metal loading, textural properties, and acid sites distribution (e.g., Al/Si molar ratio) of catalysts for hydro-coprocessing mixtures of vegetable oil and gas oil type fractions? How do these catalytic properties influence the yield and/or selectivity of the involved reactions?

On the other hand, the industrial scale-up of many of those experiments is still a remote possibility, since the reported studies have been exploratory and have not made it possible to correlate the reaction mechanisms with the intrinsic properties of the used catalysts (24). Thus, researching for key points would facilitate the development of future kinetic models and theoretical calculations that will allow the design, synthesis, and evaluation of catalysts for very specific purposes at an industrial level. The latter could be attained by the estimation of the kinetic parameters ascribed to the corresponding kinetic model as a function of the catalyst used and designed for such purpose.

1.2 HYPOTHESIS

Obtaining a cleaner diesel-like fraction during the hydro-coprocessing of a gas oil and vegetable oil blend is possible by developing a functionalized mesoporous catalyst type Ni-W/Al-SBA-15, due to the effect of the textural properties and the acidic and metallic sites of the catalyst during hydrocracking and the selective sulfur (S) and oxygen (O) removal.

Ni-W active phases are the most robust in hydroprocessing. These phases selectively remove heteroatoms allowing the increase the H:C molar ratio during the hydrogenolysis-hydrogenation

process of the hydrocarbon mixture (4). Additionally, the direct incorporation of Aluminum (Al) to SBA-15 allows conferring a moderate or slight acidity with a uniform distribution of acid sites (Brønsted and Lewis). Acidic Brønsted sites act as precursors of cracking of bonds and specific functional groups during hydroprocessing reactions (3, 26).

1.3 OBJECTIVES AND GOALS

1.3.1 General objective

To establish the influence on the catalytic activity of Ni-W type sulfided active phases, and the acid and textural properties of the Al-SBA-15 material for the development of a catalyst with a higher yield to cleaner liquid fuels in hydro-coprocessing of a mixture of gas oil and vegetable oil.

1.3.2 Specific objectives

i. To synthesize aluminum-functionalized mesoporous silica (Al-SBA-15) by a direct method as catalytic support for bifunctional catalysts for the hydro-coprocessing of a mixture of gas oil and vegetable oil.

ii. To determine the Al/Si molar ratio (acid sites distribution) that promotes the highest yield to a cleaner (less S) diesel-type fraction during the hydro-coprocessing of a mixture of gas oil with vegetable oil using a catalyst with a fixed Ni-W composition.

iii. To determine the composition of metal oxides (active phases distribution) that promotes the highest yield for the HDS reaction during the hydro-coprocessing of a mixture of gas oil and vegetable oil with a catalyst with the best Al/Si molar ratio.

iv. To evaluate the effect of temperature (T) on the diesel-type fraction yield during the hydro-coprocessing of a mixture of gas oil and vegetable oil with an enhanced Ni-W/Al-SBA-15 catalyst with the best Al/Si molar ratio and composition of metallic oxides.

1.3.3 Goals

The established goals by each one of the objectives proposed for this research are described below. The goals are described as the main products ascribed to each objective.

Objective 1

- Five mesoporous silicas functionalized with aluminum Al-SBA-15 type as reported in the literature (Al/Si molar ratio of 0.1, 0.05, 0.033, 0.025, and 0.0) with the direct synthesis method (3, 27).

Objective 2

- Five Ni-W/Al-SBA-15 catalysts with a fixed composition of metal oxides (2.5% NiO and 15% WO_3). The successive incipient wet impregnation method will be used, using the corresponding Ni and W precursor salts, $Ni(NO_3)_2.6H_2O$ and $(NH_4)_6H_2W_{12}O_{40}.H_2O$ for Ni and W respectively (19).
- Characterization of intrinsic properties of the catalytic supports and synthesized catalysts by Physisorption of N_2 at 77 K, XRD (X-ray diffraction), TEM, Pyridine-FTIR, ^{27}Al-MAS-NMR, and RAMAN spectroscopy.
- The catalytic evaluation (batch reaction for 4 h) of the effect of acidity during the hydroprocessing of a vegetable oil-gas oil mixture (20 vol.% *Jatropha curcas* L.*)* at the conditions (6 MPa and 360 °C) reported in the literature(28). The latter for the five catalysts with different Al/Si molar ratios.
- Quantification and identification of the reaction products by simulated distillation (ASTM D2887) for the quantification of the diesel-like fraction. To quantify the removal of sulfur (S) by the ASTM D-4294 or similar standard. Oxygen (O) removal will be analyzed by FTIR.

Objective 3

- Three (3) Ni-W/Al-SBA-15 catalysts with variable NiO composition (3.5, 4.5, and 5.5 wt.%) and WO_3 (18, 20, and 25 wt.%) for the best Al/Si ratio and according to previously reported catalytic evaluation results (19).
- Characterization of intrinsic properties of the catalytic supports and synthesized catalysts by Physisorption of N_2 at 77K, XRD (X-ray diffraction), *Pyridine*-FTIR, ^{27}Al-MAS-NMR, and RAMAN spectroscopy.
- The catalytic evaluation (batch reaction for 4 h) of the effect of the metallic phases during the hydroprocessing of a vegetable oil-gas oil mixture (20 vol.% *Jatropha curcas* L.*)* at the conditions (6 MPa and 360 °C) reported in the literature(28). The latter for the three catalysts with a variable composition of metallic oxides.
- Quantification and identification of the reaction products by simulated distillation (ASTM D2887) for the quantification of the diesel-like fraction. To quantify the removal of sulfur (S) by the ASTM D-4294 or similar standard. Oxygen (O) removal will be analyzed by FTIR.

Objective 4

- Catalytic evaluation of the best catalyst for the hydroprocessing of the vegetable oil-gas oil mixture (metal oxides composition and Al/Si molar ratio with a higher incidence in the HDS and higher diesel-like fraction yield, respectively) at fixed conditions of hydrogen (H_2) initial pressure and vegetable oil concentration (25, 28). Only the reaction temperature will be varied at 380 °C, 400 °C, and 420 °C.
- Quantification and identification of the reaction products by simulated distillation (ASTM D2887) for the quantification of the diesel-like fraction. To quantify the removal of sulfur (S) by the ASTM D-4294 or similar standard. Oxygen (O) removal will be analyzed by FTIR.

1.4 JUSTIFICATION

A focus of interest in research for the improvement of oil refining processes is centered in developing new catalysts that permits to convert heavy crude fractions into liquid fuel molecules (middle distillates), and cleaner (lower concentration of S, N, V, etc.) compounds without detriment to the fuel capacity of the product. In this way, reducing the environmental impact derived from the extraction, processing, and combustion of fossil fuels is sought. Hence, incorporating renewable sources into conventional refining processes, such as vegetable oil, is undoubtedly a promising alternative. However, vegetable oils are essentially a matrix of oligomeric compounds with diverse functional groups (oxygenated) whose presence negatively affects the combustion reactions in vehicles. Therefore, bifunctional catalysts (acid and hydrogenating function) are required for their processing.

Thus, the present research focuses on elucidating the effect of the intrinsic properties of an enhanced bifunctional Ni-W sulfided catalyst supported on mesoporous silica functionalized with aluminum (Al) Al-SBA-15 type in the hydro-coprocessing of a vegetable oil and gas oil mixture. Specifically, the study of the effect of the distribution of acidic sites and active sites (metallic phases) of the catalyst and the operating temperature in promoting a higher yield during the hydrodesulfurization reaction (HDS), thus as possible hydrocracking (HCK) of the components of the mixture to attain diesel-like fractions (C_{11}-C_{17}).

The results of this research will allow the development of a catalyst for the hydro-coprocessing of a mixture of vegetable oil-gas oil based on the effect of the surface chemistry of the catalyst in the hydroprocessing. These results are key data for the development of a subsequent kinetic study for the sizing and designing industrial units for the process, and further reducing the gap between experimental results and the treatment of real samples and processes.

1.5 SCOPE

This research presents the experimental results of the exploratory study of the catalytic activity for the development of a bifunctional Ni-W/Al-SBA-15 catalyst in the hydro-coprocessing of a vegetable oil-gas oil mixture at a laboratory scale. For this purpose, preliminary reactions are carried out to determine and sequentially set the best: Al/Si molar ratio, weight composition of the metal oxides (NiO and WO_3), and the operating temperature. The idea is to attain the highest yield to a cleaner and renewable diesel-like fraction by enhancing hydrodesulfurization (HDS), hydrodeoxygenation (HDO), and hydrocracking (HCK) reactions when hydro-coprocessing vegetable oil and gas oil.

Finally, it is highlighted that this research does not include the study of the effect of non-sulfided active phases (e.g., carbides, phosphides, and nitrides) since it is desired to increase the knowledge that we already have of the Ni-W sulfided active phases (typical of hydroprocessing with conventional catalysts). In addition, the study of the effect of the composition of the vegetable oil-gas oil mixture is not included, since the reactivity and effect of the catalysts as a function of the amount of vegetable oil added is unknown, but it is known that a large addition of such oil makes it possible to obtain fuels out the permitted sulfur and oxygen content for internal combustion processes. Therefore, it is a research question that remains open to future research once the results of this research are reported.

1.6 CONTRIBUTION

- Synthesis and characterization of a catalyst (different from the conventional Ni-Mo/ɤ-Al_2O_3) to attain a diesel-like fraction during the hydro-coprocessing of a mixture of vegetable oil and gas oil using functionalized mesoporous silica type Al-SBA-15 as catalytic support and active Ni-W sulfided phases.
- Catalytic evaluation of the efficiency of a catalyst (different from the conventional Ni-Mo/ɤ-Al_2O_3) to attain a diesel-like fraction during the hydro-coprocessing of a mixture of vegetable oil and gas oil using functionalized mesoporous silica Al-SBA-15 type as catalytic support and active Ni-W sulfided phases.
- Kinetic analysis procedure for an enhanced and novel Ni-W/Al-SBA-15 sulfided catalyst in terms of catalytic activity for hydro-coprocessing reactions of hydrodesulfurization (HDS), hydrodeoxygenation (HDO), and hydrocracking (HCK) of a vegetable oil and gas oil blend.

2. LITERATURE REVIEW

The oil refining process as a conventional source of energy is an energy transformation and utilization technology that is still in force today (29-32). The derived fractions with high added value are obtained by hydroprocessing (reaction at high pressure and temperature in the presence of hydrogen) using mainly heterogeneous catalysts in units or reactors with fixed bed and continuous flow (30, 33). Hydroprocessing is a set of chemical reactions that require meeting two main objectives. One of these is the removal of contaminating heteroatoms (e.g., S, N, V, etc.), deriving the reactions of Hydrodesulfurization (HDS) and Hydrodenitrogenation (HDN) and others. The second objective is to promote the reaction of hydrogen with the hydrocarbon mixture in reactions of isomerization, alkylation, and selective cracking, to increase the H:C molar ratio of the present compounds. This process is called Hydrocracking (HCK) (29). Specifically, the purpose is to obtain fractions called middle distillates (MD), from such fractions naphtha, kerosene, diesel, and jet fuel are obtained by a further separation process (33). Currently, carrying out this processing is more complicated since there are heavier crude sources (lower API) whose constituent compounds have a higher molecular weight (polyaromatic and unsaturated hydrocarbons) and a higher content of S, N, and heavy metals (3). In this sense, the research interests of refiners have been focused on the simultaneous processing of mixtures of petroleum fractions with vegetable oils. This makes it possible to obtain cleaner liquid fuels that incorporate alternative sources of energy, such as derivatives of lignocellulosic biomass, aiming at enhancing the fuel capacity of the hydrocarbons thus obtained. The latter results in a reduction in green housed effect polluting gas emissions (SO_X, NO_X, and CO_2, respectively) (33).

Thus, the most recent research for the hydro-coprocessing of vegetable oil with fractions derived from petroleum shows a growing interest in the development of catalysts based on nickel in its reduced form and supported on mesoporous nanomaterials type SBA-15 and MCM-41. In this regard, Oh *et al.*,, evaluated the performance of three bimetallic catalysts NiCu, NiZn and NiMn supported in SBA-15 in the HDO (Hydrodeoxygenation) of bio-oil at 3 MPa, 45 min and 250-350 °C, highlighting that the presence of the two metals increases the gas production performance compared to the Ni-SBA-15 catalyst(34). However, mesoporous silicas lack acidic sites and acidity to promote chemical reactions of isomerization and selective cracking of larger molecules. For this reason, it has been generated a distribution of acidic sites (Brønsted and Lewis) to materials such as SBA-15 and MCM-41, synthesizing functionalized supports such as Al-SBA-15, Zr-SBA-15, Ti-SBA-15, and others (3, 35). In this sense, Zhang *et al.*,, impregnated the reduced Ni/MCM-41 catalyst (10 wt.% Ni) with a

heteropoly acid type HPW (phosphotungstic acid) to evaluate its performance in the HCK (hydrocracking) of methyl palmitate, obtaining jet-fuel with a selectivity of 86.1%. This result is a consequence of the strong acidity of the catalysts due to the presence of HPW on their surface(36). Similarly, Tan *et al.*,, synthesized and evaluated a new reduced catalyst Ni_2P/Zr-SBA-15 (30 wt.% Ni and molar ratio Ni/P = 1) in the hydrodeoxygenation (HDO) of Jatropha oil, obtaining a yield of 60% and that was attributed to the acidity of the catalytic support generated. The reactions involved were: deoxygenation, aromatization, and cracking (26). Also, Tieuli, *et al.*,, provided insights into the HDO of bio-oil model molecules such as isoeugenol by incorporating sulfated ZrO_2 to the Ni-SBA-15 catalyst and evaluating its performance at 300 °C, 3 MPa, by using dodecane as solvent. The results showed that the incorporation method of the metals and the presence of the ZrO_2 nanoparticles decreased the catalytic activity (lower yield). The latter because the reduced active phase of nickel was inside SBA-15 tubular channels and the zirconia both internally and externally was blocking access to the metal active site. A kinetic model was also proposed that adjusted 91% to the experimental data (37). By their side, Gómez-Orozco *et al.*,, tested a ternary system (Ni, Mo, and W) as a sulfided active phase in the HDS of dibenzothiophene (DBT) at 320 °C and 5.5 MPa, and using Ti-SBA-15 as catalytic support (35). The less Ti on the catalytic support (Si/Ti molar ratio of 40) reduced HDS activity due to the hydrogenation capability of less Ti catalysts. The occurrence of tetrahedral Ti was responsible of the catalytic activity trends as previously reported. Hence, Lima *et al.*, reported the catalytic evaluation of Ni-Mo catalysts supported on SBA-15 and alumina, aiming to elucidate the influence of surface chemistry of the support on catalyst deactivation (38). The alumina supported catalyst exhibited 44% more coke deposition than the SBA-15 supported catalyst, indicating that a more acidic catalytic support facilitates a quicker catalytic deactivation by coke formation and carbon deposition. For that reason, tailoring acidic properties is important for the development of an effective catalyst. In this respect, Zhang et al synthesized an acidic Al-MCM-41 support for a Pt catalyst in the HDT of Jatropha oil at 360 °C, 4 MPa, and a LHSV of 1 h^{-1} by etching the MCM-41 support with sulfuric acid, citric acid, or hydrochloric acid (39), etching the catalytic support decreased the specific surface area (S_{BET}) but increased catalytic activity due to the increase in acid sites. Citric acid etched catalysts were the more selective to a diesel-like fraction (C_8-$C16_6$).

On the other hand, conventional catalysts for hydroprocessing are Co-Mo, Ni-Mo, and Ni-W sulfides supported on: ɤ-Al_2O_3, SiO_2-Al_2O_3, TiO_2, and zeolites type HY, USY, Hbeta, etc. Such catalysts have also been evaluated in the hydro-coprocessing of crude oil mixtures with vegetable oil. In this regard, El-Sawy *et al.*,, reports the catalytic evaluation of the binary bed (two types of catalysts), Ni-Mo/Al_2O_3 and Ni-W/SiO_2-Al_2O_3 in vacuum gas oil (VGO) and residues mixture with two types of vegetable oil waste: lubricating oil (WLO) and cooking oil (WCO). These experiments were carried

out at 7 MPa, LHSV 1.5 h^{-1}, 380-440 °C, and a concentration range of each waste oil of 10-20 vol.%. Depending on the type of waste used, the yield to diesel and kerosene was variable, and WCO promoted the formation of a greater quantity of kerosene. On the contrary, WLO promoted diesel yield. In terms of temperature, it maximized diesel production at 400 °C (2). For their part, Palos *et al.*, evaluated the performance of commercial catalysts Co-Mo/Al_2O_3, Ni-Mo/SiO_2-Al_2O_3, and Ni-W/USY in a 20 vol.% mixture of oil derived from tires and light diesel. The reaction products were analyzed by APPI/ESI FT-ICR MS, FID-MS GC X GC, and PFPD GC, showing a similar distribution and type of products for the set of catalysts studied (4).

Regarding the previous hydrotreating of vegetable oil samples, obtained by direct processing of lignocellulosic biomass, Auersvald *et al.*,, used the commercial Ni-Mo/Al_2O_3 catalyst (5.5 wt.% NiO and 28.3 wt.% MoO3) during the hydrotreating of straw oil derived from pyrolysis (240-360 °C, 2-8 MPa, WHSV = 1 h^{-1}), showing that 85% of the fuel precursors are obtained in the organic phase and miscibility with diesel for the bio-oil obtained at 360 °C and 8 MPa (40). However, since the efficiency for HDS is reduced using sulfided phases, De Paz Carmona *et al.*, evaluated molybdenum carbides and nitrides (MoC_x and MoN_x) supported on Al_2O_3, TiO_2, and ZrO_2 in the hydroprocessing of atmospheric gas oil (AGO) mixed with rapeseed oil (RSO) at different AGO/RSO ratios (330-350 °C, 5.5 MPa, WHSV = 1-2 h^{-1}). It is highlighted that the intrinsic properties of Al_2O_3 favored yielding and selectivity compared to the other supports (41).

Finally, the effect of the catalyst/bio-oil mass ratio on the catalytic cracking of bio-oil using zeolites has been studied, and a yield to deoxygenates higher than 61% was reported by increasing this ratio. Additionally, it is noted that the yield to liquid was the lowest (12-16%) for the catalyst supported in HSZM-5 due to its strong acidity at simulated FCC (Fluid Catalytic Cracking) conditions (42).

Based on the aforementioned, optimal composition and type of metallic phases (sulfided or reduced), the molar ratio of acidity precursor heteroatoms (Al, Ti, Z, or others), and the operating conditions (temperature and partial pressure of hydrogen) allow maximizing the yield or selectivity during the hydroprocessing of vegetable oil-gas oil mixtures to the compounds of interest. Scientific research has focused on conducting exploratory studies with different types of materials such as heterogeneous solid catalyst support, active phases based on Ni and their combinations with Mo and W, and different types of vegetable oil. Nonetheless, the operating conditions are based on previous or availability reports. Therefore, the hydroprocessing of mixtures of vegetable oil and heavy crude fractions is a research topic that remains open and requires a more solid knowledge for its future scaling and application at an industrial level.

3. EFFECT OF THE Al/Si MOLAR RATIO IN THE HYDRO-COPROCESSING OF A MIXTURE OF VEGETABLE AND GAS OIL WITH A Ni-W/Al(X)-SBA-15 SULFIDED CATALYST

This chapter discusses the effect of textural properties and acidity of Al(x)-SBA-15 materials as supports for Ni-W sulfided catalysts during the hydro-coprocessing of a mixture of gas oil and *Jatropha curcas* L. oil. Accordingly, this chapter describes the experimental procedure for synthesizing Al-SBA-15 by a direct method for Al/Si molar ratios of 0.1, 0.05, 0.033, 0.025, and 0.0. The composition of metallic oxides was fixed at 2.5 wt.% for NiO and 15 wt.% for WO_3. Hence, the aluminum incorporation effect on the yield of a diesel-like fraction when hydroprocessing the mixture is elucidated.

3.1. EXPERIMENTAL

3.1.1. Synthesis of Al (x)-SBA-15 catalytic supports

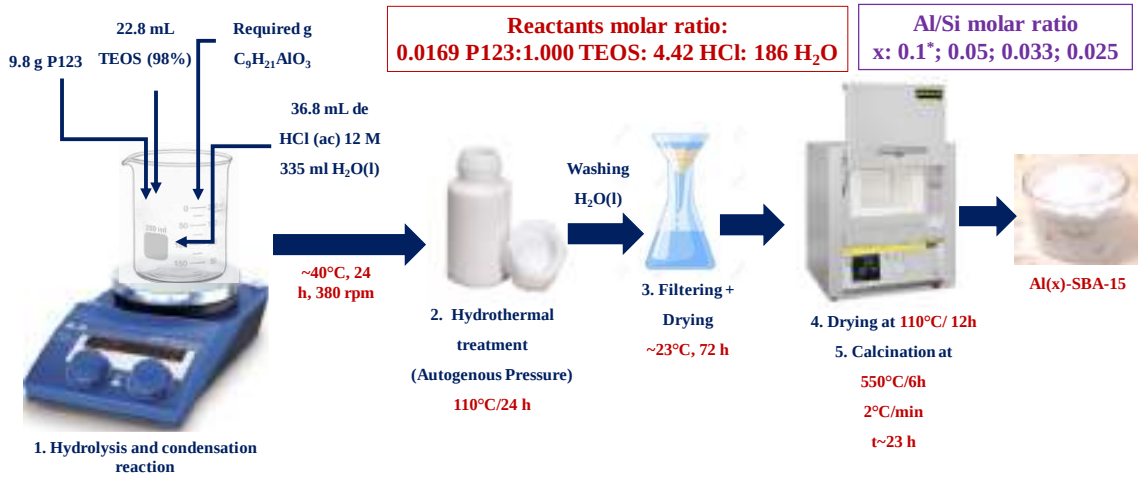

Fig. 1. Schematic procedure for Al(x)-SBA-15 synthesis. x: Al/Si molar ratio.

To set the experimental conditions for synthesizing Al modified SBA-15 materials and obtaining about 10 g of each sample, fifteen syntheses were carried out. The experimental procedure is shown in **Fig. 1,** and it is described as follows:

Silica-based Al functionalized materials were directly synthesized adapting previously reported procedures (27, 43-45). In a typical synthesis, about 9.8 g of Pluronic P123 ($EO_{20}PO_{70}EO_{20}$, M_{av} =

5800, PEG 30 wt.%, Aldrich) were dissolved in 235 mL of a 1.2 M aqueous solution of HCl (37.3 vol.%, Merck) under continuous agitation (~380 rpm). A calculated amount (depending on Al/Si molar ratio) of aluminum isopropoxide ($C_9H_{21}AlO_3$, Aldrich 98%) was dissolved in ~100 mL of a 1.2 M aqueous solution of HCl (37.3 vol.%, Merck) under continuous agitation (~500 rpm). Then, both HCl aqueous solutions were mixed and kept under agitation (~380 rpm) for 1 h. Subsequently, ~22.8 mL of tetraethyl orthosilicate ($SiC_8H_{20}O_4$, TEOS, Aldrich 98%) were added dropwise. Temperature was increased from room temperature (~25 °C) to 38 °C and kept at these conditions for 24 h. The milky suspension obtained is transferred into a PTFE closed bottle for hydrothermal treatment at 110 °C for 24 h, using a heating rate of 2 °C/min in an oven. The solid product is filtrated, flushed with deionized water, and dried at ambient conditions for 72 h. Finally, the solid product is placed on a furnace for drying at 110 °C/12 h and calcination at 550 °C/6 h to remove the template (Pluronic P123) using a heating rate of 2 °C/min. The resulting material was labeled Al(x)-SBA-15, where x is the Al/Si molar ratio.

The nominal molar ratio of reactants during the synthesis was the following: 1.0 TEOS:0.0169 P123:4.42 HCl:186 H_2O according to previously reported works (3, 21). Pristine SBA-15 catalytic support was synthesized following the previous procedure, but, without aluminum isopropoxide addition.

The synthesized catalytic supports were labeled: Al(x)-SBA-15-*n*, where *x* is the Al/Si molar ratio and *n* is the corresponding number of the synthesis.

3.1.2. Catalysts preparation

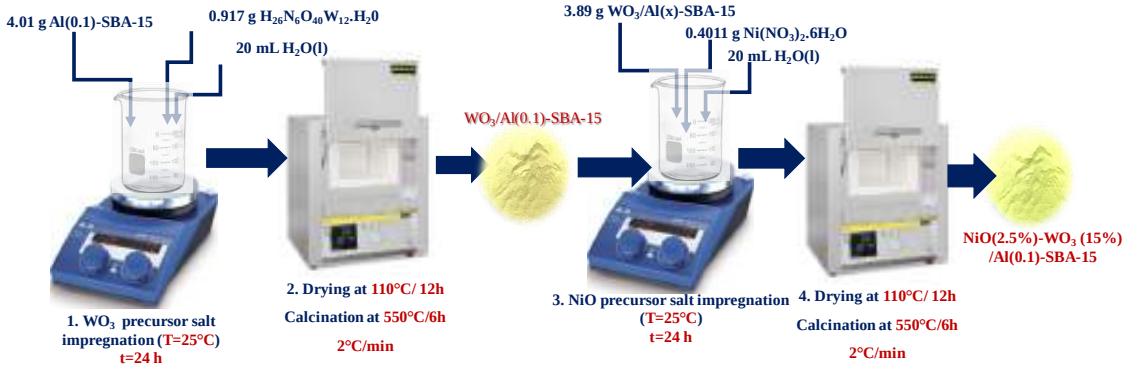

Fig. 2. Schematic procedure for NiO(2.5%)-WO_3(15%)/Al(x)-SBA-15 synthesis. x: Al/Si molar ratio.

Preliminary experiments were carried out to elucidate the effect of impregnation time and air flow during the synthesis of Ni-W/Al(x)-SBA-15 oxide phase catalysts. Catalysts preparation was carried out according to the following procedure as depicted in **Fig. 2**:

Ni-W/Al(x)-SBA-15 oxide phase catalysts were prepared by the successive incipient wetness impregnation method. A calculated amount (to get ~15 wt.% of WO_3) of ammonium metatungstate, $(NH_4)_6H_2W_{12}O_{40}.H_2O$ (Aldrich 85 wt.% WO_3) was dissolved in ~25 mL of deionized water. The previous solution was added to ~5 g of Al(x)-SBA-15 and mixed until homogenization and kept static for 24 h. The resulting material dried at 110 °C for 12 h and calcined at 550 °C for 6 h with a heating rate of 2 °C/min into a furnace. Then, the recovered solid was impregnated with ~25 mL of an aqueous solution of nickel nitrate, $NiNO_3.6H_2O$ (Aldrich, 97%) to get ~2.5 wt. % of NiO, kept static for 24 h, and subsequently dried and calcined in a furnace at the same conditions of the previous impregnation. All the synthesized solids were grounded and sieved down to a particle size between 25 and 75 μm for reaction experiments. Catalysts were labeled: Ni-W/Al(x)-SBA-15-*z*, where x is the Al/Si molar ratio and *z* is the number of the synthesis.

For Ni-W/Al(0.1)-SBA-15-1 catalyst, the impregnated solids were homogenized for 1 h, for Ni-W/Al(0.0)-SBA-15-1, the impregnated solids were homogenized for 24 h, and for Ni-W/Al(0.0)-SBA-15-2, the impregnated solids were homogenized for 24 h, but calcined with a flow rate of dry air of 500 mL min^{-1} into the furnace at the previously reported conditions.

3.1.3. Characterization

3.1.3.1. Textural Properties

Samples between 0.05 and 0.1 g were outgassed at 180 °C/12 h before analysis. Outgassed samples were analyzed in a Quantachrome ASQIA equipment for nitrogen physisorption @-196.15 °C. Isotherms were recorded with twenty acquisition points during adsorption and seventeen during desorption. Specific surface area (S_{BET}, m^2g^{-1}) was determined by the BET (Brunauer, Emmet and Teller) method at relative pressures (P/P_0) within 0.04 and 0.25 according to IUPAC recommendation (46). Pore volume (cm^3g^{-1}) was determined at 0.99 of relative pressure, while pore diameter (nm) was determined by the BJH (Bayer, Joyner and Halenda) method.

3.1.3.2. Materials Crystallinity by XRD

Previously grounded samples between 0.05 and 0.1 g were analyzed in a Rigaku Ultima IV X-ray diffractometer coupled with an ultra-high-speed detector for low angle (2θ from 0.4° to 4°) measurements. Wide angle (2θ from 10° to 80°) measurements were performed to identify changes in kind of metallic phase and crystallinity of the synthesized catalysts. Copper Kα1 radiation (1.54 A°) was employed with a speed of 0.5°min^{-1} each 0.02 s.

3.1.3.3. Porous Structure by HR-TEM

Micrographs with a magnification of ~50 nm were taken for Al(x)-SBA-15, and Ni-W/Al(0.1)-SBA-15 materials using a 200 kV JEOL (Japan) JEM-ARM200F microscope with a cold field emission gun (ColdFEG). Images acquisitions were carried out with a Orius model Gatan camera employing Gatan Microscopy Suite: Digital micrograph 2.31.734 version. These analyses were performed to elucidate changes in porous structure by Al, Ni, and W incorporation during synthesis procedure.

3.1.3.4. Materials Acid Sites Distribution (Brønsted/Lewis) by Pyridine-FTIR

About 0.03 g of each Al(x)-SBA-15 and Ni-W/Al(x)-SBA-15 materials were analyzed in an FTIR spectrometer Nicolet 8700 within a range of 400 to 4000 cm^{-1}, and an average number of scans of 50. Prior to the analysis, samples were outgassed at 400 °C. About 50 µL of Pyridine was absorbed at room temperature inside a quartz cell, and desorbed progressively under vacuum at 50, 100, 200, 300, and 400 °C.

3.1.3.5. Molecular Structure of Aluminum Species by ^{27}Al-MAS-NMR Measurements

^{27}Al Nuclear magnetic resonance (NMR) spectra were recorded in a Bruker Advance III spectrometer attached to a 4 mm magic-angle spinning (MAS) probe, using direct excitation, about 30° of pulse angle, a recycle delay of 0.1 s, and a sample spin-rate approximately of 7 kHz. Spectra were acquired at 104.26 MHz.

3.1.3.6. Chemical functional groups by RAMAN spectroscopy

RAMAN spectra were acquired in the interval of 100 to 1300 cm^{-1} in a LabRam HR8000 equipment employing a laser of 633 nm, nominal power of 13 mW, exposure time of 6 s, and an accumulation time of 8 repetitions.

3.1.3.7. FTIR spectra of liquid products during the hydro-coprocessing

IR spectra were recorded within the range of 400 to 4000 cm^{-1} in an IR 2 IlluminatIR II JY Smiths Detection apparatus coupled to an OLYMPUS BX41 optic microscope.

3.1.3.8. Electrospray ionization (ESI) mass spectrometry

ESI spectra were acquired in a Bruker Daltonics micrOTOF-Q apparatus scanning within the range of 50 to 2000 m/z and employing a positive ion polarity. Spectrum data was adjusted by subtracting sodium (Na) molecular weight (~22.99 g mol^{-1}) from m/z units to qualitatively determine the corresponding hydrocarbon fraction for representative higher intensity ions obtained.

3.1.3.9. Analysis of liquid products by ^{1}H-NMR

H^+ Liquid state Nuclear Magnetic Resonance (NMR) analyses were performed in Bruker Ascend TM apparatus for all liquids products of the hydro-coprocessing of the vegetable oil and gas oil blend and

pure *Jatropha curcas* L. oil. Samples were previously dissolved in deuterated chloroform, $CDCl_3$. Spectra were acquired at 750 MHz employing a relaxation delay of 1s, receiver gain of 4, pulse width of 8 s, and a total number of scans of 32.

3.1.4. Catalytic Evaluation

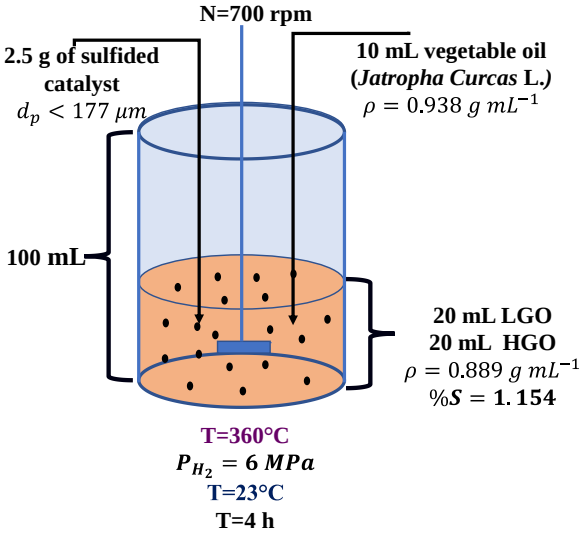

Fig. 3. Schematic procedure for catalytic evaluation of sulfided catalysts.

Hydro-coprocessing experiments were carried out in a 100 mL batch reactor Parr 4598 under the following operational conditions: 360 °C, 6 MPa of initial hydrogen (H_2) partial pressure, ~2 wt.% of sulfided catalyst, 700 rpm, and a reaction time of 4 h as shown in **Fig. 3**. Prior to the experiments, a mixture 50% vol. of LGO (Light Gas Oil) and HGO (Heavy Gas Oil) was prepared and labeled as GOM (Gas Oil Mix) GOM was further mixed with *Jatropha curcas* L. Oil (JO) to make a mixture JO/GOM volume ratio of 20/80. About 50 mL of the final mixture was loaded into the reactor with the required amount of previously sulfided Ni-W/Al(x)-SBA-15 catalyst.

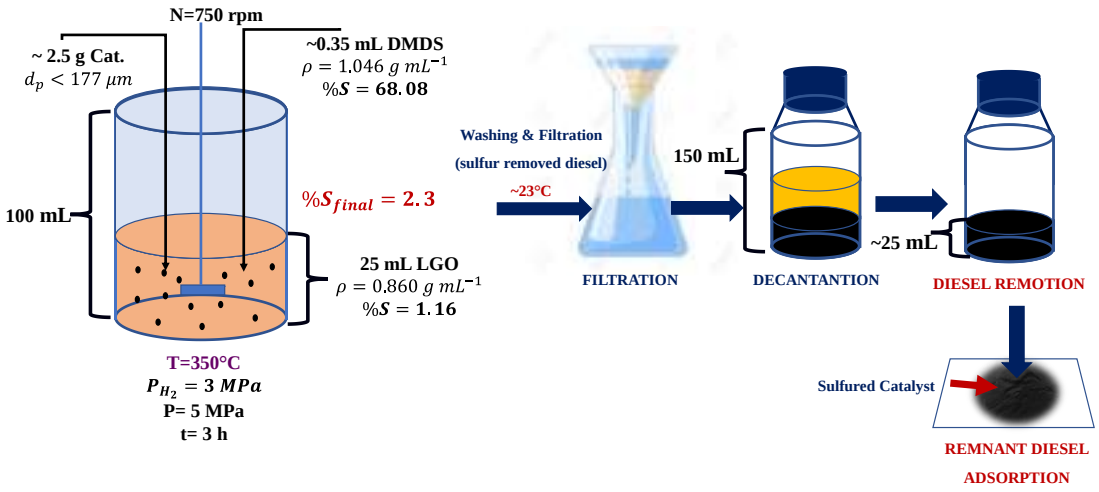

Fig. 4. Schematic procedure for sulfidation of oxide phase catalysts.

Sulfidation process (transforming NiO and WO_3 in their respective sulfides) was conducted *ex-situ* in the same batch reactor as shown in **Fig. 4**. But, using a feedstock formed by LGO (~1.4 wt.% S content) mixed with the required amount (~0.35 mL) of dimethyl disulfide (DMDS, $C_2H_6S_2$, Aldrich 99%) to attain ~2.3 wt.% of S content. Sulfided catalysts were recovered by filtration, washing with sulfur removed diesel, decantation, and adsorption of the remnant of no sulfur diesel on a paper blanket.

Reactor operating conditions are the following: 25 mL of LGO, 3 MPa of H_2(g) initial pressure, 750 rpm, 2.5 g of oxidized Ni-W precursor of the catalyst. Temperature was successively increased from ~25 °C to 150 °C, and kept for 30 min. Subsequently, the temperature was raised from 150 °C to 350 °C kept for 3 h at a heating rate of ~2.5 °C/min.

3.1.5. Catalytic Activity

3.1.5.1. Hydrodesulfurization (HDS) percentage (sulfur removal)

Sulfur content was determined according to the ASTM D4294 standard in a SINDIE 2622-10 equipment. Then, sulfur removal percentage was determined by computing the relative difference percentage between the feedstock (as reference) and the liquid product for each Ni-W/Al(x)-SBA-15 catalyst as shown in **Eqn.1**. C_{S0} and Cs are the initial and final sulfur concentrations in weight percentage.

$$\%HDS = \frac{C_{S0} - C_s}{C_s} * 100 \quad \textbf{Eqn.1}$$

3.1.5.2. Hydrodeoxygenation (HDO) percentage (oxygen removal)

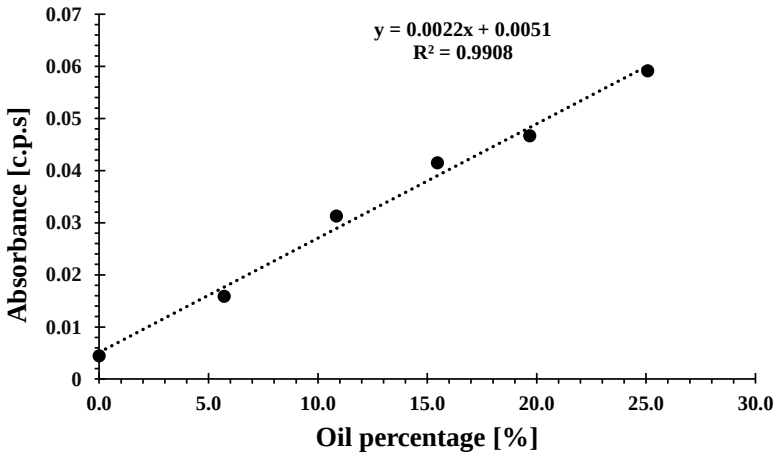

Fig. 5. Determination curve for vegetable oil composition at ~1750 cm^{-1} FTIR band.

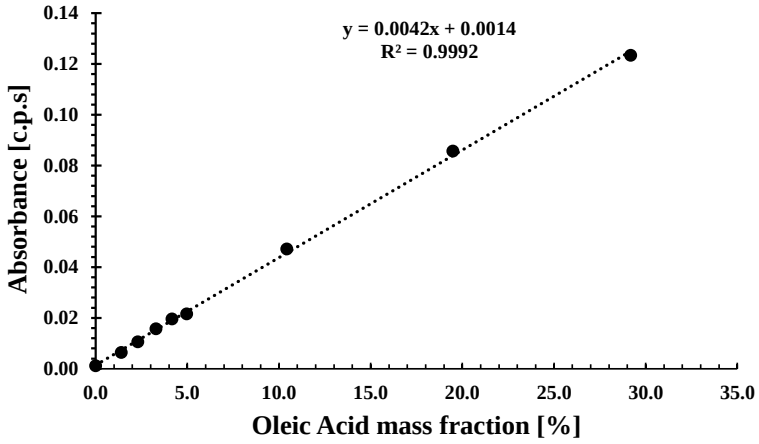

Fig. 6. Determination curve for free fatty acids composition at ~1750 cm^{-1} FTIR band.

To quantify the oxygen removal by hydro-coprocessing the feedstock with the Ni-W/Al(x)-SBA-15 catalysts, two determination curves were done using FTIR absorbances. The first curve (**Fig. 5**, R^2=0.9908) corresponded to *Jatropha curcas* L. percentage vs FTIR absorbance at ~1750 cm^{-1}, preparing samples with 0, 5.7, 10.8, 15.5, 19.7, and 25.1 wt.% of vegetable oil and the GOM. The **Fig. 6**, R^2=0.9992) corresponded to Oleic Acid *vs* FTIR absorbance at ~1710 cm^{-1}. Oleic acid (technical grade, 90%, Aldrich) was used to prepare samples with 0, 1.4, 3.3, 4.2, 5.0, 10.4, 19.5, 29.2 wt.% of oleic acid and the GOM. Hence, vegetable oil and carboxylic acids compositions were calculated, and then computing their oxygen content (%). HDO activity was expressed as the relative deviation percentage between of initial oxygen content in the GOM and the final oxygen content in the liquid product.

3.1.5.3. ASTM D2887 boiling point distributions and fraction compositions

Simulated Distillation was carried out according to the ASTM D2887 procedure in a GC-2010 Shimadzu equipment, which was set up for such purposes. Distillation curve data was analyzed in ASPEN HYSYS V9 to determine the composition of each fraction as follows: Naphtha (80 °C-180 °C), Kerosene (180 °C-240 °C), Light Diesel (240 °C-290 °C), Heavy Diesel (290 °C-340°C), Gas Oil (340 °C-370 °C), and Residue (>370 °C) Diesel-like fraction composition was computed by adding Light Diesel and Heavy Diesel compositions, respectively.

3.2. RESULTS AND DISCUSSION

3.2.1. Characterization of catalytic supports and catalysts

3.2.1.1. Effect of the synthesis conditions in the textural properties of the materials

To get ~10 g of each Al/Si molar ratio sample, at least two synthesis of each Al(x)-SBA-15 material was carried out. In **Table 1** it is reported the change in textural properties for all synthesized materials ratio as follows:

Table 1. Textural Properties for SBA-15 and Al(x)-SBA-15 synthesized materials

Sample	S_{BET} [m^2/g]	PV [cm^3/g]	PD [nm]
Al(0.0)-SBA-15-1	849.2	1.3	6.1
Al(0.0)-SBA-15-2	728.4	1.2	6.8
Al(0.0)-SBA-15-3	825.7	1.4	6.9
Al(0.0)-SBA-15-4	732.3	1.3	7.2
Al(0.0)-SBA-15-5	505.7	1.2	9.4
Al(0.1)-SBA-15-1	725.6	1.1	6.1
Al(0.1)-SBA-15-2	750.9	1.2	6.6
Al(0.1)-SBA-15-3	725.2	1.3	7.3
Al(0.05)-SBA-15-1	733.8	1.2	6.7
Al(0.05)-SBA-15-2	745.3	1.4	7.4
Al(0.033)-SBA-15-2	690.6	1.2	7.2
Al(0.033)-SBA-15-1	742.2	1.2	6.5
Al(0.025)-SBA-15-1	754.9	1.2	6.3
Al(0.025)-SBA-15-2	761.9	1.3	7.0
Al(0.025)-SBA-15-3	873.5	1.3	5.9

According to **Table 1**, at same Al/Si molar ratio materials exhibited similar textural properties (S_{BET}, PV and PD), indicating a good reproducibility of the synthesis. Specific surface area (S_{BET}), pore volume (PV) and pore diameter (PV) average changes was ~10.5%, ~8.8%, and ~10.8%, respectively.

Therefore, it cannot be stated that Al direct incorporation leaded to significant changes in mesoporosity of the SBA-15 based synthesized materials.

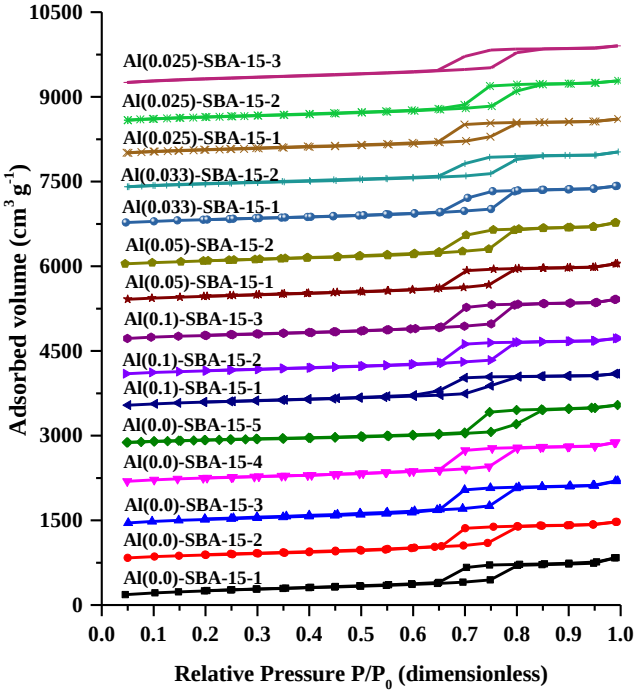

Fig. 7. Nitrogen @77 K physisorption isotherms for SBA-15, Al(x)-SBA-15-*n*, *x*: Al/Si molar ratio; *n*: synthesis number.

According to **Fig. 7**, all synthesized catalytic supports and catalysts exhibited a type IV isotherm and an H1 hysteresis loop. Type IV isotherm characterizes mesoporous materials and H1 hysteresis loop indicates tubular, uniform, and open (both sides) pores. The latter feature was evidenced for all samples. Nevertheless, a slight deformation of hysteresis loop at higher relative pressures (within 0.64 and 0.8) for Al(0.05)-SBA-15-2, Al(0.033)-SBA-15-2, and Al(0.025)-SBA-15-2 was evidenced. This deformation indicates a possible change in the uniformity of tubular pores in the material. Nevertheless, in general, all samples with the same Al/Si molar ratio showed similar isotherms among them.

Finally, Al(0.0)-SBA-15-5 and Al(0.025)-SBA-15-3 exhibited pore volumes values out the trend of the same Al/Si molar ratio catalytic supports, 9.4 nm, and 5.9 nm, respectively. For that reason, such materials were discarded for catalysts preparation procedure.

3.2.1.2. Effect of the synthesis conditions in materials crystallinity and mesoporosity

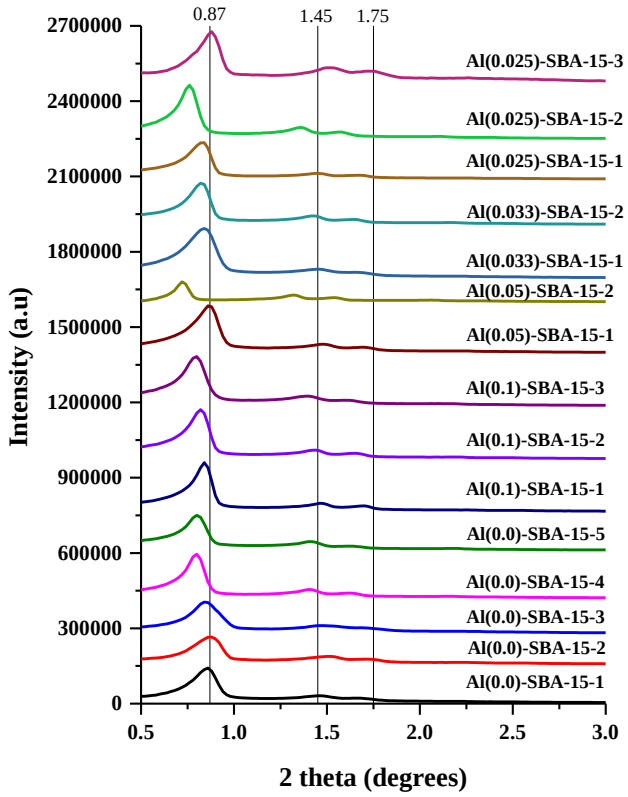

Fig. 8. Low Angle X-ray diffraction profiles for SBA-15, and Al(x)-SBA-15-*n* materials, *x*: Al/Si molar ratio; *n*: synthesis number

According to **Fig. 8**, all SBA-15 based materials with different Al/Si molar ratio exhibited three well defined peaks at 2θ: 0.8°, 1.4°, and 1.7° ascribed to the indexed planes: (100), (110), and (200). Such signals characterize hexagonal symmetry with *p6mm* space group of SBA-15. Hence, the direct synthesis of Al(x)-SBA-15 did not affect the mesoporous structure of the silica base material (SBA-15). In addition, among samples with the same Al/Si molar ratio no significative differences were observed, except the slight leftwards movement of the three characteristics peaks with a reduction in intensity of the signal. Such differences can be explained by the nature of each sample and the conditions pertaining to its measurement. In addition, **Table 2** reports the estimated wall thickness values for all synthesized materials. Planar distances for the plane (100) were computed by Bragg's law and the red parameter (a_0) was calculated by multiplying d_{100} for $2\sqrt{3}/3$. According to the data reported, higher values of a_0 indicates a leftwards displacement of the signal ascribed to plane 100 as observed for Al(0.05)-SBA-15-2, Al(0.033)-SBA-15-2, Al(0.025)-SBA-15-2. This trend could be associated with the partial and slight deformation of hysteresis loop shown in **Fig. 7**. Finally, Al(0.0)-

SBA-15-5, and Al(0.025)-SBA-15-3 depicted wall thickness values lower than their same Al/Si molar ratio counterparts. The latter, supporting the decision of discarding such materials for catalysts preparation as previously commented in **Section 3.2.1.1.**

Table 2. Wall thickness estimation for Al(x)-SBA-15 type synthesized materials.

Sample	2θ [°]	2θ [rad]	d100 [nm]	a0 [nm]	PD [nm]	Wthickness[nm]
SBA-15-1	0.86	0.015	10.3	11.9	6.1	5.8
SBA-15-2	0.88	0.015	10.0	11.6	6.8	4.8
SBA-15-3	0.88	0.015	10.0	11.6	6.9	4.7
SBA-15-4	0.8	0.014	11.0	12.7	7.2	5.5
SBA-15-5	0.81	0.014	10.9	12.6	9.4	3.2
Al(0.1)-SBA-15-1	0.84	0.015	10.5	12.1	6.1	6.0
Al(0.1)-SBA-15-2	0.82	0.014	10.8	12.4	6.6	5.8
Al(0.1)-SBA-15-3	0.8	0.014	11.0	12.7	7.3	5.4
Al(0.05)-SBA-15-1	0.86	0.015	10.3	11.9	6.7	5.2
Al(0.05)-SBA-15-2	0.76	0.013	11.6	13.4	7.4	6.0
Al(0.033)-SBA-15-1	0.84	0.015	10.5	12.1	7.2	4.9
Al(0.033)-SBA-15-2	0.82	0.014	10.8	12.4	6.5	5.9
Al(0.025)-SBA-15-1	0.84	0.015	10.5	12.1	6.3	5.8
Al(0.025)-SBA-15-2	0.78	0.014	11.3	13.1	7.0	6.1
Al(0.025)-SBA-15-3	0.88	0.015	10.0	11.6	5.9	5.7

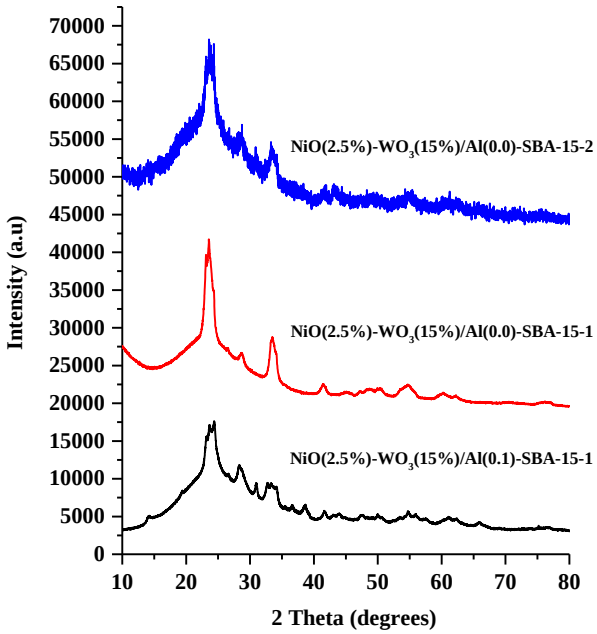

Fig. 9. Wide Angle X-ray diffraction profiles for NiO(2.5%)-WO3(15%)/Al(x)-SBA-15-*n* catalysts, x: Al/Si molar ratio; *n*: synthesis number.

Regarding the formation of metallic phases over the catalysts surface on Al(x)-SBA-15 catalytic supports, **Fig. 9** depicts XRD profiles for three catalysts loaded with NiO(2.5%) and WO_3(15%) supported on: Al(0.0)-SBA-15-1, Al(0.1)-SBA-15-1, and Al(0.0)-SBA-15-2 catalytic supports. The occurrence of partially oxidized W species at 2θ~23.7° for the catalyst supported on Al(0.0)-SBA-15-1 catalysts was evidenced. The latter due to the shortest homogenization time (~1 h) before drying and calcination. For catalysts supported on Al(0.1)-SBA-15-1, and Al(0.0)-SBA-15-2 (homogenization time of 24 h) peaks ascribed to $NiWO_4$ (PDF 00-72-0480 ICDD) were observed at 2θ: 23.7°, 33.6°, 41.6°, 54.7°, and 60.2°. In addition, the occurrence of $NiWO_4$ nanoparticles on catalysts supports was evidenced regardless the incorporation of a flow of dry air of 500 mL min^{-1} for the catalyst supported on Al(0.0)-SBA-15-2. The most intense signal was ascribed to WO_3 component in $NiWO_4$, and **Table 3** shows the average nanoparticle size as computed by Debye-Scherrer's equation (**Eqn.2**). The average nanoparticle size was ~4.7 nm. Therefore, WO_3 nanoparticles on catalysts surface is ~0.7 nm higher than 4 nm, the minimum detection limit of XRD measurements.

$$\boldsymbol{d = \frac{0.91 * \lambda}{b * \cos\theta_m}} \quad \boldsymbol{Eqn.2}$$

In equation 1, λ is the wavelength of Cu K_α radiation in nm (0.1541 nm), *b* is the FWHM (Full Width at High Maximum) at 2θ°, and θ_m is the half of the 2θ° ascribed to the most intense peak in WA-XRD diffraction patterns shown in **Fig. 8**.

Table 3. Average W nanoparticle size for catalysts as computed by Debye-Scherrer equation.

Material	θm (2θ/2) [°]	b [°]	b[rad]	d[nm]
NiO(2.5%)-WO_3(15%)/Al(0.0)-SBA-15-1	11.9826	1.9081	0.0333	4.3
NiO(2.5%)-WO_3(15%)//Al(0.1)-SBA-15-1	11.7907	1.5750	0.0275	5.2
NiO(2.5%)-WO_3(15%)//Al(0.0)-SBA-15-2	11.8454	1.8371	0.0321	4.5

3.2.1.3. Textural Properties of final catalysts and catalytic supports

Previously synthesized materials Al(0.0)-SBA-15-1, Al(0.0)-SBA-15-2, and Al(0.1)-SBA-15-1 materials were used during catalysts preparation, and Al(0.0)-SBA-15-5, and Al(0.025)-SBA-15-3 were discarded, all previously commented in **sections (3.2.1 and 3.2.2)**. Therefore, the remnant same Al/Si molar ratio synthesized materials were mixed to get the final catalytic supports for catalysts preparation. The catalysts were labeled NiO(2.5%)-WO_3(15%)/Al(x)-SBA-15 mix1, where x is the Al/Si molar ratio. To elucidate Al effect on hydro-coprocessing reactions, Al(0.0)-SBA-15 catalyst is reported for comparison purposes.

According to data reported in **Table 4**, all Al(x)-SBA-15 supports exhibited a pore volume (PV) of 1.2 cm^3g^{-1} (~6.0% of deviation) and a pore diameter (PD) of ~6.6 nm (~2.6% of deviation). Regarding

the specific surface area, S_{BET}, the average deviation in such property is ~5.6%. No linear tendence could be observed for textural properties variations with Al/Si molar ratio. Thus, the differences among such properties could be possibly attributed to inherent errors during measurements, indicating all catalytic supports shown similar properties disregarding the Al content. In addition, **Table 4** also reports the textural properties for Ni-W oxide phase catalysts (2.5 wt.% NiO, and 15 wt.% WO_3) supported on Al(x)-SBA-15 mix1 materials. Average deviations in PV and PD were ~3.6% and 2.1% respectively, while S_{BET} average deviation was ~1.5%. However, it could be observed that S_{BET} decreased at expenses of the decrease of Al/Si molar ratio, indicating that Al influenced changes in the mesoporosity when adding metals (Ni and W) on the Al(x)-SBA-15 mix1 catalytic supports. Such changes were ratified by comparing textural properties among Al(x)-SBA-15 mix1 materials with NiO(2.5%)-WO_3(15%)/Al(x)-SBA-15 mix1 oxide phase catalysts. It was evidenced the reduction of both S_{BET} and PV when adding metals on the catalysts surface or adsorption capacity, and PD remains the same. Accordingly, Ni and W species did not block pores during the synthesis of the oxide phase catalysts.

Table 4. Textural Properties for Al(x)-SBA-15 supports and Ni-W/Al(x)-SBA-15 catalysts; x: Al/Si molar ratio.

Sample	S_{BET} [m^2/g]	PV [cm^3/g]	PD [nm]
Al(0.1)-SBA-15 mix1	766.3	1.3	6.7
Al(0.05)-SBA-15 mix1	750.0	1.3	6.8
Al(0.033)-SBA-15 mix1	748.0	1.2	6.6
Al(0.025)-SBA-15 mix1	803.0	1.3	6.5
Al(0.0)-SBA-15-2	728.4	1.2	6.8
NiO(2.5%)-WO_3(15%)/Al(0.1)-SBA-15 mix1	524.3	0.9	7.0
NiO(2.5%)-WO_3(15%)/Al(0.05)-SBA-15 mix1	514.2	0.9	6.9
NiO(2.5%)-WO_3(15%)/Al(0.033)-SBA-15 mix1	513.6	0.9	6.7
NiO(2.5%)-WO_3(15%)/Al(0.025)-SBA-15 mix1	501.6	0.8	6.6
NiO(2.5%)-WO_3(15%)/Al(0.0)-SBA-15-2	516.1	0.9	6.8

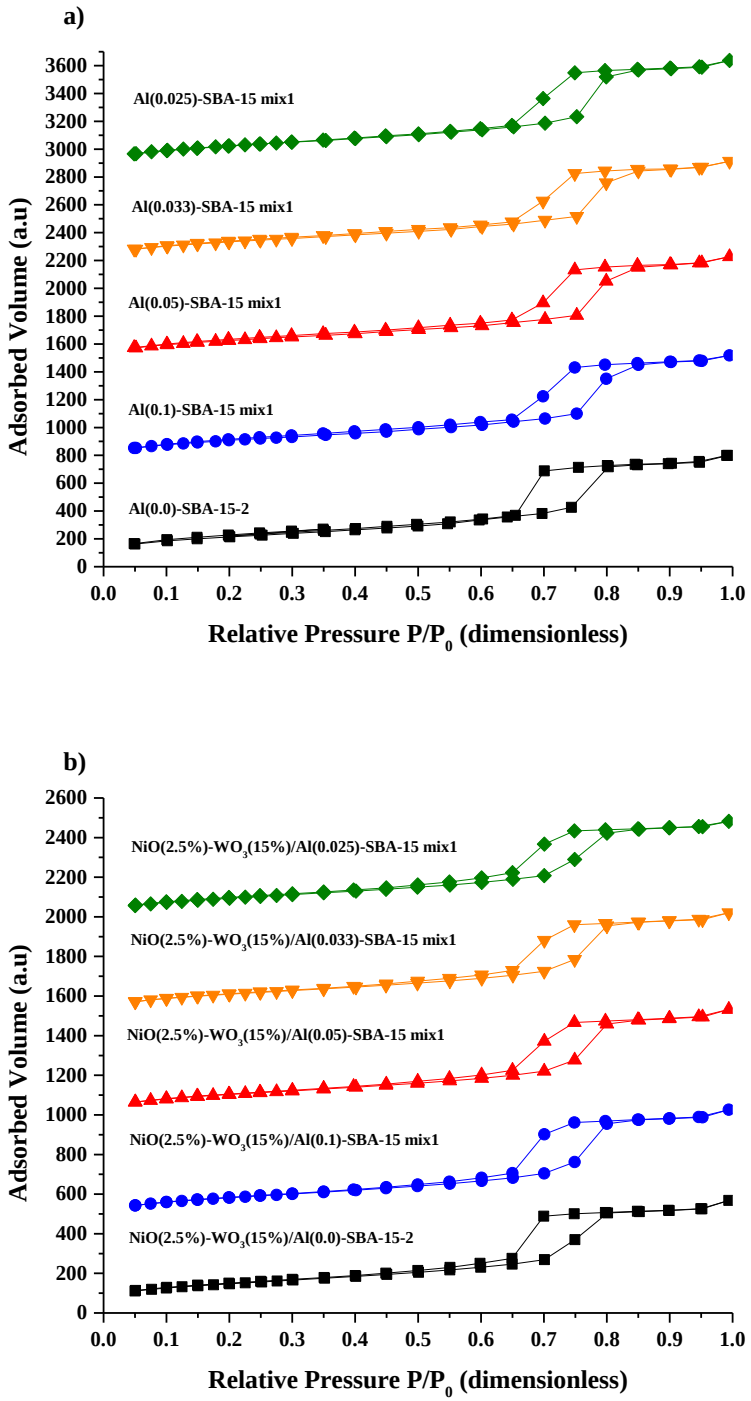

Fig. 10. N_2@-196.15 °C adsorption-desorption isotherms for a) Al(x)-SBA-15 materials b) NiO(2.5%)-WO_3(15%)/Al(x)-SBA-15 oxide phase catalysts; x: Al/Si molar ratio

Fig. 10 a) shows nitrogen physisorption isotherms for all Al(x)-SBA-15 mix1 catalytic supports and SBA-15 reference. All materials exhibited a type IV isotherm with an H1 hysteresis loop. Type IV

isotherm type indicates a mesoporous material, and the kind of hysteresis loop indicates that all materials possess tubular and uniform pores possibly opened both sides. As a result, it can be inferred that Al incorporation did not affect the structure of pores due to the no significant changes in the shape of such loop at relative pressures (P/P_0) between 0.6 and 0.8 were observed.

For NiO(2.5%)-WO_3(15%)/Al(x)-SBA-15 mix1 catalysts, **Fig. 10 b)** shows that all catalysts depicted Type IV isotherm and an H1 hysteresis loop as the pristine Al(x)-SBA-15 mix1 catalytic supports. Nevertheless, in comparison with isotherms presented in **Fig. 10 a)**, those catalysts shown a decrement of the adsorbed volume due to the reduction and partial deformation of the hysteresis loop at relative pressures (P/P_0) between 0.6 and 0.8. Such hysteresis deformation indicates a change in pores shape by Ni and W incorporation on the catalysts surface, and the lowest Al/Si molar ratio catalyst depicted the more reduced hysteresis loop. Therefore, the lowest adsorption capacity as previously stated.

3.2.1.4. Mesoporous structure of Al(x)-SBA-15 mix1 catalytic supports and Ni-W/Al(x)-SBA-15 mix1 catalysts crystallinity

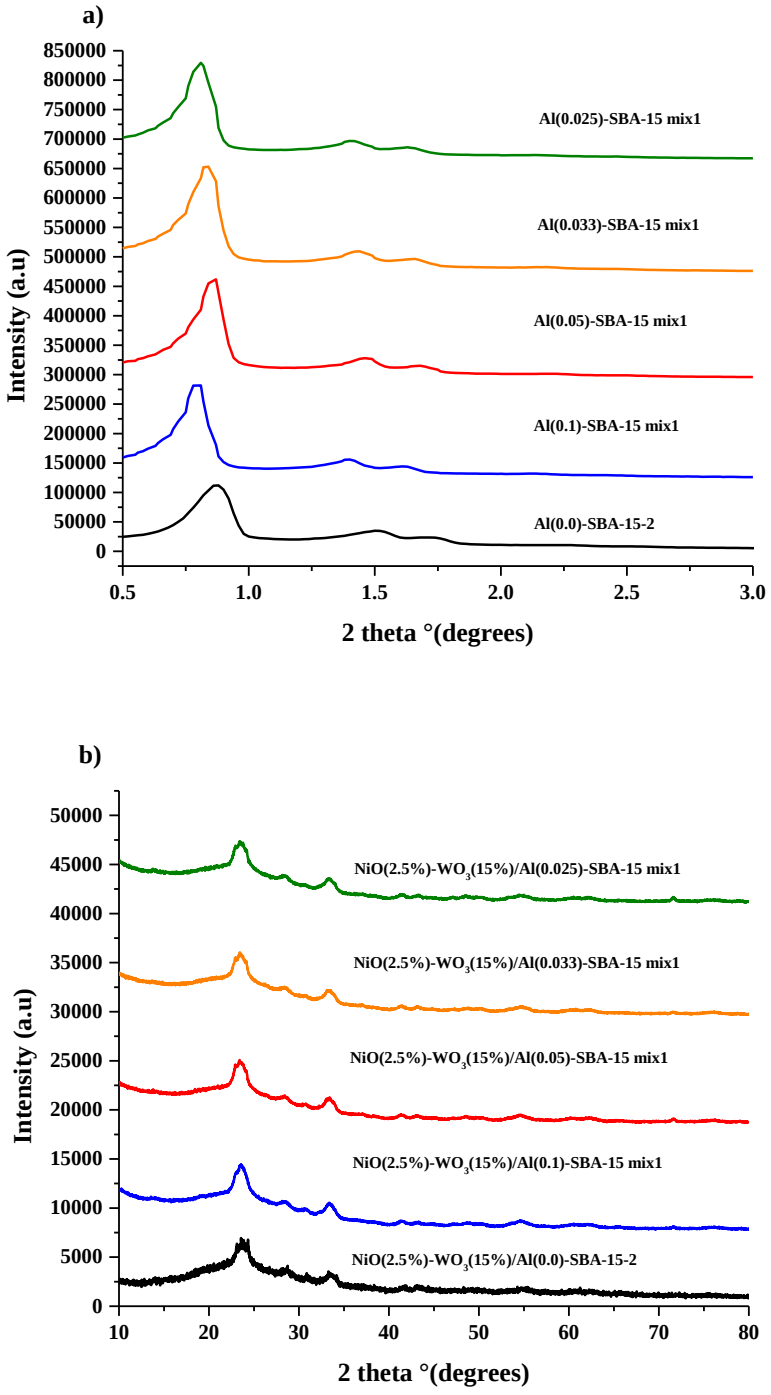

Fig. 11. XRD patterns for a) Al(x)-SBA-15 mix1 materials (LA, low angle), b) NiO(2.5%)-WO3(15%)/Al(x)-SBA-15 oxide phase catalysts (WA, wide angle); x: Al/Si molar ratio.

Fig. 11. a) depicts low angle X-ray diffraction (LA-XRD) profiles for Al(x)-SBA-15, and SBA-15 reference. All materials exhibited three well defined peaks at 2θ: 0.8° 1.4° and 1.7° ascribed to indexed planes (100), (110), and (200), respectively. The occurrence of such peaks indicates that all materials possess a hexagonal symmetry with *p6mm* space group of SBA-15(47). The direct incorporation of Al during the synthesis of Al(x)-SBA-15 mix1 materials did not alter the ordering pattern of SBA-15. Therefore, Al might be incorporated as extra-framework Al or at lower Al/Si molar ratio it might be completely incorporated into silica framework.

Regarding wide angle X-ray diffraction (WA-XRD) in **Fig. 11. b)**, all catalysts samples depicted peaks at 2θ: 23.6°, 33.6°, 41.6°, 54.7°, and 60.2°. Such peaks could be ascribed to $NiWO_4$ (PDF 00-0072-0480 ICDD)(48), indicating the formation of a mixed compound of W and Ni components during catalysts preparation. On the other hand, WO_3 species signals are ascribed at 2θ: 23.1°, 23.6°, and 24.3°. Hence, the acute signal at ~23.6° could be associated to WO_3. No occurrence of signals for NiO at 2θ: 37.4°, 43.4°, and 62.7° were observed(49-51). Hence, the latter ratifies the mixture among Ni and W precursors previously commented. Regarding to Al species, no signal could be observed, suggesting that there were not Ni, W, and Al mixed phases or either those were below the detection limit of XRD, well dispersed and had small particle size. Additionally, WA-XRD profile for NiO(2.5%)-WO_3(15%)/Al(x)-SBA-15 mix1 catalysts and NiO(2.5%)-WO_3(15%)/Al(0.0)-SBA-15-2 (no Al content) were the same. Hence, the formation of any phase related to Al was not clearly evidenced. Finally, $NiAl_2O_4$ signals ascribed at 2θ: 19.3°, 31.5°, 37.2°, 45.2°, 59.9°, and 65.7° were not observed (52).

Table 5. Crystallite size [nm] for WO_3 in NiO(2.5%)-WO_3(18%)/Al(x)-SBA-15 catalysts, x: Al/Si molar ratio.

Catalyst	θm (2θ/2) [°]	b [°]	b[rad]	d[nm]
NiO(2.5%)-WO_3(15%)/Al(0.0)-SBA-15-2	11.8454	1.8371	0.0321	4.5
NiO(2.5%)-WO_3(15%)/Al(0.1)-SBA-15 mix1	11.7489	1.8904	0.0330	4.3
NiO(2.5%)-WO_3(15%)/Al(0.05)-SBA-15 mix1	11.7020	1.8992	0.0331	4.3
NiO(2.5%)-WO_3(15%)/Al(0.033)-SBA-15 mix1	11.6999	1.9031	0.0332	4.3
NiO(2.5%)-WO_3(15%)/Al(0.025)-SBA-15 mix1	11.7155	1.8666	0.0326	4.4

According to the information given in **Table 5**, all catalysts exhibited an average particle size ~4.4 nm. Particle size was computed by **Eqn.2** for the strongest signal at 2θ ~ 23.6° for WO_3 diffraction signal, and *b* is the Full Width at Half Maximum (FWHM) of such peak. It is noteworthy that the minimum particle size that can be observed by XRD is ~4 nm. Therefore, catalysts average particle size was 0.3 nm larger that such a minimum.

3.2.1.5. Porous structure of catalytic supports and catalysts

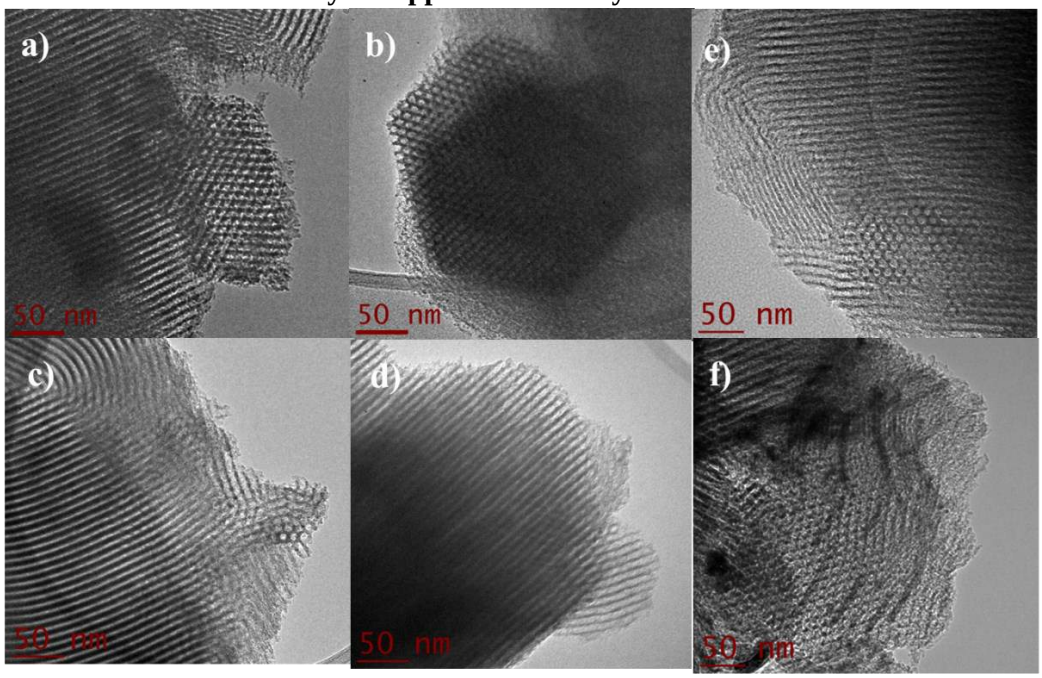

Fig. 12. HR-TEM micrographs for Al(x)-SBA-15 mix1 supports and catalyst, a) Al(0.0)-SBA-15 mix1, b) Al(0.1)-SBA-15 mix1, c)Al(0.05)-SBA-15 mix1, d) Al(0.033)-SBA-15 mix1, e) Al(0.025)-SBA-15 mix1, f) NiO(2.5%)-WO_3(15%)/Al(0.1)-SBA-15 mix1. x: Al/Si molar ratio.

As far as can be observed in **Fig. 12**, Al(x)-SBA-15 mix1 samples clearly exhibited the hexagonal 2D-array of cylindrical pores as LA-XRD diffractograms indicated (**Section 3.2.4**). For all materials tubular uniform channels were observed. Hence, it was confirmed that direct Al incorporation did not influence significant changes in the mesoporous pattern of SBA-15 by the proposed method of synthesis. Accordingly, those results suggests that Al species might be uniformly distributed on silica surface for Al(x)-SBA-15 mix1 catalytic supports. In addition, in **Fig. 12f)** it can be observed that Ni and W nanoparticles were grouped or agglomerated over Al(0.1)-SBA-15 mix1 as it was shown in **Table 5** for the size of WO_3 nanoparticles. The latter indicates that $NiWO_4$ formed was not distributed homogeneously over the catalytic support.

3.2.1.6. Materials Acid Sites Distribution (Brønsted/Lewis) by *Py*-FTIR

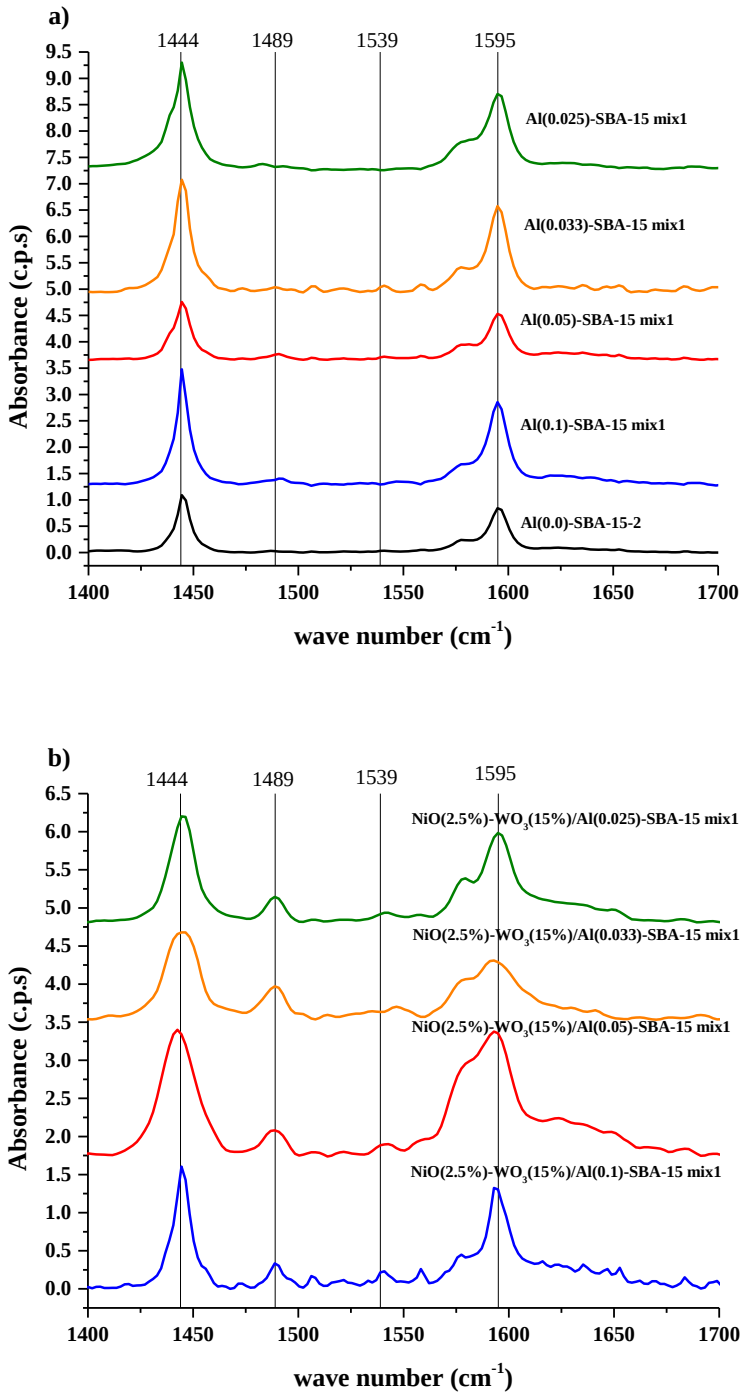

Fig. 13. *py*-FTIR spectra at 50 °C a) Al(x)-SBA-15 mix1 catalytic supports, b) NiO(2.5%)-WO_3(15%)/Al(x)-SBA-15 mix1 oxide phase catalysts. x: Al/Si molar ratio.

Acid sites (Brønsted and Lewis) distribution can be qualitatively analyzed by Py-FTIR spectra. In such spectra, three main bands could be observed. First, about 1444 cm^{-1} ascribed to Lewis (L) acid

sites, second, about 1489 cm^{-1} ascribed to Brønsted and Lewis (B+L) acid sites, and about 1539 cm^{-1} ascribed to Brønsted (B) acid sites. The band about 1598 cm^{-1} corresponds to the vibrational modes of pyridine adsorbed on the materials surface. Accordingly, in **Fig. 13 a),** for catalytic supports, there were not observed intense signals about the occurrence of Brønsted acid sites, instead it was observed that the predominant signal of Lewis acid sites. In general, Lewis and Brønsted acid sites bands increased with *Al* content in comparison with Al(0.0)-SBA-15 mix1 reference. On the other hand, **Fig. 13 b)** for NiO(2.5%)-WO_3(15%)/Al(x)-SBA-15 mix1 oxide phase catalysts, it was observed that there was an increase in intensity of both bands (Brønsted and Lewis), indicating that Ni and W incorporation enhanced the formation of acid sites on the catalysts surface.

Table 6. Brønsted acid sites concentration for NiO(2.5%)-WO_3(18%)/Al(x)-SBA-15 catalysts, x: Al/Si molar ratio.

Material\ T[°C]	Brønsted sites [mmol g^{-1}]				
	50	100	200	300	400
NiO(2.5%)-WO_3(15%)/Al(0.1)-SBA-15 mix1	0.040	0.007	0.005	0.006	0.004
NiO(2.5%)-WO_3(15%)/Al(0.05)-SBA-15 mix1	0.050	0.021	0.010	0.002	0.001
NiO(2.5%)-WO_3(15%)/Al(0.033)-SBA-15 mix1	0.028	0.013	0.002	0.000	0.000
NiO(2.5%)-WO_3(15%)/Al(0.025)-SBA-15 mix1	0.023	0.015	0.007	0.001	0.000

For NiO(2.5%)-WO_3(15%)/Al(x)-SBA-15 mix1 oxide phase catalysts, presented in this work, the amount of pyridine adsorbed (mmol g^{-1}) on Brønsted acid sites is depicted in **Table 6**. At temperatures higher than 50 °C the amount of pyridine adsorbed on Brønsted acid sites (mmol g^{-1}) decreased dramatically (about 98%) for all catalysts. For example, for NiO(2.5%)-WO_3(15%)/Al(0.05)-SBA-15 mix1, Brønsted sites concentration decreased from 0.050 mmol g^{-1}(50 °C) to 0.001 mmol g^{-1}(400 °C). However, NiO(2.5%)-WO_3(15%)/Al(0.05)-SBA-15 mix1 catalyst exhibited the highest concentration of Brønsted acid sites of 0.050 mmol g^{-1} at 50 °C. Regarding the latter, Jaroszewska *et al.,* reported a similar result, 0.057 mmol g^{-1}, for an Pt/Al(0.14)-SBA-15 catalyst at 150 °C (27). Similarly, as Li *et al.*, reported for Al(0.2)-SBA-15, and Ni-W/Al(0.2)-SBA-15 a total Brønsted acid sites concentration of 0.043 mmol g^{-1}, and 0.023 mmol g^{-1} respectively at 200 °C (51).

Table 7. Lewis' acid sites concentration for NiO(2.5%)-WO_3(18%)/Al(x)-SBA-15 catalysts, x: Al/Si molar ratio.

Material\ T[°C]	Lewis sites [mmol g^{-1}]				
	50	100	200	300	400
NiO(2.5%)-WO_3(15%)/Al(0.1)-SBA-15 mix1	0.790	0.190	0.060	0.040	0.020
NiO(2.5%)-WO_3(15%)/Al(0.05)-SBA-15 mix1	1.450	0.180	0.050	0.030	0.030
NiO(2.5%)-WO_3(15%)/Al(0.033)-SBA-15 mix1	0.600	0.140	0.050	0.020	0.010
NiO(2.5%)-WO_3(15%)/Al(0.025)-SBA-15 mix1	0.660	0.170	0.040	0.010	0.000

On the other hand, **Table 7** shows the amount of pyridine adsorbed (mmol g^{-1}) on Lewis acid sites for Ni-W/Al(x)-SBA-15 mix1 oxide phase catalysts. At temperatures higher than 50 °C the amount of pyridine adsorbed on Lewis acid sites (mmol g^{-1}) decreased dramatically (about 97.9%) for all catalysts. For instance, for NiO(2.5%)-WO_3(15%)/Al(0.05)-SBA-15 mix1, Lewis sites concentration decreased from 1.450 mmol g^{-1}(50 °C) to 0.030 mmol g^{-1}(400 °C). In comparison, Jaroszewska *et al.*,, reported a similar result, 0.089 mmol g^{-1} for an Pt/Al(0.14)-SBA-15 catalyst at 150 °C(27). Similarly, Li *et al.*,, reported for Al(0.2)-SBA-15, and Ni-W/Al(0.2)-SBA-15(51) a total Lewis acid sites concentration of 0.209 mmol g-1, and 0.332 mmol g^{-1}, respectively at 200 °C. Hence Ni-W/Al(x)-SBA-15 mix1 catalysts presented in this work showed a higher concentration of Lewis acid sites than Brønsted acid sites and compared to previously reported measurements for similar materials.

Finally, the dramatical decrease in concentration of both kind of acid sites (Brønsted and Lewis) at temperatures higher than 100 °C indicated that the oxide phase catalysts presented in this study possess weak acidity, and for that reason pyridine is readily desorbed.

3.2.1.7. Molecular Structure of Aluminum Species by ^{27}Al-MAS-NMR Measurements

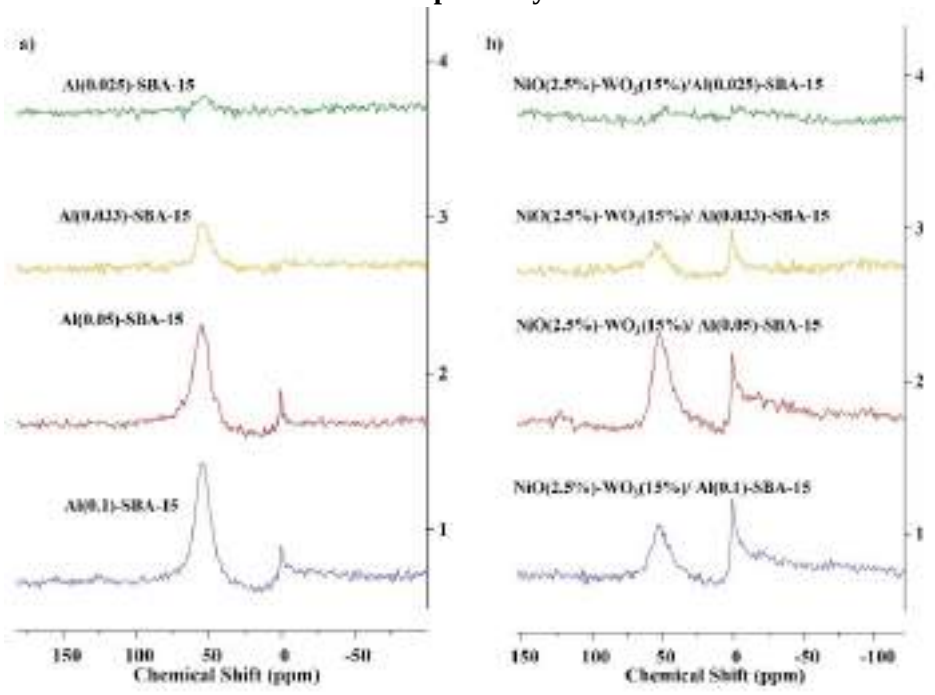

Fig. 14. ^{27}Al-MAS-NMR spectra a) Al(x)-SBA-15 catalytic supports, b) NiO(2.5%)-WO_3(15%)/Al(x)-SBA-15 oxide phase catalysts. x: Al/Si molar ratio.

Nuclear magnetic resonance (NMR) in the solid state provides information regarding chemical structure of specific elements in a material. In this case, ^{27}Al-MAS-NMR spectra for Al(x)-SBA-15

mix1 and NiO(2.5%)-WO_3(15%)/Al(x)-SBA-15 mix1 is shown in **Fig. 14** for *Al* species. Specifically, in **Fig. 14 a)** it could be observed that most of the *Al* added during the synthesis of Al(x)-SBA-15 mix1 catalytic supports was directly incorporated into the Si framework of SBA-15. The latter, due to the occurrence and intensity of the signal at about 53 ppm ascribed to tetrahedral aluminum(53-55). It is noteworthy that, the occurrence of octahedral aluminum species (extra framework *Al*) at a chemical shift about 0 ppm is evidenced for the highest Al/Si molar ratios (0.1 and 0.05). For NiO(2.5%)-WO_3(15%)/Al(x)-SBA-15 mix1 in **Fig. 14 b)**, the occurrence of both kind of *Al* species was also evident. In comparison with Al(x)-SBA-15 mix1 results in **Fig. 12 a)**, the intensity of octahedral *Al* was increased by the addition of *Ni* and *W*, suggesting that *Ni* and *W* interacted with *Al*. However, for the catalyst NiO(2.5%)-WO_3(15%)/Al(0.025)-SBA-15 mix1 the corresponding signals to tetra and octahedral aluminum species were not clearly observed.

3.2.1.8. Chemical functional groups by RAMAN spectroscopy

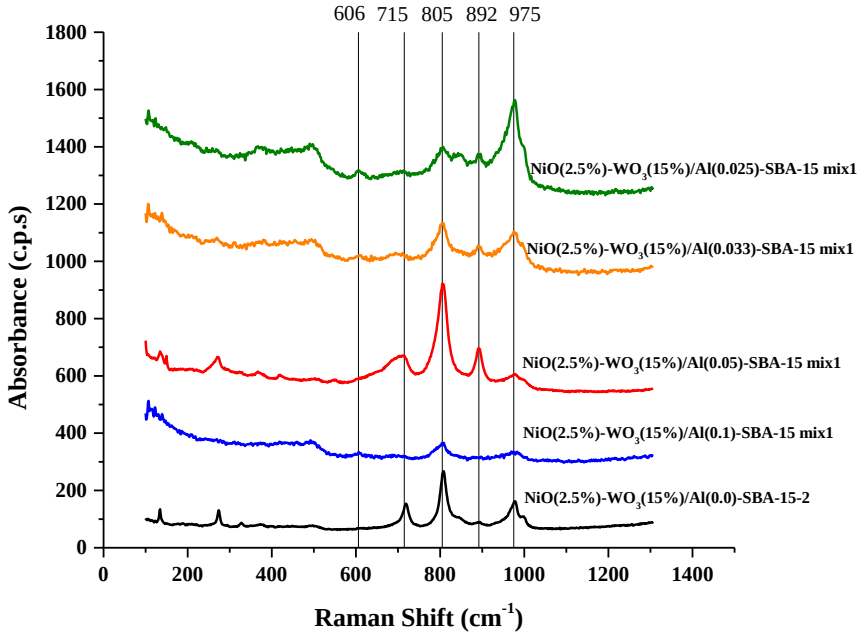

Fig. 15. RAMAN spectra for NiO(2.5%)-WO_3(15%)/Al(x)-SBA-15 oxide phase catalysts. x: Al/Si molar ratio.

According to the spectra presented in **Fig. 15**, the occurrence of different functional groups on the surface for NiO(2.5%)-WO_3(15%)/Al(x)-SBA-15 mix1 catalysts varies in function of Al/Si molar ratio. In common, there were bands at 715 cm^{-1} and 805 cm^{-1}, which are ascribed to WO_3 species in agreement with the WA-XRD profile shown in **Fig. 11 b)** and data reported in **Table 5.** An extra common band was observed at about 970 cm^{-1} for all NiO(2.5%)-WO_3(15%)/Al(x)-SBA-15 mix1 oxide phase catalysts. For NiO(2.5%)-WO_3(15%)/Al(0.025)-SBA-15 mix1 oxide phase catalyst such

signal was the highest. That signal could be associated with the formation to an octahedrally coordinated tungsten compound for $NiWO_4$ (56). Regarding the latter, catalysts with Al/Si molar ratios of 0.05 and 0.033 exhibited a sharper signal at ~892 cm^{-1}, corresponding to $NiWO_4$, specifically to vibrational modes for distorted and octahedral WO_6 clusters as reported by Lima *et al.*(57). Finally, for NiO(2.5%)-WO_3(15%)/Al(0.025)-SBA-15 it was observed a weak signal at 606 cm^{-1} ascribed to $NiAl_2O_4$(58). Nevertheless, the presence of *Ni* and *Al* compounds was not detected by WA-XRD measurements as reported in **Section 3.2.1.4**. On the other hand, the formation of Aluminum Tungstate was discarded since there was no signal about 1054 cm^{-1} for any of the catalysts (56).

3.2.1.9. FTIR spectra of liquid products obtained from the hydro-coprocessing of the vegetable oil and gas oil

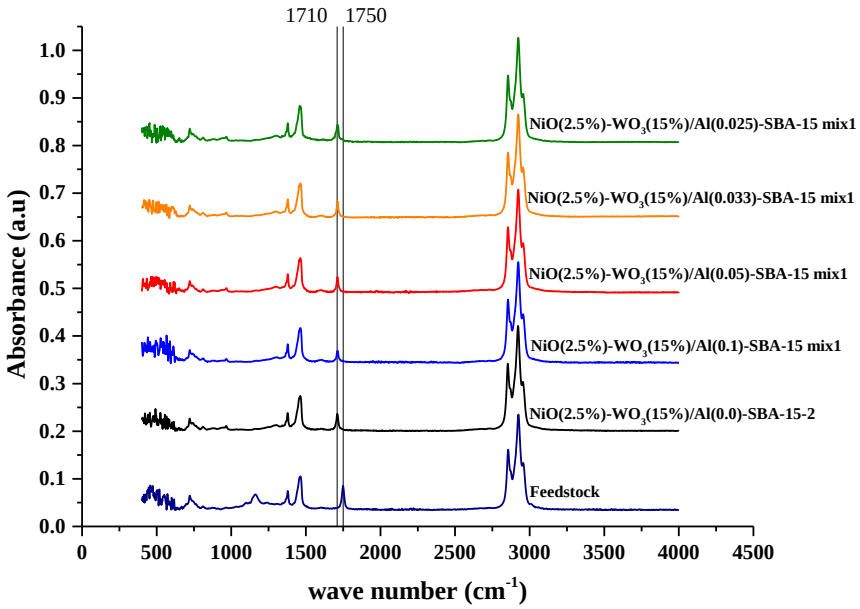

Fig. 16. FTIR spectra for liquid products using NiO(2.5%)-WO_3(15%)/Al(x)-SBA-15 oxide phase catalysts. x: Al/Si molar ratio

According to **Fig. 16**, major changes in FTIR spectra were qualitatively observed by comparing the feedstock spectrum with the liquid products spectra for NiO(2.5%)-WO_3(15%)/Al(x)-SBA-15 mix1 catalysts and the NiO(2.5%)-WO_3(15%)/Al(0.0)-SBA-15-2 catalyst reference. The band at about 1160 cm^{-1}, ascribed to C-O bond disappeared completely, indicating that HDO of vegetable oil occurs via separation of linear hydrocarbons from carboxylic acid chains during HDO from carbon and oxygen simple bond. On the other hand, the band about 1750 cm^{-1}, ascribed to carbonyl group (acyl groups) appeared leftwards to about 1710 cm^{-1}. The latter indicates that there was a change in product distribution and molecules containing the carbonyl group due to hydroprocessing from triglyceride to carboxylic acid(59). Such change was the highest for NiO(2.5%)-WO_3(15%)/Al(0.1)-SBA-15

mix1, which showed the lowest intensity for the ~1710 cm^{-1} FTIR band. However, it is noteworthy that by FTIR analysis it cannot be determined if the reduction of 1710 cm^{-1} band was derived from the decomposition of only one carboxylic acid or a group of compounds with similar carbon and oxygen double bond groups. The latter due to that *Jatropha curcas* L. oil possesses three kinds of fatty acids: oleic, linoleic, and linolenic acids, which exhibits the same characteristic band. Therefore, the band at ~1710 cm^{-1} corresponds to a lump or group for those fatty acids.

3.2.1.10. Qualitative hydrocarbon distribution by ESI mass spectrometry

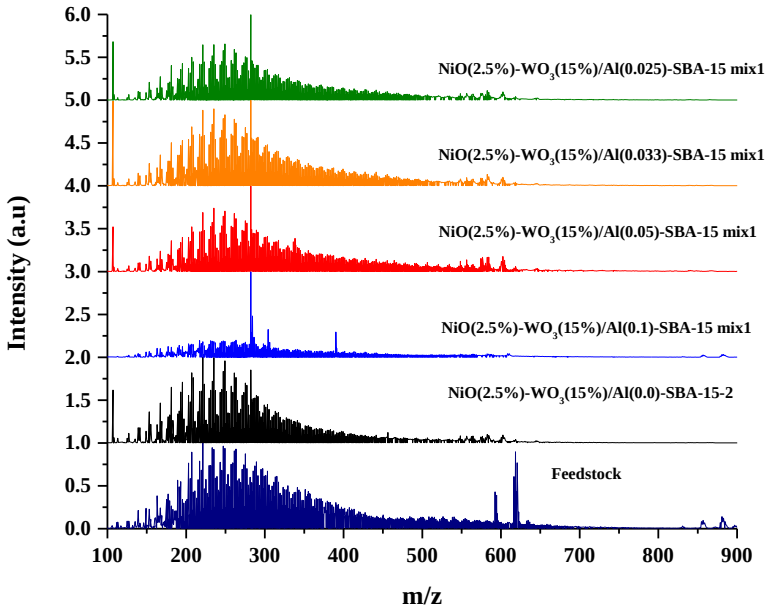

Fig. 17. ESI-MS spectra for the liquid product of NiO(2.5%)-WO_3(15%)/Al(x)-SBA-15 mix1 sulfided phase catalysts and the feedstock. x: Al/Si molar ratio.

In **Fig. 17** are depicted the ESI-MS spectra for all the liquid products during hydroprocessing the mixture of vegetable oil and gas oil. According to the results, all samples exhibited the occurrence of most of the fractions within the m/z range between 200 and 400, such range corresponds to C_{14} to C_{29} hydrocarbons. Nevertheless, the mixture (feedstock) exhibited a intense signal at m/z ~619.16 corresponding to the C_{44} alkane chain, followed by the signal at m/z of ~591.108 for C_{42}, and the occurrence of signals between C_{59} and C_{63} at 829.550 and 885.654, respectively. Hence, the feedstock possessed a major concentration of heavy fractions. On the other hand, when using NiO(2.5%)-WO_3(18%)/Al(x)-SBA-15 sulfided catalysts, lower Al/Si molar ratios resulted in higher occurrence of lighter fractions. Specifically, for Ni-W/Al(0.1)-SBA-15 mix1, it was observed the strongest signal at 282.25 corresponding to C_{18}-C_{20} hydrocarbons, followed by the signals at m/z of 304.23 and 390.28

ascribed to C_{21} and C_{28}, respectively. Even so, the signal ascribed to C_{18}-C_{20} might be possible attributed to some type of free fatty acids presented in *Jatropha Curcas* L. oil into the feedstock. Therefore, depending on the *Al* content (Al/Si molar ratio) hydroprocessing of vegetable oil occurs via formation of free fatty acids, such as oleic acid, which were later hydroconverted in lighter hydrocarbons (C_{14} to C_{29}). The less *Al* on the catalysts the higher concentration of lighter fractions within m/z range between 200 and 400. The more *Al* on the catalysts the highest content of free fatty acids in the product mixture. On the other hand, FTIR results (**Section 3.1.7**) indicated that the highest reduction of carbonyl group at ~1710 cm^{-1} was observed at Al/Si molar ratio of 0.1. Therefore, hydroconversion of acyl groups in triglycerides into fatty acids could be observed. In addition, NiO(2.5%)-WO_3(18%)/Al(0.1)-SBA.15 mix1 sulfided catalyst evidenced a lower occurrence of lighter hydrocarbons fractions.

3.2.1.11. ^{1}H-NMR spectra for liquid products and vegetable oil

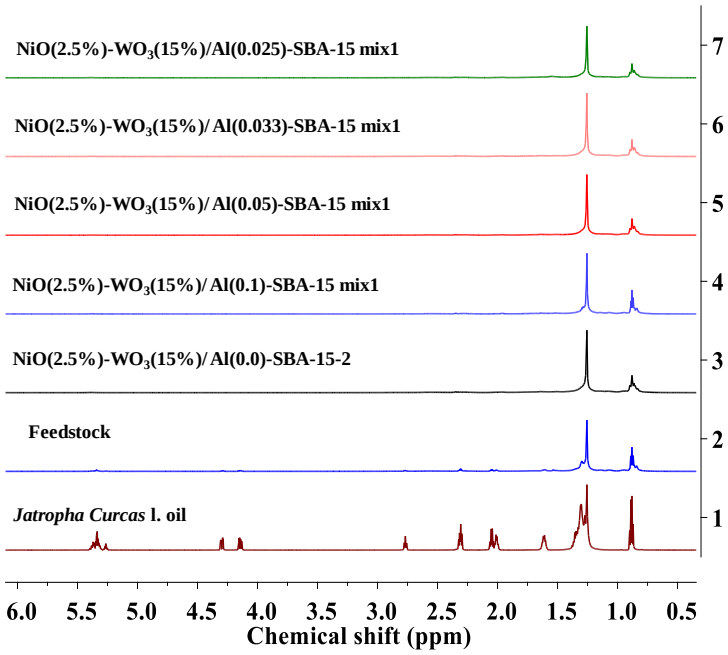

Fig. 18. ^{1}H-NMR spectra for the liquid product of NiO(2.5%)-WO_3(15%)/Al(x)-SBA-15 mix1 sulfided phase catalysts and the feedstock. x: Al/Si molar ratio.

Fig. 18 depicts H-NMR spectra for the liquid products from hydro-coprocessing the mixture of vegetable oil and gas oil. There, it is also presented the spectrum for *Jatropha curcas* L. oil as a reference for comparative purposes. According to the figure, about 9 signals could be clearly observed for pure vegetable oil at 0.89 ppm for fatty acids excluding linolenic acid, 1.31 ppm and 1.61 ppm for acyl chains, 2.04 ppm for mono- and polyunsaturated fatty acids, 2.31 ppm for acyl chains in

unsaturated fatty acids, 2.77 ppm for linoleic and linolenic acid, 4.27 ppm and 5.28 ppm for triacylglycerols, and at 5.35 ppm for mono- and polyunsaturated fatty acid (60, 61). The latter signals could be observed for the feedstock at lower intensity due to the concentration of vegetable oil in such mixture (~20% v/v). However, by comparing with the spectra of liquid products for NiO(2.5%)-WO_3(15%)/Al(x)-SBA-15 mix1 and NiO(2.5%)-WO_3(15%)/Al(0.0)-SBA-15-2 sulfided catalyst, it could be observed only two signals at 1.31 ppm and 0.89 ppm. As a result, hydro-coprocessing the mixture occurred via conversion of fatty acids via HDO of the vegetable oil component to hydrocarbons. The occurrence of the remaining signals indicated that there are fractions of acyl group components unconverted to carboxylic acid. The latter in agreement with FTIR spectra in **Section 3.2.1.9** for the analysis of the band at about 1710 cm^{-1}, which remained disregarding *Al* content. Signals at higher chemical shift of 1.31 ppm were not detectable when using NiO(2.5%)-WO_3(15%)/Al(x)-SBA-15 mix 1 sulfided catalysts. Therefore, mono- and polyunsaturated fatty acid in the vegetable oil were completely hydroconverted.

3.2.2. Catalytic evaluation of NiO(2.5%)-WO_3(15%)/Al(x)-SBA-15 mix1 sulfided catalysts

3.2.2.1. Effect of the Al content in the hydrodesulfurization properties of NiO(2.5%)-WO_3(15%)/Al(x)-SBA-15 sulfided catalysts

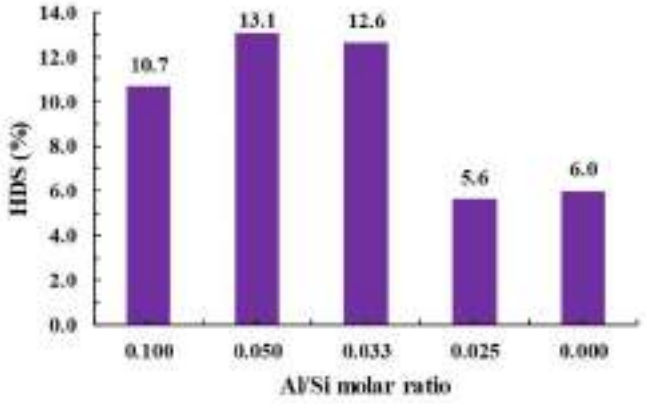

Fig. 19. HDS expressed as sulfur removal percentage for NiO(2.5%)-WO_3(15%)/Al(x)-SBA-15 mix1 oxide phase catalysts. x: Al/Si molar ratio.

Fig. 19 depicts changes in sulfur removal expressed as %HDS as function of Al/Si molar ratio. According to the results, there was not a linear tendency between the %HDS and the *Al* content. It could only be inferred that the sulfided catalyst NiO(2.5%)-WO_3(15%)/Al(0.05)-SBA-15 mix1 demonstrated the highest sulfur removal yield (13.1%), the catalysts NiO(2.5%)-WO_3(15%)/Al(0.025)-SBA-15 mix1, and NiO(2.5%)-WO_3(15%)/Al(0.0)-SBA-15-2 evidenced similar results, 5.6, and 6.0%, respectively. A plausible explanation for such trend could be related

with that *Al* was undetectable by ^{27}Al-MAS-NMR for the catalyst with Al/Si molar ratio of 0.025 as shown in **Fig. 14 b)**. The less *Al* on the catalysts the less HDS activity. Hence, Al influences sulfur removal reactions via HDS at the reaction conditions evaluated. Additionally, it could also be inferred that catalysts acidity influenced sulfur removal. The latter due to that NiO(2.5%)-WO_3(15%)/Al(0.05)-SBA-15 mix1 catalyst displayed the highest occurrence of Brønsted and Lewis acid sites and the highest HDS activity as shown in **Table 6**, and **Fig. 13** respectively.

3.2.2.2. Effect of the Al content in the Hydrodeoxygenation (HDO) properties of Ni-W/Al(x)-SBA-15 mix1 sulfided catalysts

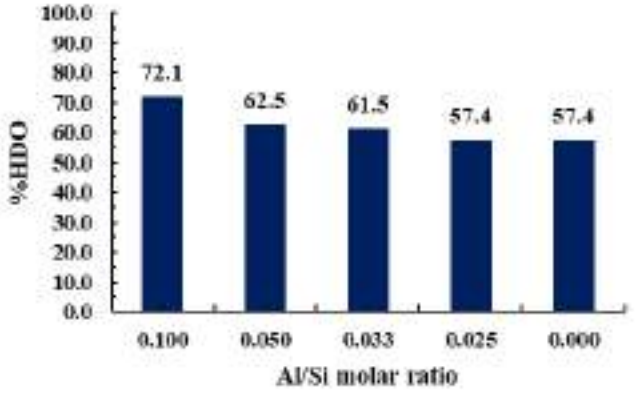

Fig. 20. HDO conversion as the reduction of absorbance at FTIR band of about 1710 cm^{-1} for NiO(2.5%)-WO_3(15%)/Al(x)-SBA-15 mix1 oxide phase catalysts. x: Al/Si molar ratio.

Fig. 20 depicts changes in the conversion of HDO from results of the FTIR absorption band ascribed to carbonyl group for carboxylic acid (about 1710 cm^{-1}) as function of Al/Si molar ratio. %HDO decreased at expenses of Al/Si molar ratio, indicating that a major incorporation of Al promotes the carboxylic acid formation from triglycerides during the hydro-coprocessing the mixture of vegetable oil and gas oil. The highest HDO yield was for NiO(2.5%)-WO_3(15%)/Al(0.1)-SBA-15 mix1 (72.1%), and the lowest for NiO(2.5%)-WO_3(15%)/Al(0.025)-SBA-15 mix1(30.9%). The absence of Al in the catalyst, NiO(2.5%)-WO_3(18%)/Al(0.0)-SBA-15-2, showed a 57.4% of HDO as observed for NiO(2.5%)-WO_3(15%)/Al(0.025)-SBA-15 mix1. However, as previously mentioned. The best yield was attained at the highest Al/Si molar ratio. Hence, aluminum effect in HDO was clearly demonstrated. The previous results agreed to the qualitative FTIR analysis shown in **Section 3.2.1.9**.

By comparing HDO and HDS yields, the HDO prevailed over the HDS at the highest Al/Si molar ratio as shown in the previous section (**Section 3.2.2.1**) where NiO(2.5%)-WO_3(15%)/Al(0.1)-SBA-15 sulfided catalyst did not show the highest HDS activity. In this respect, Sépulveda *et al.*,(62) demonstrated that during the co-processing of guaiacol and 4,6-DMDBT with sulfided ReS_2/SiO_2 and ReS_2/Al_2O_3 catalysts, guaiacol inhibited HDS rate and catalysts acidity influenced HDO. They also

highlighted that water formation as byproduct during the HDO also might decrease HDS activity. Water formation could promote the occurrence of oxy-sulfides and oxides over the catalysts surface. It was stated by Infantes-Molina *et al.*(63), during HDO of phenol the oxidation/hydroxylation of ruthenium sulfide (RuS_2) phase occurred forming a ruthenium oxy-sulfided and ruthenium oxide. The latter according to XPS measurements for the spent catalysts supported on SBA-15 and modified with Ir or Pd, RuS_2/SBA-15. On the other hand, Şenol *et al.*,(64) studied H_2S effect during the HDO of aromatic and aliphatic oxygenates. HDO conversion for phenol decreasing at expenses of increasing H_2S content. On the contrary, increasing hydrogen sulfide content during HDO of methyl heptanoate enhanced HDO conversion. As a result, one can infer that hydrogen sulfide formation during HDS improves HDO reactions when hydro-coprocessing sulfur and oxygenated compounds.

For our NiO(2.5%)-WO_3(15%)/Al(0.1)-SBA-15 mix1 sulfided catalyst, a higher HDO could lead to a higher production of water, reducing the occurrence of sulfided active sites via formation of Ni and W oxy-sulfides and oxides. In this respect, a gas phase H_2/H_2S blend is required to reactivate the catalysts, restoring the fully sulfided coordinated metal sulfide. Hence, hydrogen sulfide formation during HDS enhanced HDO by regenerating the active sites used during HDO. Additionally, there might be a competition among oxygenated and sulfur compounds on reacting over the surface of the catalysts as the above mentioned authors have reported before by mean of experiments with sulfur and oxygenated model compounds(63, 64). Therefore, the catalytic activity observed on simultaneous HDO-HDS with NiO(2.5%)-WO_3(15%)/Al(x)-SBA-15 mix1 sulfided catalysts may be governed by the catalyst's regeneration step in the catalytic cycle, specifically, after oxygen removal.

According to the latter, it is not always possible to attain a catalyst with the best yielding for HDO and HDS simultaneously when hydro-coprocessing a mixture of vegetable oil and gas oil. Intrinsic properties of the catalyst like acidity and metallic character influences the catalytic activity. As a result, tailoring such properties will depend on the final purpose of the catalyst. In this research our purpose is obtaining a catalyst yielding a diesel-like fraction with the less sulfur content as possible.

3.2.2.3. Effect of the Al content in the Hydrocracking (HCK) properties of Ni-W/Al(x)-SBA-15 sulfided catalysts

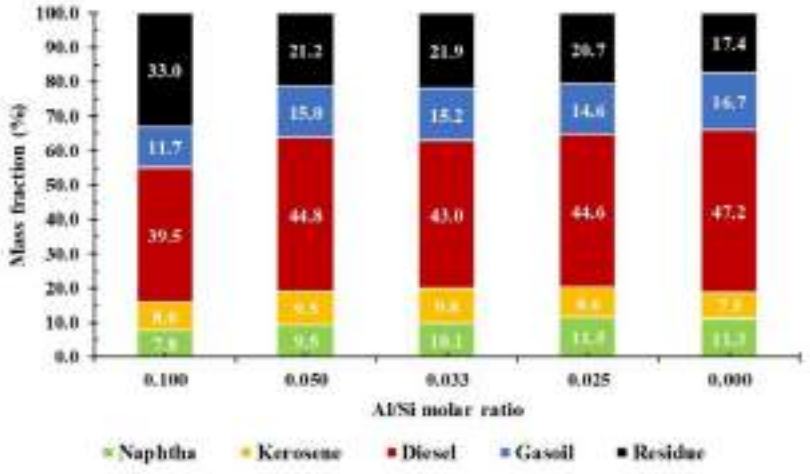

Fig. 21. Lumps mass fraction percentage distribution for NiO(2.5%)-WO_3(15%)/Al(x)-SBA-15 mix1 oxide phase catalysts. x: Al/Si molar ratio.

ASTM D2887 simulated distillation curves were processed in ASPEN HYSYS V9 to compute the corresponding mass fractions for five fractions: Naphtha, Kerosene, Diesel, Gasoil, and Residue. According to the results shown in **Fig. 21**, the highest content of *Al* evidenced the lowest diesel-like fraction percentage (39.5%) for NiO(2.5%)-WO_3(15%)/Al(0.1)-SBA-15 mix1 catalyst, and the catalyst with Al/Si molar ratio of 0.0 showed the highest yield (47.2%). However, Ni-W/Al(0.05)-SBA-15 mix1 showed a 44.8% diesel-like fraction percentage, which is 2.4% units lesser than NiO(2.5%)-WO_3(15%)/Al(0.0)-SBA-15-2. The same tendency was observed for the other NiO(2.5%)-WO_3(18%)/Al(x)-SBA-15 mix1 sulfided catalysts. Accordingly, it could not be concluded that Al content did not influence HCK reactions, instead it was clear that Al/Si molar ratio of 0.05 promoted the highest yield to a diesel-like fraction when hydro-coprocessing the mixture of vegetable oil and gas oil. Similar trends could be observed for the other fractions. Specifically, residue mass fraction was reduced from 33% to 20.3% by hydro-coprocessing the feedstock with Ni-W/Al(x)-SBA-15 mix1 sulfided catalysts with Al/Si molar ratio higher than 0.1. One way to explain the latter results relies on the fact that at higher *Al* content the catalysts exhibited the occurrence of grouped metallic phases with ~4.4 nm of WO_3 crystallite size over the catalyst surface as shown in TEM micrograph in **Fig. 12 f)** and **Table 5**, respectively**.** Catalytic activity depends strongly on the way the active phases distribute on the catalysts surface, and it was shown in **Fig. 15** for RAMAN spectra, that aluminum incorporation influenced chemical structure of the catalysts. As a result, an improvement in hydrotreating reactions (HDS and HDO) when aluminum was added to the synthesis of the catalytic support was observed. Accordingly, aluminum addition favored the heteroatoms removal instead of hydrocracking at the reaction conditions employed as previously commented in

sections **3.2.2.1** and **3.2.2.3**. In addition, it has been also reported that for $NiWO_4$ sulfided catalysts there is an enhancement in HDS activity due to the formation of a single layer of a sulfided phase over the catalysts surface as detected by temperature programmed sulfidation (48). Hence, *Al* incorporation seemed to influence the formation of a single $NiWO_4$ sulfided phase due to that RAMAN spectra for NiO(2.5%)-WO_3(15%)/Al(x)-SBA-15 catalysts showed decreased intensity for the signal at ~970 cm^{-1} for higher Al/Si molar ratios, thus promoting hydrotreating reactions. On the other hand, the occurrence of an acute signal at 2θ of 23.6° for WO_3 (**Fig. 11** for WA-XRD) suggests the formation of the type II active phase (multi-layer) ascribed to the corresponding sulfide, which can be ratified by the acute signal at ~805 cm^{-1} in the RAMAN spectra at higher Al/Si molar ratios. Acute RAMAN signals suggest less dispersed active phases while wider signals more dispersed active phases. However, type II active phase enhanced HDS and hydrogenation (HG) activity of dibenzothiophene (DBT) in comparison to type I active phase (single layer) using Ni-Mo and Co-Mo sulfided catalysts supported on γ-Al_2O_3 as reported by Kagami *et al.* (65). For that reason, the catalytic activity is not necessarily governed by active phase dispersion on the catalyst surface, rather by the type of active phase site. In our case, as shown in **Fig. 14** for ^{27}Al-MAS-NMR spectra, Aluminum interacted with metals increasing octahedral coordination at expenses of decreasing the tetrahedral. Consequently, the interaction among metals and the Al_2O_3 formed during the synthesis of Al(x)-SBA-15 supports gave birth to the already mentioned type II and type I active phases sites on the sulfided catalysts.

Finally, as evidenced in **Fig. 21**, WO_3 and $NiWO_4$ as oxide precursors for a sulfided active phase improved hydrocracking reactions as demonstrated by the formation of higher contents of diesel, naphtha, and kerosene fractions with the no Al sulfided catalyst, NiO(2.5%)-WO_3(15%)/Al(0.0)-SBA-15-2.

3.3. Conclusions

Hydro-coprocessing a mixture of *Jatropha curcas* L. oil and gas oil blend was evaluated employing a series of unconventional NiO(2.5%)-WO_3(15%)/Al(x)-SBA-15 mix1 sulfided catalysts. Al effect in hydroprocessing relied on promoting heteroatoms (S and O) removal instead of hydrocracking reactions as was demonstrated by testing NiO(2.5%)-WO_3(15%)/Al(0.0)-SBA-15-2 sulfided catalyst (no Al). In addition, that sulfided catalyst enhanced the highest diesel-like fraction yield of about 47.2% compared to 44.8% for NiO(2.5%)-WO_3(15%)/Al(0.05)-SBA-15 mix1 sulfided catalyst as a direct effect of $NiWO_4$ as active phase. However, NiO(2.5%)-WO_3(15%)/Al(x)-SBA-15 mix1 sulfided catalysts could remove about 1267 ppm of sulfur in the feedstock and about 57.3% of acyl groups in vegetable oil. Therefore, these catalysts are promising candidates for getting cleaner (less

S), greener and lighter hydrocarbons blend via hydroprocessing of vegetable oil and gas oil blends. Finally, Al direct incorporation during the synthesis of SBA-15 did not collapse the mesostructured ordering pattern of SBA-15 maintaining textural properties, generating acidity, and promoting hydroprocessing reactions on the catalysts surface.

4. EFFECT OF THE NiO AND WO_3 COMPOSITION IN THE HYDRO-COPROCESSING OF A MIXTURE OF GAS OIL AND VEGETABLE OIL WITH A NiO(y)- WO_3(z)/Al(0.05)-SBA-15 SULFIDED CATALYST

This chapter discusses the effect of textural properties and metallic oxides (NiO and WO_3) load for Ni-W sulfided catalysts supported in an Al(0.05)-SBA-15 material during the hydro-coprocessing of a mixture of gas oil and *Jatropha curcas L.* oil. The Al(0.05)-SBA-15 was selected due to the highest Brønsted acid sites concentration (0.053 mmol g^{-1}) and HDS yield (13.1%) in previous experiments shown in **Chapter 3**, **sections 3.2.1.6** and **3.2.2.1**, respectively. Accordingly, this chapter describes the experimental procedure for synthesizing and evaluating NiO(y)-WO_3(z)/Al(0.05)-SBA-15 sulfided catalysts, where *y* is the composition of NiO, and *z* is the composition of WO_3. The composition of metallic oxides varies at 3.5 wt.%, 4.5 wt.%, and 5.5 wt.% for NiO and 18 wt.%, 20 wt.% , and 25 wt.% for WO_3. Thus, the effect of metallic loading on hydrodesulfurization (HDS) and hydrodeoxygenation (HDO) when hydroprocessing the mixture is elucidated.

4.1. EXPERIMENTAL

4.1.1. Synthesis of Al(0.05)-SBA-15 catalytic support

Al(0.05)-SBA-15 was synthesized three times following the procedure reported in section **3.1.1**. The synthesized materials were labeled as Al(0.05)-SBA-15-*n*, where *n* is the number of the synthesis following the numbering given to the same material in **Chapter 3.**

4.1.2. Catalyst preparation

NiO(*y*)-WO_3(*z*)/Al(0.05)-SBA-15 oxide phase catalysts were prepared following the same procedures reported in Chapter 3, section **3.1.2**, *y* and *z* are the weight percentages of NiO and WO_3, respectively.

4.1.3. Characterization

Catalytic supports and catalysts were characterized by: N_2 physisorption at -196.15 °C, LA-XRD (low angle X-ray diffraction), WA-XRD (wide angle X-ray diffraction), ^{27}Al-MAS-NMR, and RAMAN spectroscopy, as described in **sections 3.1.3.1**, **3.1.3.2**, **3.1.3.5**, and **3.1.3.6**, respectively. Liquid products of catalytic evaluation were characterized by: FTIR, and ^{1}H-NMR as described in sections **3.1.3.7** and **3.1.3.9,** respectively.

4.1.4. Catalytic Evaluation

Previously sulfided NiO(y)-WO_3(z)/Al(0.05)-SBA-15 catalysts were tested in the hydro-coprocessing of the mixture vegetable oil (*Jatropha curcas* L. oil) and gas oil following the sulfidation and reaction procedures as reported in **Section 3.1.4**.

4.1.5. Catalytic Activity

Hydro-coprocessing reactions were analyzed in terms of sulfur removal (%HDS), oxygen removal (%HDO), and diesel-like fraction yield for HCK. Procedures and expression of results were calculated as reported in **Section 3.1.5**.

4.2. RESULTS AND DISCUSSION

4.2.1. Characterization of catalytic supports and catalysts

4.2.1.1. Mesoporous structure and crystallinity of Al(0.05)-SBA-15 materials and NiO(y)-WO_3(z)/Al(0.05)-SBA-15 oxide phase catalysts

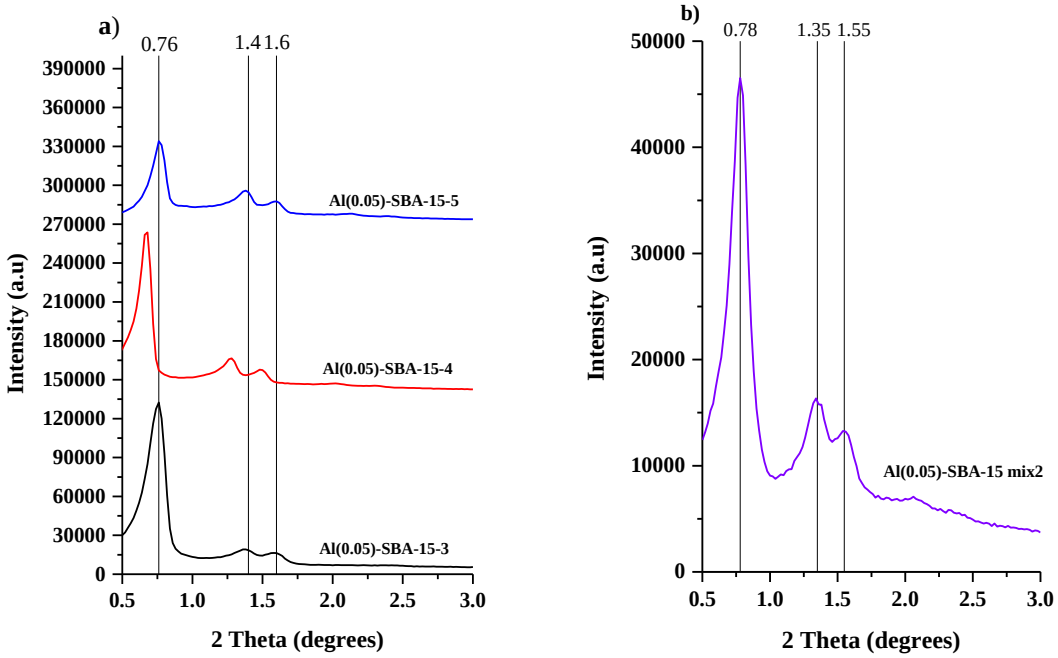

Fig. 22. Low Angle X-ray diffraction profiles for : a) Al(0.05)-SBA-15-n materials, b) Al(0.05)-SBA-15 mix2, n: synthesis number.

According to the **Fig. 22 a)** the three synthesis of Al(0.05)-SBA-15 catalytic support evidenced three clear signals at 2θ: 0.8°, 1.4° and 1.6° ascribed to the indexed planes (100), (110), and (200) respectively. Such planes characterize the hexagonal symmetry with *p6mm* space group. Differences in signal intensity and 2θ displacement were observed, indicating that it is not possible attaining the same Al(0.05)-SBA-15 material. Nevertheless, signals occurrence ratifies the mesostructured pattern. Therefore, Al(0.05)-SBA-15-3, Al(0.05)-SBA-15-4 and Al(0.05)-SBA-15-5 materials were mechanically mixed with the Al(0.05)-SBA-15 mix1 remnant used in catalyst preparation in **Chapter 3**. In **Fig.22 b)** it is depicted the LA-XRD profile for the final mixture of Al(0.05)-SBA-15 mix2

material. The final mixture retains the mesostructured pattern by exhibiting the same signals at same 2θ° as previously commented.

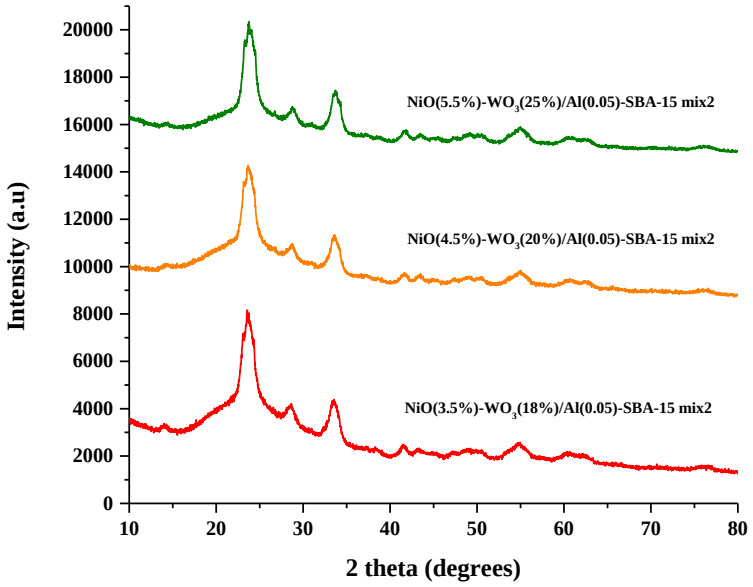

Fig. 23. Wide Angle X-ray diffraction profiles for NiO(y)-WO_3(z)/ Al(0.05)-SBA-15 mix2 oxide phase catalysts. y: NiO weight percentage, z: WO_3 weight percentage.

On the other hand, **Fig. 23** shows the WA-XRD profiles for the three NiO(y)-WO_3(z)/Al(0.05)-SBA-15 mix 2 catalysts. As far as can be observed, all catalysts exhibited signals at 2θ° at 23.7°, 29.1°, 33.7°, 41.8°, and 54.7°, indicating the occurrence of $NiWO_4$ as previously reported in **Section 3.2.1.4.** The most intense signals at 2θ° of 23.7° and 33.9° corresponds to tetragonal WO_3. The crystallite particle size for WO_3 was computed by Debye-Scherrer's equation and reported in **Table 8.** According to the latter, depending on the WO_3 load the particle size increased. The more tungsten is incorporated the bigger nanoparticle size. The average WO_3 crystallite size was 5.1 nm.

Table 8. Crystallite size [nm] for WO_3(y) in NiO(y)-WO_3(z)/Al(0.05)-SBA-15 catalysts. y: NiO weight percentage, z: WO_3 weight percentage.

Material	θm(2θ/2) [°]	b [°]	b[rad]	d[nm]
NiO(3.5%)-WO_3(18%)/Al(0.05)-SBA-15 mix2	11.8322	1.7012	0.0297	4.8
NiO(4.5%)-WO3(20%)/Al(0.05)-SBA-15 mix2	11.8655	1.6351	0.0285	5.0
NiO(5.5%)-WO3(25%)/Al(0.05)-SBA-15 mix2	11.9137	1.5400	0.0269	5.3

4.2.1.2. Textural properties of NiO(y)-WO_3(z)/Al(0.05)-SBA-15 mix2 oxide phase catalysts

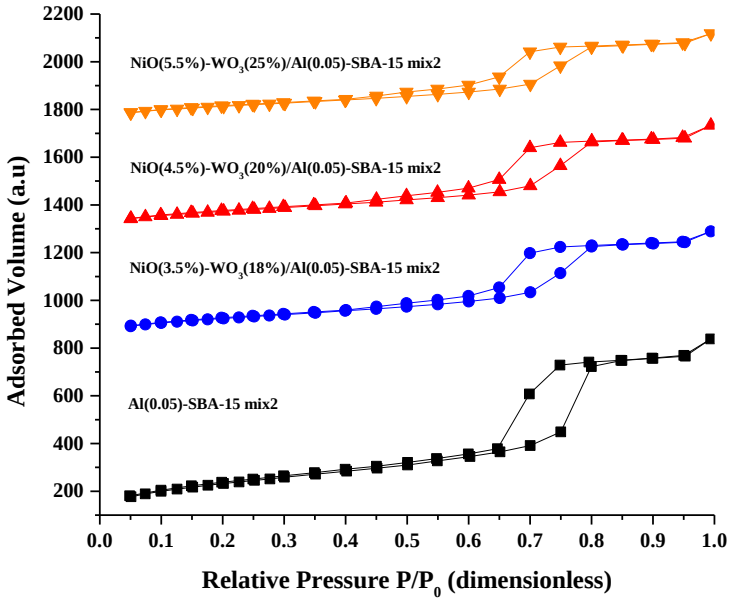

Fig. 24. N_2@-196.15 °C adsorption-desorption isotherms NiO(y)-WO_3(z)/Al(0.05)-SBA-15 mix2 and Al(0.05)-SBA-15 mix2 catalytic support. Y: NiO weight percentage, z: WO_3 weight percentage.

NiO(y)-WO_3(z)/Al(0.05)-SBA-15 mix2 oxide phase catalysts exhibited a type IV isotherm with a hysteresis loop H1 type as shown in **Fig. 24**. By comparing Al(0.05)-SBA-15 mix2 supports with the catalysts, it could be observed a reduction in the size of such hysteresis loop at relative pressures (P/P_0) between 0.7 and 0.8. Hence, it was inferred that Ni and W incorporation decreased adsorption capacity. In addition, Al(0.05)-SBA-15 mix2 exhibited a slight deformation of the plateau in the hysteresis loop at relative pressures (P/P_0) between 0.7 and 0.8, suggesting that the shape of cylindrical pores might be slightly altered in the final catalytic support. It is noteworthy remembering that this material is the mixture of different synthesis for the same Al/Si molar ratio (0.05) as commented in **Section 4.1.1** and **4.2.1.1.**

Regarding the effect of incorporating Ni and W over Al(0.05)-SBA-15 mix2 catalytic support, **Table 9** reports the textural properties of NiO(y)-WO_3(z)/Al(0.05)-SBA-15 mix2 oxide phase catalysts. Incorporating Ni and W decreased pore volume (PV) and specific surface area (S_{BET}). The first effect ratifies the reduction of adsorption capacity as previously commented, and the second effect suggests that Ni and W could possibly block the porous and change mesoporosity of the material as shown in **Fig. 24** due to the reduction and change in the shape of the hysteresis loop. However, pore diameter (PD) values were in average 6.7 nm. Therefore, no obstruction of pores was confirmed. The more

metallic load (NiO and WO_3) the less values of S_{BET}, confirming the change in mesoporosity when adding metals. In addition, the catalyst with higher WO_3 nanoparticle size (**Table 8**) possessed the lowest S_{BET} and PV. Hence, the highest metallic load the highest nanoparticle size and the lowest textural properties and mesoporosity.

Table 9. Textural Properties for NiO(y)-WO_3(z)/Al(0.05)-SBA-15 mix2 oxide phase catalysts and support. *y*: NiO weight percentage, z: WO_3 weight percentage.

Sample	S_{BET} [m^2/g]	PV [cm^3/g]	PD [nm]
Al(0.05)-SBA-15 mix2	803.1	1.3	6.5
NiO(3.5%)-WO_3(18%)/Al(0.05)-SBA-15 mix2	458.4	0.8	6.7
NiO(4.5%)-WO_3(20%)/Al(0.05)-SBA-15 mix2	434.1	0.8	6.9
NiO(5.5%)-WO_3(25%)/Al(0.05)-SBA-15 mix2	374.5	0.6	6.8

4.2.1.3. Chemical functional groups by RAMAN spectroscopy

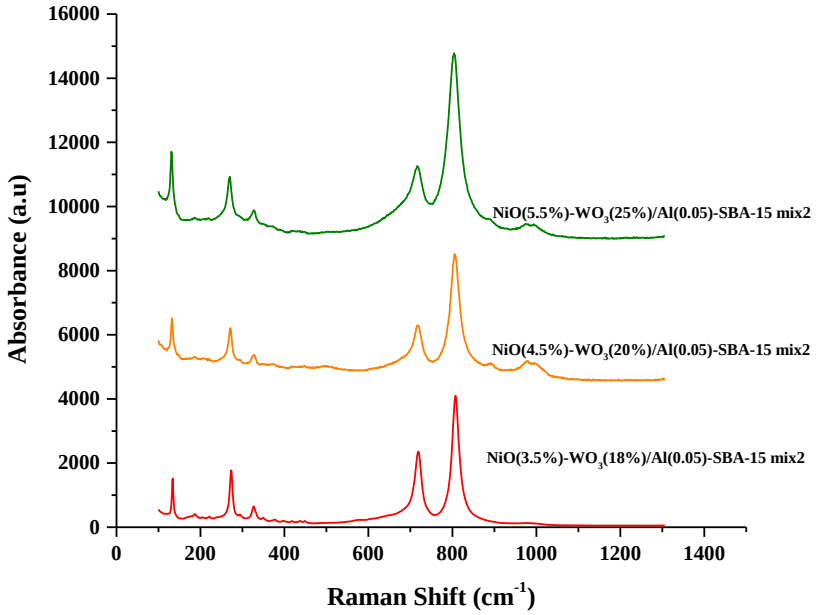

Fig. 25. RAMAN spectra for NiO(y)-WO_3(z) /Al(0.05)-SBA-15 mix2 oxide phase catalysts. y: NiO weight percentage, z: WO_3 weight percentage.

NiO(y)-WO_3(z)/Al(0.05)-SBA-15 mix2 oxide phase catalysts exhibited a similar RAMAN spectra as observed in **Fig. 25**. In common there were bands at Raman shift at 715 cm^{-1} and 805 cm^{-1}, which are ascribed to WO_3 species in agreement with the WA-XRD profile shown in **Fig. 23** and data reported in **Table 8**, indicating the occurrence of higher WO_3 nanoparticles at expenses of increasing metallic load. Nevertheless, an extra and broad band between 970 cm^{-1} and 1000 cm^{-1} could be observed for higher metallic loading (NiO and WO_3 weight percentages) catalysts. That signal at ~970 cm^{-1}

corresponds to an octahedrally coordinated tungsten compound (56, 57). On the other hand, the bands at about 130 cm^{-1}, 270 cm^{-1}, and 330 cm^{-1} could be ascribed to tungstate ions, WO_4^{-2}, ratifying the formation of $NiWO_4$ as previously reported for a similar material (66). Signals at Raman shift higher than 1054 cm^{-1} were not observed. As a result, the occurrence of nickel or tungsten aluminates was discarded.

4.2.1.4. Molecular Structure of Aluminum Species by ^{27}Al-MAS-NMR Measurements

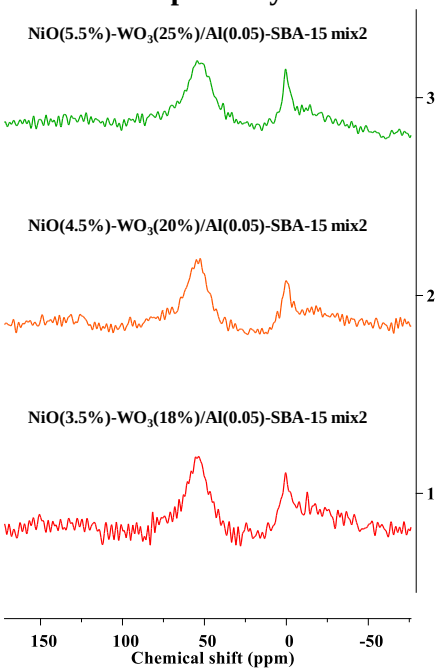

Fig. 26. 27Al-MAS-NMR spectra for NiO(y)-WO3(z) /Al(0.05)-SBA-15 mix2 oxide phase catalysts. y: NiO weight percentage, z: WO3 weight percentage.

As far as could be observed in **Fig. 26**, disregarding metallic load, all NiO(y)-WO_3(z)/Al(0.05)-SBA-15 mix 2 oxide phase catalysts clearly exhibited two signals at chemical shifts of about 53 ppm and 0 ppm, corresponding to tetrahedral and octahedral aluminum species, respectively(67-69). The ^{27}Al-MAS-NMR spectrum for the NiO(3.5%)-WO_3(18%)/Al(0.05)-SBA-15 mix2 oxide phase catalyst slightly showed less signal intensity, suggesting minor changes in Al species content. By comparing the spectrum with that shown in **Fig. 14 b) Section 3.2.1.8** for NiO(2.5%)-WO_3(15%)/Al(0.05)-SBA-15 mix1 oxide phase catalyst, no major differences were observed. As a result, increasing the metallic load (NiO and WO_3 compositions) seemed to not influence *Al* coordination into the NiO(y)-WO_3(z)/Al(0.05)-SBA-15 mix2 oxide phase catalysts.

4.2.1.5. FTIR spectra of liquid products during the hydro-coprocessing of the vegetable oil and gas oil

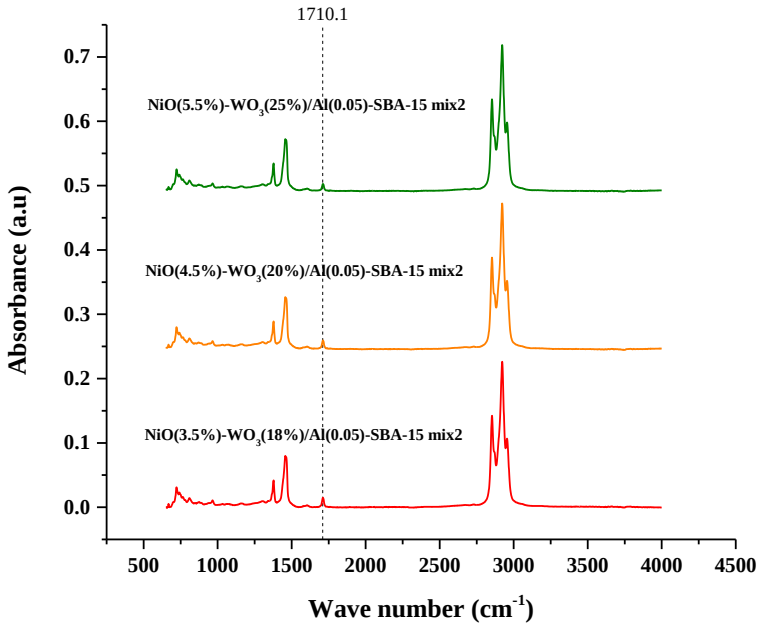

Fig .27. FTIR spectra for liquid products using NiO(y)-WO_3(z) /Al(0.05)-SBA-15 mix2 oxide phase catalysts. y: NiO weight percentage, z: WO_3 weight percentage.

Fig. 27 shows FTIR spectra for the liquid product of the hydro-coprocessing of the mixture vegetable oil and gas oil with the NiO(y)-WO_3(z)/Al(0.05)-SBA-15 mix2 sulfided catalysts. The corresponding bands at ~1168 cm^{-1} ascribed to simple bond, C-O, disappeared completely. The band at ~1710 cm^{-1} ascribed to double bond, C=O, in the carboxylic acid group was reduced on function of the metallic load as follows: NiO(3.5%)-WO_3(18%)/Al(0.05)-SBA-15 mix2<NiO(4.5%)-WO_3(20%)/Al(0.05)-SBA-15 mix2<NiO(5.5%)-WO_3(25%)/Al(0.05)-SBA-15 mix2. Therefore, the more Ni and W over the catalysts surface the more degradation of free fatty acids into hydrocarbons. The bands about 2750 cm^{-1} to 3000 cm^{-1}, and 1250 cm^{-1} to 1500 cm^{-1}, correspond to methyl and methylene groups on hydrocarbons. On the other hand, by comparing FTIR spectra with the shown in **Fig. 16** (section 3.2.1.9), it was observed that the signal at ~1750 cm^{-1} of the feedstock and ascribed to triglycerides disappeared, ratifying the conversion from triglycerides into free fatty acids. Additionally, at the same Al/Si molar ratio (0.05) but higher metallic load, from 17.5% to 30.5%, most of the carboxylic acids in the *Jatropha curcas* L. oil were hydroconverted in linear hydrocarbons as previously commented.

4.2.1.6. ^{1}H-NMR spectra for liquid products and vegetable oil

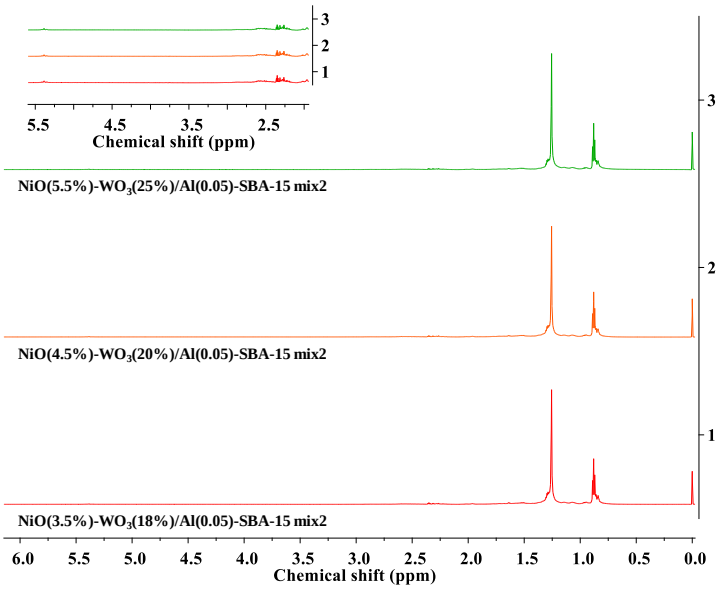

Fig. 28. ^{1}H-NMR spectra for the liquid product of NiO(y)-WO_3(z) /Al(0.05)-SBA-15 mix2 sulfided phase catalysts. y: NiO weight percentage, z: WO_3 weight percentage.

According to **Fig. 28** for ^{1}H-NMR spectra, after hydro-coprocessing the mixture of vegetable oil and gas oil with NiO(y)-WO_3(z)/Al(0.05)-SBA-15 mix2 sulfided catalysts, only two signals were clearly observed at chemical shift of 0.89 ppm and 1.31 ppm for all the liquid products. The latter signals are ascribed to unconverted unsaturated acyl groups in vegetable oil, and the –(CH_3)- and –$(CH_2)_3$- groups into the gas oil counterpart. Hence, most of the components were hydrocarbons derived of hydro-coprocessing the mixture. On the other hand, some traces of the signals at chemical shift of 2.31 ppm and 5.35 ppm remained as shown in zoomed part in **Fig. 28**, indicating that unconverted fatty acid chains remained at low concentrations. Therefore, HDO of the mixture occurred via oxygen removal of acyl groups from triglycerides into fatty acid chains, which latter were hydroconverted into hydrocarbons as confirmed by the no occurrence of *Jatropha curcas* L. signals at chemical shifts higher than 1.31 ppm as shown in **Fig. 18 Section 3.2.1.11**.

4.2.1.7. Qualitative hydrocarbon distribution by ESI mass spectrometry

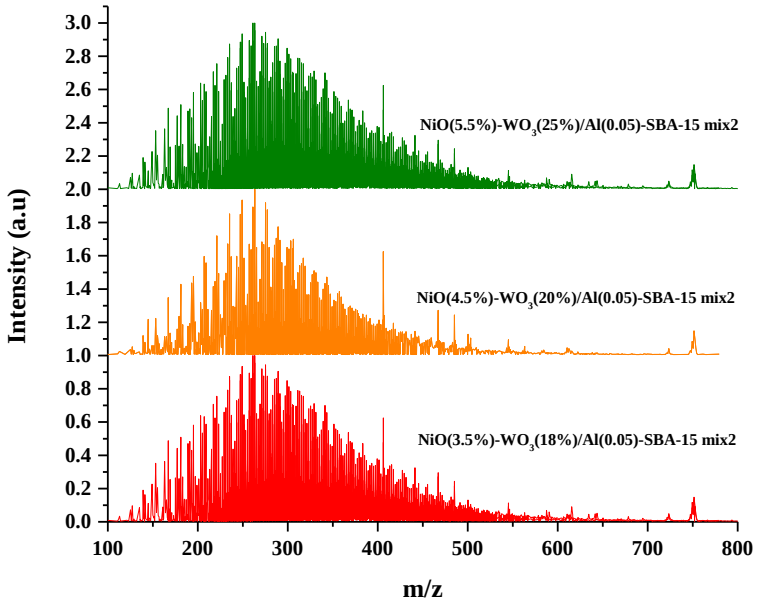

Fig. 29. ESI-MS spectra for the liquid product of NiO(y)-WO_3(z) /Al(0.05)-SBA-15 mix2 oxide phase catalysts. y: NiO weight percentage, z: WO_3 weight percentage.

A qualitative analysis of hydrocarbon distribution can be carried out by positive ion mode ESI-MS spectra as shown in **Fig. 29**. Accordingly, increasing *NiO* and *WO_3* the highest values showed the lowest occurrence of heavier hydrocarbon fractions at m/z within the range of 600 and 800 ascribed to C_{43} to C_{57} hydrocarbons, and di and triglycerides. The latter could be observed for the liquid product for the NiO(5.5%)-WO_3(25%)/Al(0.05)-SBA-15 mix2 sulfided catalyst. For the NiO(4.5%)-WO_3(20%)/Al(0.05)-SBA-15 mix2 sulfided catalyst (24.5% of metallic load) there were signals at m/z between 400 and 600, and 700 to 800 ascribed to C_{29} and C_{43}, and C_{50} and C_{57} hydrocarbons, respectively. Hence, hydro-coprocessing of the mixture vegetable oil and gas oil might occur via rupture of triglyceride bonds into free fatty acids and subsequently into hydrocarbons as suggested by ^{1}H-NMR analysis in **Section 4.2.1.6**. Finally, for the NiO(3.5%)-WO_3(18%)/Al(0.05)-SBA-15 mix2 sulfided catalyst, it was observed a slightly broader distribution of lighter hydrocarbons within the m/z range of 200 to 400 ascribed to C_{14} and C_{29} hydrocarbons. Therefore, this catalyst could enhance the highest diesel-like fraction as compared with the other catalysts.

4.2.2. Catalytic evaluation of NiO(y)-WO_3(z)/Al(0.05)-SBA-15 sulfided catalysts

To elucidate the effect of metallic load during hydro-coprocessing the mixture vegetable oil and gas oil, NiO(y) and WO_3(z) weight percentages were added and labeled as "metallic load". Data is presented accordingly.

4.2.2.1. Effect of metallic load in the hydrodesulfurization properties of NiO(y)-WO_3(z)/Al(0.05)-SBA-15 sulfided catalysts

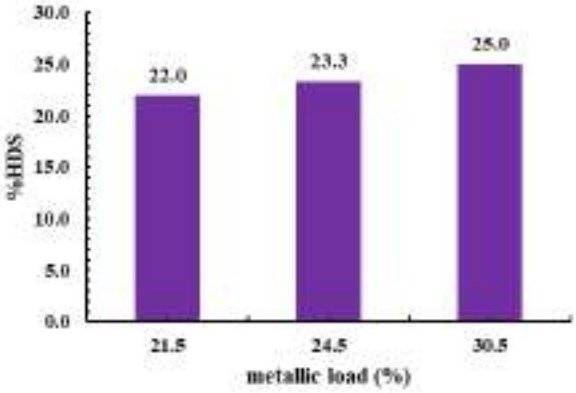

Fig. 30. HDS expressed as sulfur removal percentage for NiO(y)-WO_3(z) /Al(0.05)-SBA-15 mix2 oxide phase catalysts. y: NiO weight percentage, z: WO_3 weight percentage.

An increasing linear tendency could be observed for sulfur removal (%HDS) by using NiO(y)-WO_3(z)/Al(0.05)-SBA-15 mix2 sulfided catalysts for the hydro-coprocessing of the mixture *Jatropha curcas* L. oil and gas oil as it is illustrated in **Fig. 30**. Accordingly, the higher metallic load (30.5%) the most sulfur removal (25.0%). The order is the following: NiO(3.5%)-WO_3(18%)/Al(0.05)-SBA-15 mix2<NiO(4.5%)-WO_3(20%)/Al(0.05)-SBA-15 mix2<NiO(5.5%)-WO_3(25%)/Al(0.05)-SBA-15 mix2. The latter implies an average increase of 11.9% in sulfur removal when adding more Ni and W by compared with results reported in **Fig. 19**, **Section 3.2.2.1** for NiO(2.5%)-WO_3(15%)/Al(0.05)-SBA-15 mix1 sulfided catalyst. Therefore, hydrodesulfurization properties of $NiWO_4$ and WO_3 oxide phase precursors (**Fig. 23, Section 4.2.1.1**) of sulfided phases was elucidated as it has been previously reported by other authors (48).

4.2.2.2. Effect of metallic load in the hydrodeoxygenation (HDO) properties of NiO(y)-WO_3(z)/Al(0.05)-SBA-15 sulfided catalysts.

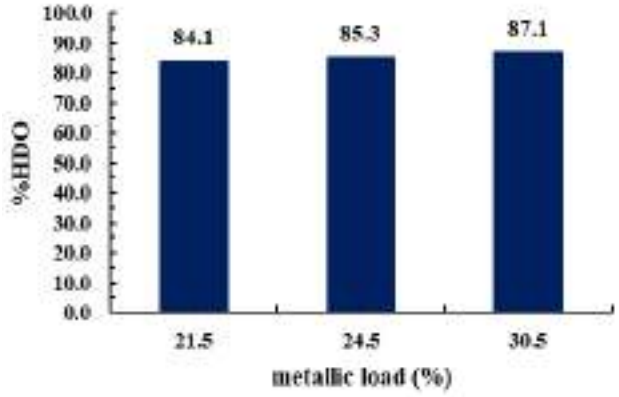

Fig. 31. HDO expressed as the reduction of absorbance at FTIR band of about 1710 cm^{-1} for NiO(y)-WO_3(z) /Al(0.05)-SBA-15 mix2 oxide phase catalysts. y: NiO weight percentage, z: WO_3 weight percentage.

The effect of the overall metallic load can be observed in **Fig. 31**. A linear tendence could be observed, indicating that the more Ni and W the more HDO activity. Accordingly, the highest reduction (87.1%) in the FTIR band about 1710 cm^{-1} was observed for the NiO(5.5%)-WO_3(25%)/Al(0.05)-SBA-15 mix2 sulfided catalyst. Therefore, the highest metallic load enhanced the conversion of free fatty acids in lighter hydrocarbons. HDO activity order is the following: NiO(3.5%)-WO_3(18%)/Al(0.05)-SBA-15 mix2< NiO(4.5%)-WO_3(20%)/Al(0.05)-SBA-15 mix2< NiO(5.5%)-WO_3(25%)/Al(0.05)-SBA-15 mix2. On the other hand, by comparing these results with the previously reported for the NiO(2.5%)-WO_3(15%)/Al(0.05)-SBA-15 mix1 sulfided catalyst in **Section 3.2.2.2**, it could be observed that HDO activity increased about 24.6% by increasing the metallic load to the highest point, from 17.5% to 30.5%. As a result, the occurrence of higher contents of WO_3 and $NiWO_4$ improved heteroatoms removal reactions as previously stated by HDS results in **Section 4.2.2.1** and **Fig. 30**. This tendence could be explained according to **Fig. 25** for RAMAN spectra, which depicted an acute and broad signal at Raman shifts of 805 cm^{-1} and 975 cm^{-1}, respectively. Specifically, the signal at ~975 cm^{-1} corresponds to $NiWO_4$, and it could be only observed for a metallic load higher than 21.5%. Additionally, as shown in **Fig. 23** and **Table 8** for WA-XRD, it could be observed that the highest metallic load the highest WO_3 nanoparticle size. Therefore, one may infer that type II (multi-layer) active metal phase was formed on the catalysts surface. The latter in agreement with the work previously reported by Kagami et al (65), where hydrotreating reactions (i.e., HDS) were improved by the occurrence of type II of active metal sites.

4.2.2.3. Effect of metallic load in the hydrocracking properties of NiO(y)-WO_3(z)/Al(0.05)-SBA-15 sulfided catalysts.

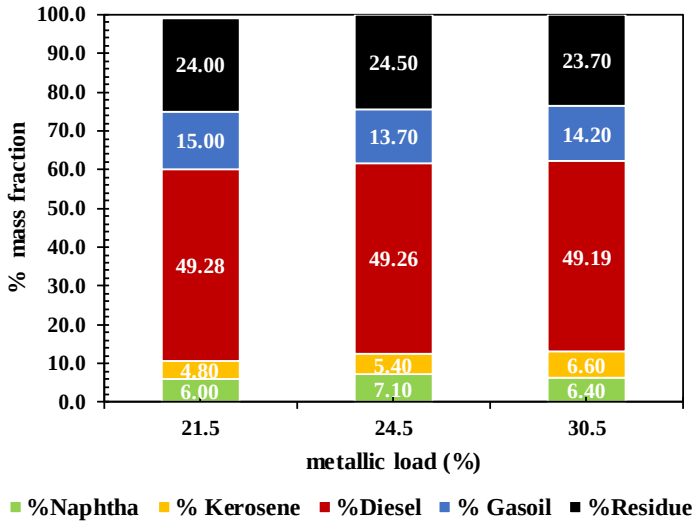

Fig.32. Lumps mass fraction percentage distribution for NiO(y)-WO_3(z)/Al(0.05)-SBA-15 mix2 oxide phase catalysts. y: NiO weight percentage, z: WO_3 weight percentage.

According to the information given in **Fig. 32**, the highest diesel-like fraction yield (49.29%) was attained with the NiO(3.5%)-WO_3(18%)/Al(0.05)-SBA-15 mix2 sulfided catalyst, and the lowest (42.19%) for the highest metallic load catalyst, the NiO(5.5%)-WO_3(25%)/Al(0.05)-SBA-15 mix2. On the other hand, lighter hydrocarbons (naphtha, kerosene, and diesel) yield was the highest (62.2%) for the NiO(5.5%)-WO_3(25%)/Al(0.05)-SBA-15 mix2 sulfided catalyst and the lowest (60.0%) for the lowest metallic load. In addition, heavier fractions (gasoil and residue) yield exhibited the following order: NiO(5.5%)-WO_3(25%)/Al(0.05)-SBA-15 mix2 < NiO(4.5%)-WO_3(20%)/Al(0.05)-SBA-15 mix2< NiO(3.5%)-WO_3(18%)/Al(0.05)-SBA-15 mix2. As a result, major differences can be explained on the fact that at the highest metallic load, the highest yield (13%) to lighter hydrocarbons (naphtha and kerosene) and the lowest yield (37.8%) to heavier ones (gasoil and residue). Therefore, increasing Ni and W content over the catalysts surface promoted the HCK of heavier fractions into lighter ones. The latter, in addition to the effect of increasing HDS and HDO conversions as shown in **Fig. 30** and **Fig. 31**.

The latter can be ratified by comparing the diesel-like fraction yield between the NiO(y)-WO_3(z)/Al(0.05)-SBA-15 sulfided catalysts with the NiO(2.5%)-WO_3(15%)/Al(0.05)-SBA-15 mix1 sulfided catalyst in **Fig. 21, Section 3.2.2.3**. It could be observed that a higher metallic load enhanced the diesel-like fraction from 44.8% to 49.3% in average, ratifying the effect of metallic load on HCK during hydro-coprocessing the mixture vegetable oil and gasoil. At this point, it is important to mention that due to Al/Si molar ratio is fixed in 0.05, no effect of *Al* could be observed and more

importantly, no differences in trends in hydrotreating reactions (HDT) like HDS and HDO. For that reason, it was ratified that the interaction of Ni and W with Al affected HDT reactions. In this case, as observed in **Fig. 26** for ^{27}Al-MAS-NMR spectra, disregarding the metallic load the coordination of *Al* is the same. Hence, activity changes can be readily attributed to the type of active phase site on the catalyst surface.

4.3. CONCLUSIONS

NiO(y)-WO_3(z)/Al(0.05)-SBA-15 oxide phase catalysts were satisfactorily synthesized. Increasing the metallic load reduced the S_{BET}, and PV or adsorption capacity of the oxide phase catalysts due to the formation of larger WO_3 nanocrystals with an average size of 5.1 nm as evidenced with WA-XRD measurements. Nevertheless, using the corresponding sulfided catalysts during the hydro-coprocessing of a mixture vegetable oil (*Jatropha curcas* L. oil) and gas oil resulted in enhancing HDS and HDO reactions by increasing the overall metallic load (NiO and WO_3 compositions) to the highest point (30.5%). Specifically, sulfur and oxygen removal were the highest for the NiO(5.5%)-WO_3(25%)/Al(0.05)-SBA-15 mix2 sulfided catalyst. On the other hand, the diesel-like yield was about 49.3% for the three catalysts with different metallic load 21.5%, 24.5%, and 30.5%, respectively. However, the corresponding yield to lighter fractions (naphtha and kerosene) was the highest for the NiO(5.5%)-WO_3(25%)/Al(0.05)-SBA-15 mix2 sulfided catalyst, due to the HCK of heavier fractions into lighter ones into the mixture. Therefore, the NiO(5.5%)-WO_3(25%)/Al(0.05)-SBA-15 mix2 sulfided catalyst was the best catalyst. In that sense, that catalyst is a promising candidate for hydro-coprocessing reactions, opening the research field on getting cleaner, liquid and lighters hydrocarbons to satisfy energetic demand worldwide.

5. EFFECT OF THE OPERATING TEMPERATURE IN THE HYDRO-COPROCESSING OF A MIXTURE OF GAS OIL AND VEGETABLE OIL WITH A Ni-W/Al(X)-SBA-15 SULFIDED CATALYST

This chapter discusses the effect of reaction temperature during the hydro-coprocessing of a mixture of gas oil and *Jatropha curcas* L. oil using a NiO(5.5%)-WO_3(25%)/Al(0.05)-SBA-15 sulfided catalyst. Accordingly, this chapter describes the experimental procedure for evaluating a Ni-W/Al-SBA-15 catalyst with the best set of metallic oxides composition and Al/Si molar ratio based on the catalytic test reported in previous chapters. The operating temperature varies at 380 °C, 400 °C, and 420 °C. Therefore, temperature dependance on hydrodesulfurization (HDS), hydrodeoxygenation (HDO), and diesel-like fraction yield or hydrocracking (HCK) when hydro-coprocessing the mixture is elucidated.

5.1. EXPERIMENTAL

5.1.1. Catalyst preparation

A NiO(5.5%)-WO_3(25%)/Al(0.05)-SBA-15 mix2 oxide phase catalyst was prepared following the same procedures reported in **Chapter 3, Section 3.1.2**. The previously synthesized Al(0.05)-SBA-15 mix 2 material (**Chapter 4**, **Section 4.1.2**) was used as catalytic support for the catalyst preparation procedure.

5.1.2. Characterization

The solid catalyst was characterized by: N_2 physisorption at -196.15 °C, LA-XRD (low angle X-ray diffraction), WA-XRD (wide angle X-ray diffraction), ^{27}Al-MAS-NMR, and RAMAN spectroscopy, as described in **sections 3.1.3.1**, **3.1.3.2**, **3.1.3.5**, and **3.1.3.6,** respectively. Liquid products of catalytic evaluation were characterized by: FTIR, and ^{1}H-NMR as described in sections **3.1.3.7** and **3.1.3.9,** respectively.

5.1.3. Catalytic Evaluation

Previously sulfided NiO(5.5%)-WO_3 (25%)/Al(0.05)-SBA-15 mix2 catalyst was tested in the hydro-coprocessing of the mixture vegetable oil (*Jatropha curcas* L. oil) and gas oil following the sulfidation and reaction procedures as reported in **Section 3.1.4**.

5.1.4. Catalytic Activity

Hydro-coprocessing reactions were analyzed in terms of sulfur removal (% HDS), oxygen removal (% HDO), and diesel-like fraction yield for HCK. Procedures and expression of results were calculated as reported in **Section 3.1.5**.

5.2. RESULTS AND DISCUSSION

5.2.1. Characterization of the catalyst

5.2.1.1. Mesoporous structure and crystallinity of NiO(5.5%)-WO_3(25%)/Al(0.05)-SBA-15 oxide phase catalyst

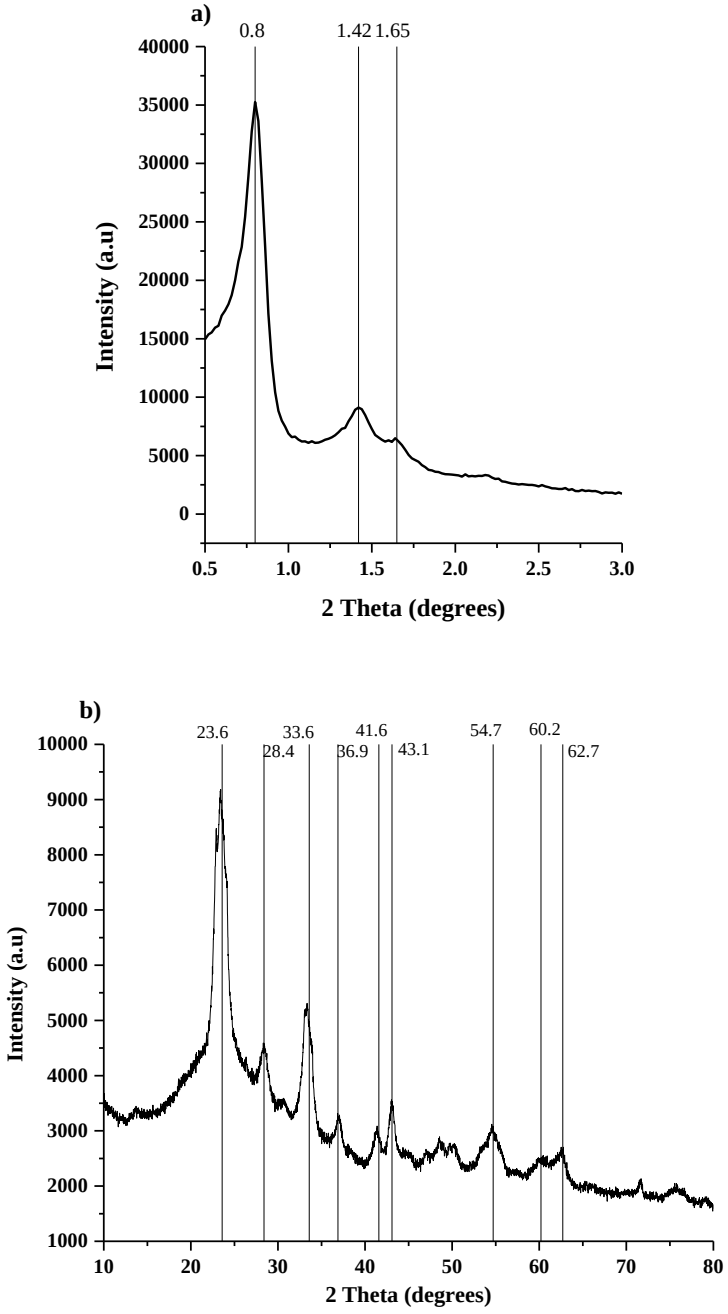

Fig. 33. XRD patterns for NiO(5.5%)-WO_3(25%)/Al(0.05)-SBA-15 mix2 oxide phase catalyst a) Low Angle (LA), b) Wide Angle (WA).

As it is shown in **Fig. 33 a)** for LA-XRD profiles, the NiO(5.5%)-WO_3(25%)/Al(0.05)-SBA-15 mix 2 catalyst exhibited the corresponding peaks for indexed planes (100), (110), and (200) ascribed to SBA-15 at 2θ° about 0.8°, 1.4°, and 1.7°, respectively. Therefore, Ni and W incorporation on the catalyst surface did not alter the mesostructured pattern and *p6mm* hexagonal symmetry as depicted in **Fig. 11**, **Chapter 3**, and **Fig. 22 b)**, **Chapter 4** for the pristine Al(0.05)-SBA-15 catalytic support. On the other hand, **Fig. 33 b)** shows the WA-XRD profile for the NiO(5.5%)-WO_3(25%)/Al(0.05)-SBA-15 mix 2 catalyst. As far as it can be observed, the occurrence of WO_3 could be detected at 2θ° of 23.6°, 28.4°, 33.3°, and 41.6°. WO_3 average particle size was 5.2 nm computed by the Debye-Scherrer's equation. $NiWO_4$ formation could be also detected by the occurrence of the signals at 23.7°, 28.4°, 33.6°, 41.6°, 46°, 48.5°, 49°, and 54.7° (70). In addition, signals ascribed to NiO could be observed at 2θ° of 36.9°, 43.1°, and 71.5°. Finally, the observed signals at 2θ° of 48.5° and 49° might be possibly ascribed to monoclinic Al_2O_3 (52). However, the absence of signals at 2θ: 19.3°, 31.5°, 37.2°, 45.2°, 59.9°, and 65.7° for $NiAl_2O_4$ ratified the no occurrence of mixed compounds of Ni and Al_2O_3(52). At this point it is important to mention that ^{27}Al-MAS-NMR spectra in **Fig. 26** for the NiO(y)-WO_3(z)/Al(0.05)-SBA-15 mix 2 oxide phase catalysts (**Chapter 4, Section 4.2.1.4**) demonstrated that extra-framework *Al* (octahedral) was increased when *Ni* and *W* were incorporated on pristine Al(0.05)-SBA-15 support in **Fig. 14** (**Chapter 3, Section 3.2.1.7**). Therefore, at the highest metallic load (30.5%) WA-XRD diffraction profiles made it clearer the occurrence of *Al* species over the catalyst surface.

5.2.1.2. Textural properties of NiO(5.5%)-WO_3(25%)/Al(0.05)-SBA-15 oxide phase catalyst

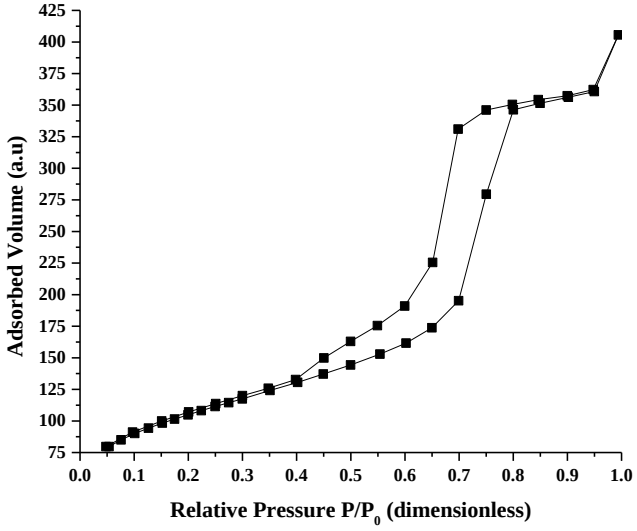

Fig. 34. N_2@-196.15 °C adsorption-desorption isotherms NiO(5.5%)-WO_3(25%)/Al(0.05)-SBA-15 mix2 and Al(0.05)-SBA-15 mix2 catalytic support.

As shown in **Fig. 34**, NiO(5.5%)-WO_3(25%)/Al(0.05)-SBA-15 mix 2 oxide phase catalyst exhibited a Type IV isotherm with and Type I hysteresis loop. The latter ratifies the mesoporosity of the catalyst and the tubular shape of the porous, respectively. There were no major differences in shape by comparing with the isotherm shown in **Fig. 24** for the similar catalyst synthesized therein. On the other hand, regarding textural properties, for the NiO(5.5%)-WO_3(25%)/Al(0.05)-SBA-15 mix2 oxide phase catalyst, those were the following: 366.8 m^2 g^{-1}, 0.6 cm^3 g^{-1}, and 6.9 nm for S_{BET}, PV and average PD, respectively. In comparison with the textural properties reported in **Table 9,** S_{BET} decreased about 2%, PV remained the same (less than 1%), and PD increased about 1.5%.

5.2.1.3. Chemical functional groups by RAMAN spectroscopy

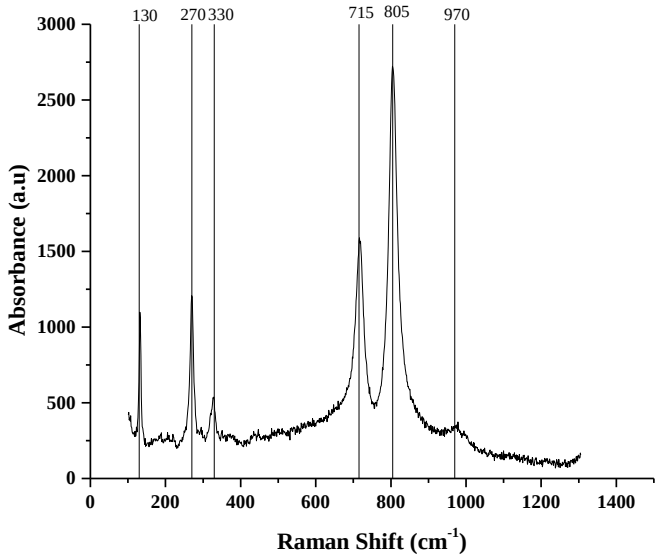

Fig. 35. RAMAN spectrum for NiO(5.5%)-WO_3(25%) /Al(0.05)-SBA-15 mix2 oxide phase catalyst.

According to **Fig. 35**, the oxide phase catalyst, NiO(5.5%)-WO_3(25%)/Al(0.05)-SBA-15 mix2, exhibited the most intense signals at a RAMAN shift of 805 cm^{-1} and 715 cm^{-1}, corresponding to WO_3 and WO_X oxides. On the other hand, the occurrence of $NiWO_4$ on the catalysts surface could be observed by the signal at 970 cm^{-1} for an octahedral coordinated W compound, and the signals at 130 cm^{-1}, 270 cm^{-1}, and 330 cm^{-1} for WO_4^{-1} species as it was previously discussed in **Chapter 4 , Section 4.2.1.3** for the similar NiO(5.5%)-WO_3(25%)/Al(0.05)-SBA-15 mix2 catalyst. The previous results agreed with the WA-XRD diffraction profiles discussion given in **Section 5.2.1.1**. Specifically, the intensity of the RAMAN signals might be an indicative of that bigger nanoparticles of *W* were formed, WO_3 particle average size was about 5.2 nm. Hence, it was confirmed the occurrence of a *Ni* and *W*

mixed phase during the synthesis of the catalyst in its oxide state. The absence of signals at RAMAN shifts higher than 1054 cm^{-1} implied the absence of *Ni* and *W* aluminates on the surface of the catalyst.

5.2.1.4. Molecular Structure of Aluminum Species by ^{27}Al-MAS-NMR Measurements

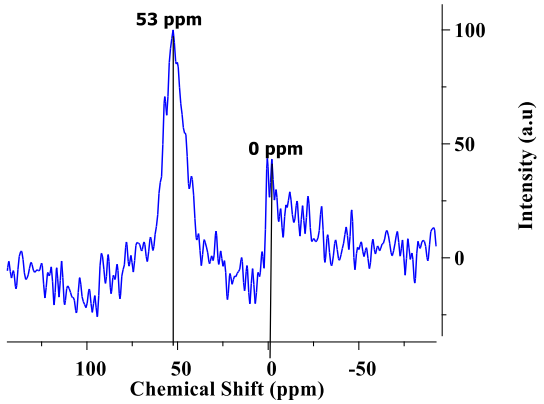

Fig. 36. ^{27}Al-MAS-NMR spectra for NiO(5.5%)-WO_3(25%) /Al(0.05)-SBA-15 mix2 oxide phase catalyst.

According to the spectrum shown in **Fig. 36**, the most intense signal could be found at a chemical shift of 53 ppm, followed by a signal at 0 ppm. Such signals correspond to tetrahedral and octahedral aluminum species, respectively (67). Therefore, in the final NiO(5.5%)-WO_3(25%)/Al(0.05)-SBA-15 mix2 oxide phase catalyst most of the aluminum got incorporated into the silica framework, while a remnant of such aluminum prevailed as extra-structural as evidenced by the occurrence of the octahedral signal. Those results agreed with those shown in **Chapter 4**, S**ection 4.2.1.4**, **Fig. 26** for the same metallic load (30.5%) catalyst.

5.2.1.5. FTIR spectra of liquid products during the hydro-coprocessing of the vegetable oil and gas oil

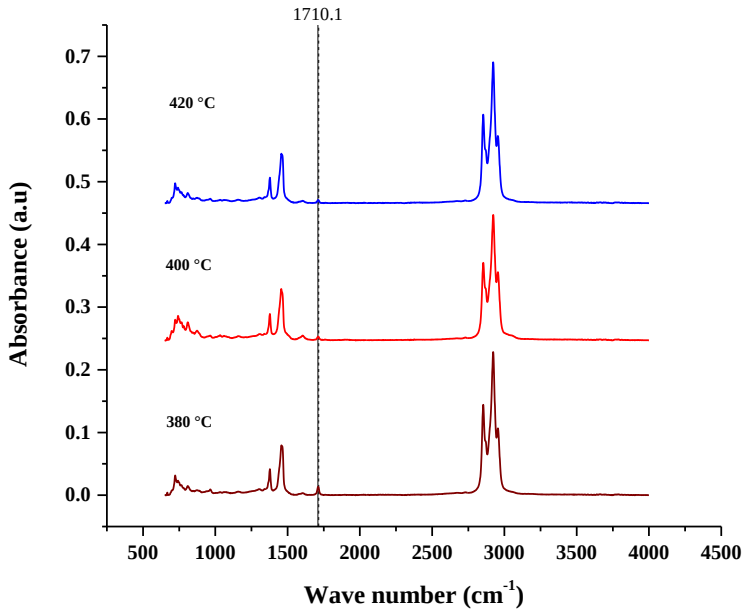

Fig. 37. FTIR spectra for liquid products using NiO(5.5%)-WO_3(25%) /Al(0.05)-SBA-15 mix2 oxide phase catalyst.

FTIR spectra for the liquid products during the hydro-coprocessing of the vegetable oil and gas oil mixture at different reaction temperatures is shown in **Fig. 37**. Accordingly, it could be observed the complete reduction (~100%) of the bands at 1168 cm^{-1} and 1710 cm^{-1} corresponding to C-O and C=O bonds, respectively. Hence, a complete HDO of the vegetable oil was elucidated. It is important to mention the absence of the band about 1743 cm^{-1} ascribed to triglycerides. Therefore, all vegetable oil was hydroconverted into free fatty acids and subsequently into hydrocarbons as evidenced by the bands between 1250-1500 cm^{-1} and 2750 and 3000 cm^{-1} for methyl and methylene groups. The highest reduction in the 1710 cm^{-1} band was observed at 420 °C followed by 400 °C, and finally at 380 °C.

Finally, by comparing the FTIR spectra in **Fig. 37** with the shown in **Fig. 27** (**Chapter 4, Section 4.2.1.5**) for the similar NiO(5.5%)-WO_3(25%)/Al(0.05)-SBA-15 mix 2 sulfided catalyst it could be observed that increasing the temperature from 360 °C to 420 °C favored HDO of the vegetable oil as evidenced by the almost complete reduction of the band at 1710 cm^{-1}.

5.2.1.6. ^{1}H-NMR spectra for liquid products during the hydro-coprocessing of the reaction mixture

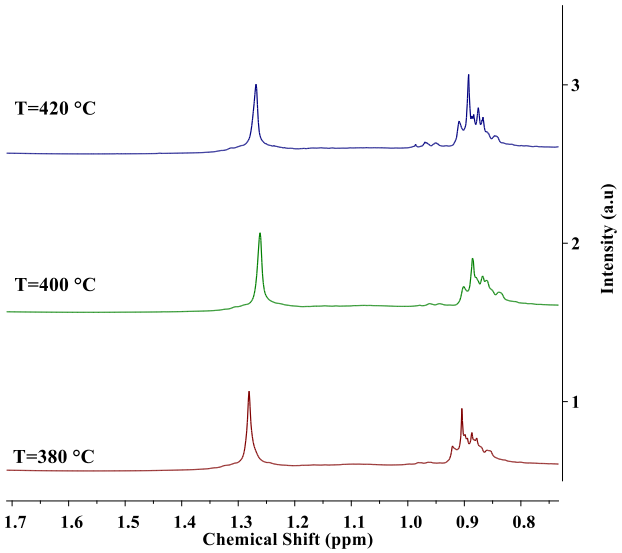

Fig. 38 ^{1}H-NMR spectra for the liquid product of NiO (5.5%)-WO_3(25%)/Al(0.05)-SBA-15 mix2 sulfided catalyst at different reaction temperature (T): 380 °C, 400 °C, and 420 °C.

In **Fig. 38** is shown the ^{1}H-NMR spectra for the liquid product during hydro-coprocessing experiments with the final NiO(5.5%)-WO_3(25%)/Al(0.05)-SBA-15 mix2 sulfided catalyst. Only two intense signals at 0.9 ppm and 1.3 ppm could be clearly observed. Such signals correspond to methyl and methylene hydrocarbons groups. Accordingly, increasing the reaction temperature (T) from 380 °C to 420 °C enhanced the HDO of the triglycerides derived from the vegetable oil (*Jatropha curcas* L. oil) in the feedstock. Additionally, the corresponding signal at 0.9 ppm became more intense at the highest T (420 °C), indicating a major concentration of lighter hydrocarbons. The previous results agreed well with FTIR spectra shown in **Fig.37**, which evidenced an almost complete HDO of the vegetable oil and the formation of hydrocarbons during hydro-coprocessing.

Finally, by comparing the results given in **Fig. 38** for the catalyst with a metallic load of 30.5% with the similar results given in **Fig. 28 (Chapter 4, Section 4.2.1.6)** for catalytic experiments at 360 °C. it could be inferred that increasing the reaction temperature favored HDO. The latter due to the absence of acyl groups signals at a chemical shift higher than 1.6 ppm.

5.2.1.7. Qualitative hydrocarbon distribution by ESI mass spectrometry

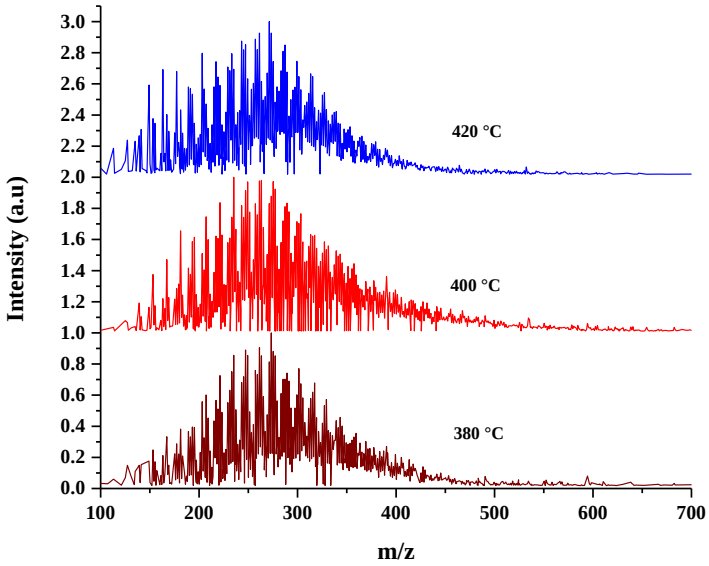

Fig. 39. ESI-MS spectra for the liquid product of NiO(5.5%)-WO_3(25%) /Al(0.05)-SBA-15 mix2 oxide phase catalyst.

Ion positive ESI-MS spectra is shown in **Fig. 39.** Accordingly, it could be observed that by increasing temperature from 380 °C to 420 °C increased the occurrence of fractions at m/z between 150 and 200. Hence, the presence of lighter hydrocarbons was evidenced. Additionally, the major concentration of hydrocarbons at m/z within 200 to 400 for C_{14}-C_{29} was observed at 380 °C and the lowest for 400 °C. Therefore, the higher temperature the lower concentration of a diesel-like fraction by the hydroconversion of heavier fractions into lighter ones during hydro-coprocessing the mixture vegetable oil and gas oil. The latter could be explained by the leftwards displacement of the distribution curve at expenses of increasing the reaction temperature. In addition, ESI-MS results agreed well with ^{1}H-NMR result shown in **Fig.38** due to at 420 °C the highest occurrence of lighter hydrocarbons was evidenced by both characterization techniques, ratifying the thermal effect on HCK during the hydro-coprocessing of the mixture of *Jatropha curcas* L. oil and gas oil used as feedstock.

5.2.2. Catalytic evaluation of NiO(5.5%)-WO_3(25%)/Al(0.05)-SBA-15 sulfided catalyst

5.2.2.1. Effect of temperature in the hydrodesulfurization properties of NiO(5.5%)-WO_3(25%)/Al(0.05)-SBA-15 sulfided catalyst

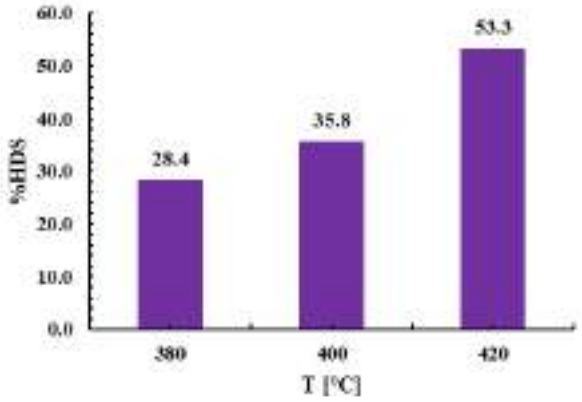

Fig. 40. HDS expressed as sulfur removal percentage for NiO(5.5%)-WO_3(25%) /Al(0.05)-SBA-15 mix2 oxide phase catalyst.

The effect of temperature in HDS activity could be observed in **Fig. 40**. HDS activity increased as follows: 420 °C > 400 °C > 380 °C. Accordingly, the highest sulfur removal (53.3%) was attained at 420 °C, and the lowest (28.4%) at 380°C.

In comparison, HDS activity reached the highest increase of 28.3% by comparing with the results shown in **Fig. 30** (**Chapter 4, Section 4.2.2.1**) for a similar NiO(5.5%)-WO_3(25%)/Al(0.05)-SBA-15 mix2 sulfided catalyst, and increasing temperature from 360 °C to 420 °C. Therefore, at higher conversion (46.7%), fixed Al/Si molar ratio (0.05) and fixed metallic load (30.5 %), HDS activity is mainly increased on function of the reaction temperature.

5.2.2.2. Effect of temperature in the hydrodeoxygenation (HDO) properties of NiO(5.5%)-WO_3(25%)/Al(0.05)-SBA-15 sulfided catalyst

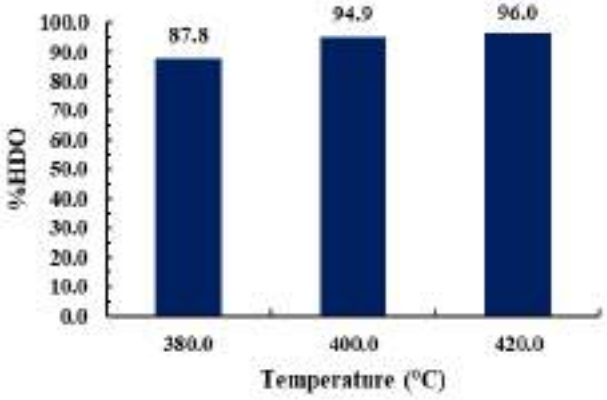

Fig. 41. HDO expressed as the reduction of absorbance at FTIR band of about 1710 cm^{-1} for NiO(5.5%)-WO_3(25%)/Al(0.05)-SBA-15 mix2 oxide phase catalyst.

In **Fig.41** it could be observed that increasing the reaction temperature from 380 °C to 420 °C increased HDO activity from 87.8% to a 96%. In comparison, HDO activity was 87.1% (**Chapter 4, section 4.2.2.2**) at 360 °C, which is 0.7% and 8.2% lower than results at 380 °C and 420 °C. Therefore, by using the same formulation catalyst, NiO(5.5%)-WO_3(25%)/Al(0.05)-SBA-15 mix2, the expected increase in HDO activity as function of the temperature was clearly evidenced.

5.2.2.3. Effect of temperature in the hydrocracking properties of NiO(5.5%)-WO_3(25%)/Al(0.05)-SBA-15 sulfided catalyst

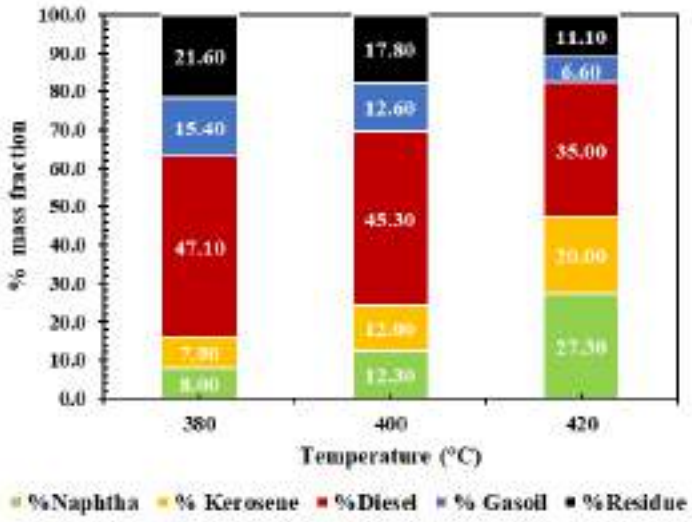

Fig. 42. Lumps mass fraction percentage distribution for NiO(5.5%)-WO_3(25%)/Al(0.05)-SBA-15 mix2 oxide phase catalyst.

The effect of the temperature (T) in the ASTM D2887 boiling point distributions is shown in **Fig. 42**. As it could be observed, increasing T to its highest value (420 °C) improved the hydrocracking (HCK) reaction during the hydro-coprocessing of the mixture *Jatropha curcas* L. oil and gas oil. Specifically at 420 °C, a 27.3% of Naphtha and a 20.0% of Kerosene were produced at expenses of reducing Residue and Gasoil fractions to 11.10% and 6.6%, respectively. On the other hand, the diesel-like fraction was reduced from 47.10% to 35% by increasing T from 380 °C to 420 °C, and a decreasing tendence in the mass percentage of the other heavier and lighter fractions was evidenced. At this point, it is important to mention that with a similar formulation catalyst (5.5% of NiO, 25% of WO_3, and an Al/Si molar ratio of 0.05) reported in **Fig. 32** (**Chapter 4**, **Section 4.2.2.3)**, it was observed a 49.3% of a diesel-like fraction at 360 °C, which is higher than the reported in this **Chapter 5**. According to the latter, the observed effect of reducing heavier components composition by HCK could be only improved by thermal effects.

Finally, it is worth mentioning that due to the temperature did enhance the production of a liquid mixture of a lighter (Naphtha and Kerosene), cleaner, and greener mixture of hydrocarbons, the choice of the suitable temperature will depend on enhancing the yield to a determined fraction of interest for refiners.

5.3. CONCLUSIONS

A sulfided NiO(5.5%)-WO3(25%)/Al(0.05)-SBA-15 catalyst was synthesized and tested in the hydro-coprocessing of a mixture of vegetable oil (*Jatropha curcas* L. oil) and a gas oil mix aiming at determining the best reaction temperature from 380 °C to 420 °C in terms of HDT (heteroatoms removal) and HCK (diesel-like fraction yield). At a fixed *Al* content (Al/Si molar ratio of 0.05) and metallic load of 30.5% (5.5% of NiO and 25% of WO_3) it was observed that metallic content enhanced HDS and HDO at a maximum of 53.5% and 96%, respectively with the higher reaction temperature (420 °C). Therefore, it could be concluded that reaction temperature influenced HDT reactions. Nevertheless, the diesel-like yield decreased 12.1% units by increasing the temperature, ratifying the thermal and no catalytic effect on HCK during the hydro-coprocessing. As a result, to promote the highest diesel-like yield it is recommended for refiners using the lowest reaction temperature (360 °C). However, the liquid product obtained at 420 °C is the hybrid fuel with the highest composition of lighter and cleaner (less sulfur) hydrocarbons, which are of interest to satisfy energetic demand by conventional processes.

6. KINETICS OF THE HYDRO-COPROCESSING OF THE MIXTURE OF VEGETABLE OIL AND GAS OIL WITH A SULFIDED NiO(5.5%)-WO_3(15%)/Al(0.05)-SBA-15 CATALYST

This chapter discusses the kinetics for HDS (hydrodesulfurization), HDO (hydrodeoxygenation), and HCK (hydrocracking) reactions during the hydro-coprocessing of a mixture of gas oil and *Jatropha Curcas* L. oil with the final NiO(5.5%)-WO_3(25%)/Al(0.05)-SBA-15 mix2 sulfided catalyst (**Chapter 5**). The corresponding kinetic parameters were estimated and analyzed looking for correlating them with the catalytic activity results previously discussed in **Chapter 4** and **Chapter 5** of the present document.

6.1. EXPERIMENTAL

6.1.1. Experimental data and reaction conditions for kinetic analysis

The effect of the reaction temperature (T) during the hydro-coprocessing of the mixture vegetable oil (*Jatropha curcas* L. oil) and gas oil with a sulfided NiO(5.5%)-WO_3(25%)/Al(0.05)-SBA-15 mix2 catalyst was elucidated in **Chapter 5 (Fig. 42)**. Accordingly, at T higher than 400 °C, thermal or non-catalytic effects could be observed in HCK due to Naphtha and Kerosene fractions yield increased 23.4%, and 33.0%, respectively with respect to data shown in **Fig. 32**. For a kinetic analysis procedure, catalytic experiments were conducted using the same sulfided NiO(5.5%)-WO_3(25%)/Al(0.05)-SBA-15 mix2 catalyst at 1 h, 2 h, 3 h, and 4 h of reaction time. The following T were chosen: 360 °C, 380 °C, and 400 °C. Other reaction conditions remained the same as reported in **Chapter 3, Section 3.1.4.** In addition, for oxygen concentration, the linear correlations from determination curves for FTIR bands at 1710 cm^{-1}, and 1750 cm^{-1} were used to calculate the amount of free fatty acids and triglycerides in the liquid products and feedstock, respectively (**Chapter 3, Section 3.1.5.2, Fig. 5 and Fig. 6**). Then, the calculated content was later converted in oxygen concentration (wt.%). Hence, HDO kinetic was measured in terms of oxygen removal from the feedstock. The initial content of oxygen was 2.18 wt.% for a 20 wt.% of *Jatropha curcas* L. oil in the reaction mixture.

Table 10. Experimental data of concentration (wt.%) for the feedstock and the liquid products of hydro-coprocessing a vegetable oil and gas oil blend with a sulfided NiO(5.5%)-WO_3(25%)/Al(0.05)-SBA-15 mix2 catalyst.

Type of reaction	Interest compound	T [°C]	Time [h]	Concentration [wt.%]
HDS	Sulfur	360	0	1.10
			1	0.97
			2	0.87
			3	0.86
			4	0.82
		380	1	0.86
			2	0.84
			3	0.81
			4	0.79
		400	1	0.76
			2	0.74
			3	0.72
			4	0.71
HDO	Oxygen	360	0	2.18
			1	1.18
			2	0.78
			3	0.59
			4	0.28
		380	1	0.92
			2	0.54
			3	0.44
			4	0.27
		400	1	0.61
			2	0.50
			3	0.35
			4	0.11
HCK	Residue fraction	360	0	52.50
			1	26.80
			2	22.40
			3	23.90
			4	23.66
		380	1	24.70
			2	24.10
			3	20.10
			4	21.60
		400	1	20.80
			2	18.90
			3	18.70
			4	17.80

According to the latter, **Table 10** summarizes the experimental data for the three hydro-coprocessing reactions: HDS, HDO, and HCK at the chosen reaction conditions. Concentrations of the interest compounds (sulfur, oxygen, and residue fraction) were given in weight percentage (wt.%).

6.1.2. Kinetic parameter estimation procedure

MATLAB R2023a and the optimization function "*fmincon*" were used to determine the best set of kinetic parameters: activation energy (E_A), collision factor (A_0), α, γ, and the HDO reaction order (b) in function of the proposed model for the respective hydro-coprocessing reaction (HDS, HDO or HCK). Reaction rate constants were computed using **Eqn.3** for the Arrhenius' equation, and the objective function was the square sum of errors (SSE) as shown in **Eqn.4** as follows:

$$k_i = A_{0_i} e^{\frac{-E_{A_i}}{R_u T}} \quad \boldsymbol{Eqn.3}$$

$$SSE = \sum_{i=1}^{N} \left[\frac{y_{calc_i} - y_{exp_i}}{y_{exp_i}} \right]^2 \quad \boldsymbol{Eqn.4}$$

R_u is the universal constant of gases [J mol^{-1}K^{-1}], T is the reaction temperature [K], y_{calc} and y_{exp} are the calculated and experimental mass fractions of the interest component, all in the liquid mixture of hydro-coprocessing the mixture vegetable oil and gas oil. Finally, b is the HDO reaction order.

A five-lumped (Naphtha, Kerosene, Diesel, Gasoil, and Residue) kinetic model was proposed as a first approach to model HCK reaction rates. The latter based on some literature reports for HCK of petroleum derived feedstocks (71, 72). The resulting ordinary differential equations (ODE) set of material balances for each lump, the parity plot, and the corresponding kinetic parameters can be found in **Appendix 1**. The SSE value computed by ***Eqn.4*** was 0.0643, and the reaction orders a= 2 and β=1.59 for products derived from Residue and Gasoil, respectively. Nevertheless, the five-lumped model did not fit well the heavier fractions (Residue and Gasoil) compositions in the reaction mixture as observed in the parity plot in **Appendix 1**. Therefore, the HCK kinetic was modeled in terms of determining the portion of more reactive compounds that could be readily hydroconverted in lighter hydrocarbons. Hence, α is the fraction of more reactive HCK compounds, $1-\alpha$ is the fraction of less reactive HCK compounds.

On the other hand, the HDS kinetic was modeled using the final approach for HCK, understanding that heavier petroleum sources possess recalcitrant sulfur compounds. Then, γ is the fraction of less recalcitrant sulfured compounds, $1-\gamma$ is the fraction of recalcitrant sulfured compounds. Finally, HDO was assessed using a power law model where b is the HDO reaction order.

6.2. RESULTS AND DISCUSSION

6.2.1. Kinetics and parameter estimation for HDS reactions

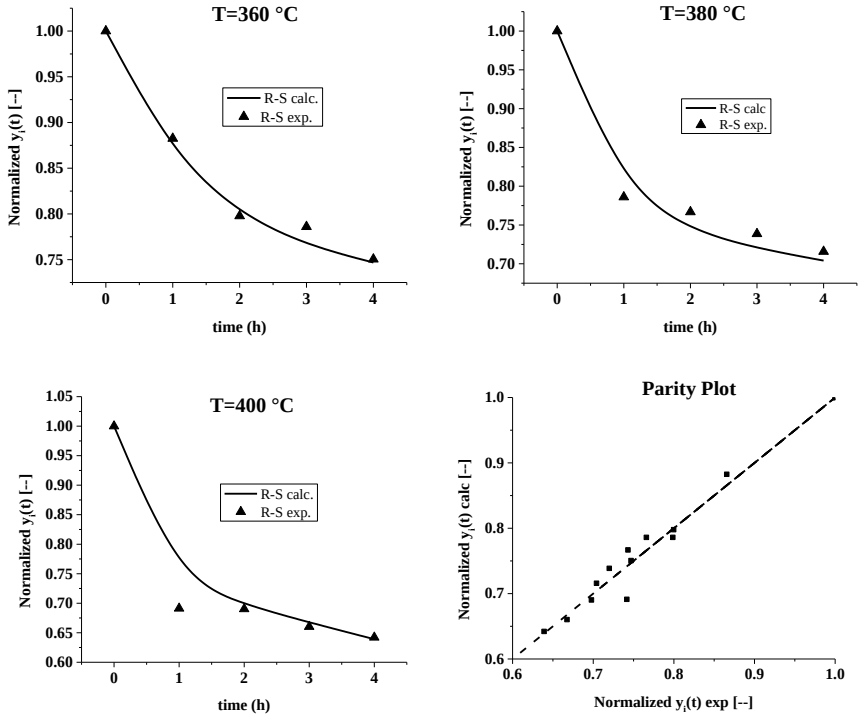

Fig. 43. Kinetics and parity chart for HDS reactions using the NiO(5.5%)-WO_3(25%)/Al(0.05)-SBA-15 mix2 sulfided catalyst at different reaction temperatures (T) and time (h).

The **Fig. 43** shows the kinetics and parity chart for HDS reactions in terms of sulfur removal at different reaction times and reaction temperatures. Sulfur concentration was normalized by dividing all concentrations in the initial point (1.098 wt.% of S). At higher reaction temperatures and reaction times higher than 1 h most of the sulfur in the feedstock was removed via HDS route. However, for the several reaction conditions (380 °C, and 400 °C), it was observed that the changes in normalized sulfur content were small, indicating the difficulty of removing S from recalcitrant compounds derived from the HGO (heavy gas oil) of the feedstock. For that reason, two first order HDS reactions were established, one for less recalcitrant sulfur compounds, and the other one for more recalcitrant sulfur compounds in the feedstock as it has been previously reported by Rodríguez *et al.*(73), and considering that both reactions yielding the same hydrodesulfured products. The kinetic model proposed was the following:

For the sulfur compounds:

Reaction 1 $S_1 = \gamma S \rightarrow Products$ $\boldsymbol{Eqn.5}$

Reaction 2 $S_2 = (1-\gamma)S \rightarrow Products$ $\boldsymbol{Eqn.6}$

Total sulfur $S_1 + S_2 = \mathrm{S}$ $\boldsymbol{Eqn.7}$

$$\frac{dS_1}{dt} = -k_1 S_1 \quad \boldsymbol{Eqn.8}$$

$$\frac{dS_2}{dt} = -k_2 S_2 \quad \boldsymbol{Eqn.9}$$

Solving ***Eqn. 8*** and ***Eqn. 9*** with the initial conditions *t=0*, $S_1 = S_{1_0}$ and $S_2 = S_{2_0}$, the solutions were:

$$S_1 = S_{1_0} e^{-k_1 t} \ \boldsymbol{Eqn.10}$$

$$S_2 = S_{2_0} e^{-k_2 t} \ \boldsymbol{Eqn.11}$$

Replacing ***Eqn. 10*** and ***Eqn. 11*** in ***Eqn. 7***:

$$S = S_{1_0} e^{-k_1 t} + S_{2_0} e^{-k_2 t}$$

Using ***Eqn. 5*** and ***Eqn. 6*** to express S_{1_0} and S_{2_0} in terms of γ:

$$S = \gamma S_0 e^{-k_1 t} + (1-\gamma) S_0 e^{-k_2 t}$$

Dividing both sides by S_0:

$$\frac{S}{S_0} = \gamma e^{-k_1 t} + (1-\gamma) e^{-k_2 t} \ \boldsymbol{Eqn.12}$$

Setting the normalized sulfur concentration as: $\frac{S}{S_0} = S_N$ and replacing in ***Eqn. 12***:

$$S_N = \gamma e^{-k_1 t} + (1-\gamma) e^{-k_2 t} \ \boldsymbol{Eqn.13}$$

For the products:

According to ***Reaction 1 (Eqn.5)*** and ***Reaction 2 (Eqn.6)***, the change in products (*P*) was expressed as:

$$\frac{dP}{dt} = k_1 S_1 + k_2 S_2 \ \boldsymbol{Eqn.14}$$

Replacing in ***Eqn.10*** and ***Eqn.11*** in ***Eqn.14***:

$$\frac{dP}{dt} = k_1 S_{1_0} e^{-k_1 t} + k_2 S_{2_0} e^{-k_2 t}$$

Using ***Eqn. 5*** and ***Eqn. 6*** to express S_{1_0} and S_{2_0} in terms of γ:

$$\frac{dP}{dt} = k_1\gamma S_0 e^{-k_1 t} + k_2(1-\gamma)S_0 e^{-k_2 t}$$

Dividing both sides by S_0:

$$\frac{d\left(\frac{P}{S_0}\right)}{dt} = k_1\gamma e^{-k_1 t} + k_2(1-\gamma)e^{-k_2 t} \quad \boldsymbol{Eqn.15}$$

Setting the normalized sulfur concentration as: $\frac{P}{S_0} = P_N$ and replacing in ***Eqn. 15***:

$$\frac{dP_N}{dt} = k_1\gamma e^{-k_1 t} + k_2(1-\gamma)e^{-k_2 t} \quad \boldsymbol{Eqn.16}$$

S_1 and S_2 are the less recalcitrant and recalcitrant contents of sulfured compounds, respectively, S_0 is the initial sulfur content, S is the final sulfur content, all in mass fraction. Finally, S_N and P_N are the normalized (dimensionless) overall sulfur and products concentration, respectively.

The results of kinetic parameter estimation are reported in **Table 11**, the optimized SSE value was 0.0088. The parity plot in **Fig. 43** exhibited that most of the normalized sulfur compositions were on the straight line, indicating a good fit between experimental and simulated data.

Table 11. Kinetic parameters for HDS during the hydro-coprocessing a vegetable oil and gas oil blend with a sulfided NiO(5.5%)-WO_3(25%)/Al(0.05)-SBA-15 mix2 catalyst

Rate Constant	**T [°C]**			**Kinetic Parameter**			
k_i **[h^{-1}]**	**360**	**380**	**400**	**E_A [kJ mol^{-1}]**	**A_0 [h^{-1}]**	***γ***	***1-γ***
$\mathbf{k_1}$	0.7642	1.5073	2.8556	116.79	$3.2955x10^9$	0.2398	0.7602
$\mathbf{k_2}$	0.0082	0.0194	0.0434	147.38	$1.1827x10^{10}$		

According to **Table 11** only a 23.98% of the sulfur compounds could readily be hydrodesulfured, and the remaining 76.02% slightly reacted over the NiO(5.5%)-WO_3(25%)/Al(0.05)-SBA-15 mix2 sulfided catalyst. The latter, by comparing the rate constants for each HDS reaction. Rate constants for the less recalcitrant compounds (γ) were about 100 times higher than for the recalcitrant compounds (1- γ). Therefore, HDS kinetic was clearly influenced by the type of sulfured compound in the feedstock. It has been previously reported that HDS of larger and recalcitrant compounds and molecules is not an easy task due to steric hindrance to remove S from the compound (73-76). On the other hand, as it was previously stated in **Chapter 3, Sections 3.2.2.1 and 3.2.2.2**, HDS reactions might promote HDO reactions via hydrogen sulfide (H_2S) formation, increasing HDO at expenses of decreasing HDS (62). Besides, water formation as byproduct of HDO could diminish the number of catalytic active sites, and there could be a competition between HDO and HDS for the same sulfided

active sites (77). Nevertheless, no matter the cause of the low HDS activity, the effect of the temperature in HDS reactions could be ratified by observing that for both kind of sulfured compounds, the reaction rates Increased as the reaction temperature increased. The latter is confirmed by comparing **Fig.30** and **Fig.40** in **Chapter 4** and **Chapter 5**, respectively, for HDS yields using the same sulfided catalyst, the NiO(5.5%)-WO_3(25%)/Al(0.05)-SBA-15 mix 2.

Finally, in **Table 12** is reported the initial HDS rates for both proposed reactions using ***Eqn. 5*** and ***Eqn. 6*** and taking the initial sulfur concentration [mass fraction]. Similar trends as the reported in **Table 11** for Arrhenius' rate constants due to the reaction order is 1.

Table 12. Initial reaction rates for HDS during the hydro-coprocessing a vegetable oil and gas oil blend with a sulfided NiO(5.5%)-WO_3(25%)/Al(0.05)-SBA-15 mix2 catalyst.

Initial reaction rate	T [°C]		
	360	380	400
$-r_{S_1}$ [h^{-1}]	0.0084	0.0166	0.0314
$-r_{S_2}$ [h^{-1}]	0.0001	0.0002	0.0005

6.2.2. Kinetics and parameter estimation for HDO reactions

A power law kinetic model was proposed for modeling HDO reactions of the vegetable oil in the feedstock as shown in $\boldsymbol{Eqn.17}$, where *O* is the oxygen content [mass fraction] and *b* is the reaction order.

$$\frac{dO}{dt} = -k_1 O^b \quad \boldsymbol{Eqn.17}$$

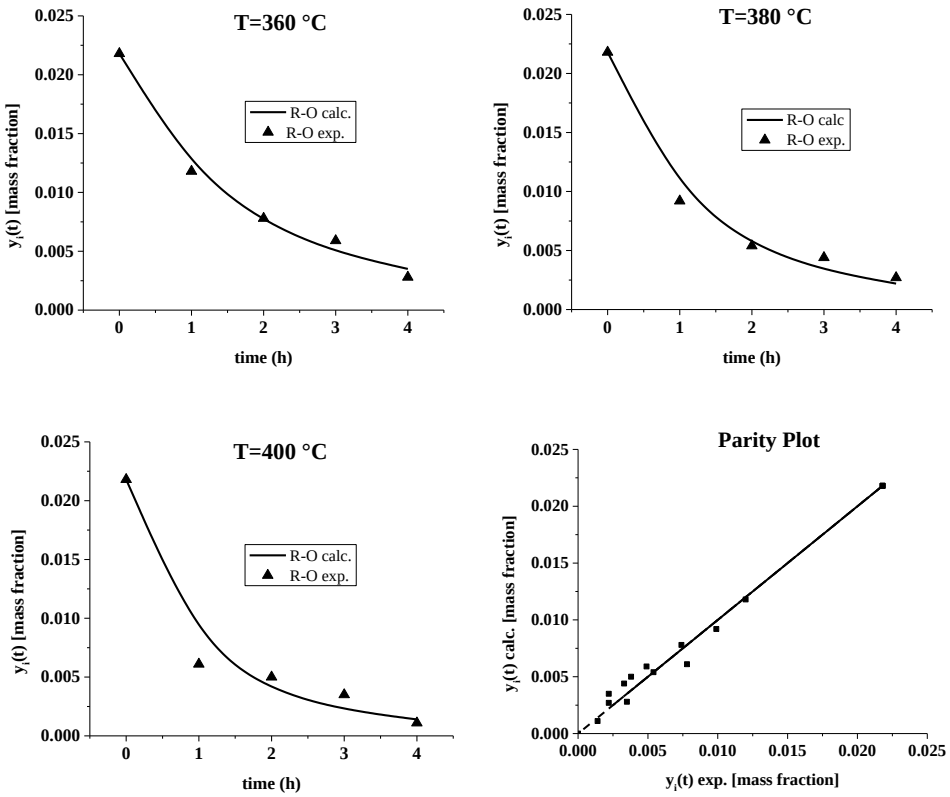

Fig. 44. Kinetics and parity chart for HDO reactions using the NiO(5.5%)-WO_3(25%)/Al(0.05)-SBA-15 mix2 sulfided catalyst at different reaction temperatures (T) and time (h).

The results of kinetic parameter estimation is reported in **Table 13**, and the SSE value at the optimum condition was 0.5299. The parity plot in **Fig. 44** exhibited that most of the oxygen contents were on the straight line, indicating a good fit between experimental and calculated data. Therefore, the power law model proposed (**Eqn. 17**) was adequate for modeling oxygen removal reactions during the hydro-coprocessing of the mixture vegetable oil and gas oil.

Table 13. Kinetic parameters for HDO during the hydro-coprocessing a vegetable oil and gas oil blend with a sulfided NiO(5.5%)-WO_3(25%)/Al(0.05)-SBA-15 mix2 catalyst.

Rate Constant	T [°C]			Kinetic Parameter		
k_i [h^{-1}]	360	380	400	E_A [kJmol^{-1}]	A_0 [h^{-1}]	*b*
k_1	3.0681	4.2353	5.7355	55.424	1.1461×10^5	1.3959

Table 14. Initial reaction rated for HDO during the hydro-coprocessing a vegetable oil and gas oil blend with a sulfided NiO(5.5%)-WO_3(25%)/Al(0.05)-SBA-15 mix2 catalyst.

Initial reaction rate	T [°C]		
	360	380	400
$-r_O$ [h^{-1}]	0.0147	0.0203	0.0275

According to data presented in **Table 13**, HDO of the vegetable oil in the feedstock follows a 1.4 order power law kinetics, and the rate constants increased on function of the reaction temperature (T) in agreement with catalytic activity results shown in **Chapter 4**, **Section 4.2.2.2**, and **Chapter 5**, **Section 5.2.2.2** for **Fig. 31,** and **Fig. 41**, respectively. In addition, by comparing the magnitude of reaction rates in **Table 14** with those reported in **Table 11** for HDS reactions, it could be observed that HDO rates were at least twice higher than those for the HDS of less recalcitrant sulfured compounds. As a result, one might infer that HDO reactions were mainly favored rather than HDS reactions, reaffirming the possibility that H_2S production during HDS enhanced oxygen removal (62), and that there might be a competition between HDO and HDS for reacting in the sulfided metallic phases over the catalyst surface(78, 79).

6.2.3. Kinetics and parameters estimation for HCK reactions

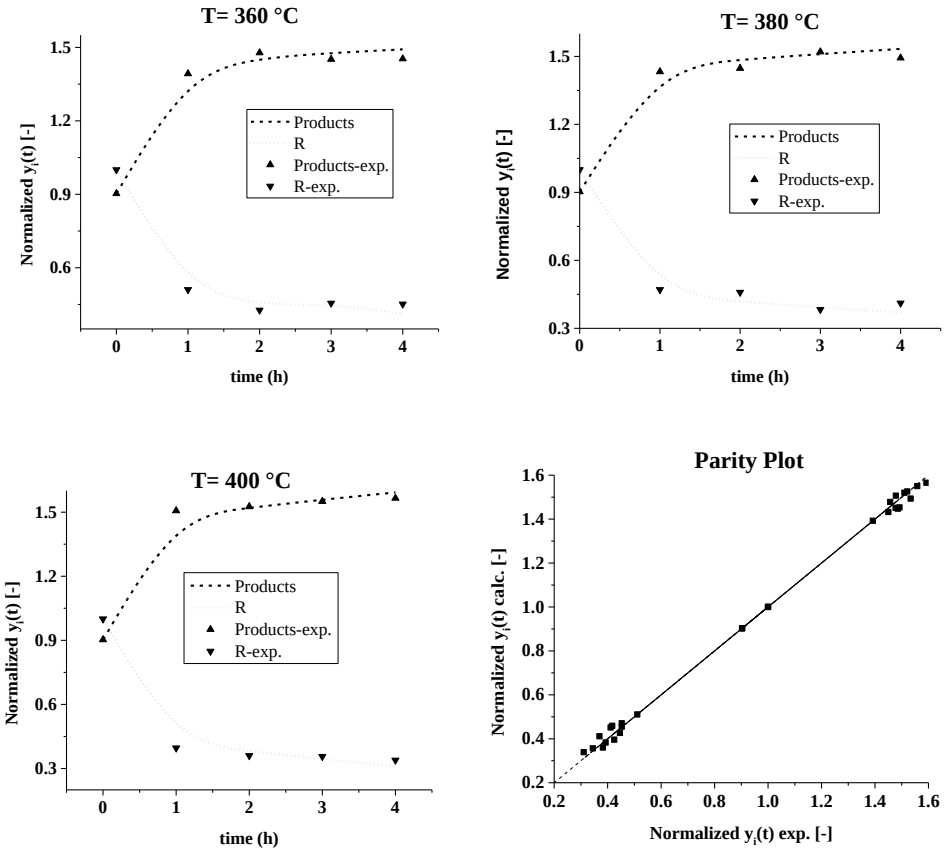

Fig. 45. Kinetics a parity chart for HCK reactions using the NiO(5.5%)-WO_3(25%)/Al(0.05)-SBA-15 mix2 sulfided catalyst at different reaction temperatures (T) and time (h).

In **Fig. 45** it could be observed the kinetics for the HCK reaction of the heavier fraction, Residue, which was hydroconverted in a combined group (Products) of lighter hydrocarbons at different

reaction time and temperature (T). Products fraction corresponds to the addition of the ASTM D2887 lumps labeled as: Naphtha, Kerosene, Diesel, and Gasoil according to the procedure reported in **Chapter 3**, **Section 3.1.5.3**. At higher reaction times than 1 h and independently of the reaction temperature, the residue fraction composition remained almost the same, indicating that isomerization, alkylation, and HCK reactions of the heavier fractions in the feedstock were less promoted by the intrinsic properties (i.e., acidity and metallic character) of the sulfided NiO(5.5%)-WO_3(25%)/Al(0.05)-SBA-15 mix2 catalyst. For that reason, the two reactions first order kinetic model proposed for HDS reactions (73) was adapted for HCK reactions as follows:

For the residue fraction (the reactant):

$$\textbf{Reaction 3} \quad R_1 = \alpha R \rightarrow Products \quad \boldsymbol{Eqn.18}$$

$$\textbf{Reaction 4} \quad R_2 = (1-\alpha)R \rightarrow Products \; \boldsymbol{Eqn.19}$$

$$\boldsymbol{Total\ residue} \quad R_1 + R_2 = \mathrm{R} \quad \boldsymbol{Eqn.20}$$

$$\frac{dR_1}{dt} = -k_1 R_1 \; \boldsymbol{Eqn.21}$$

$$\frac{dR_2}{dt} = -k_2 R_2 \; \boldsymbol{Eqn.22}$$

Solving ***Eqn. 18*** and ***Eqn. 19*** with the initial conditions *t=0*, $R_1 = R_{1_0}$ and $R_2 = R_{2_0}$, the solutions were:

$$R_1 = R_{1_0} e^{-k_1 t} \; \boldsymbol{Eqn.23}$$

$$R_2 = R_{2_0} e^{-k_2 t} \; \boldsymbol{Eqn.24}$$

Replacing ***Eqn. 23*** and ***Eqn. 24*** in ***Eqn.20***:

$$R = R_{1_0} e^{-k_1 t} + R_{2_0} e^{-k_2 t}$$

Using ***Eqn. 18*** and ***Eqn. 19*** to express R_{1_0} and R_{2_0} in terms of α:

$$R = \alpha R_0 e^{-k_1 t} + (1-\alpha) R_0 e^{-k_2 t}$$

Dividing both sides by R_0:

$$\frac{R}{R_0} = \alpha e^{-k_1 t} + (1-\alpha) e^{-k_2 t} \; \boldsymbol{Eqn.25}$$

Setting the normalized sulfur concentration as: $\frac{R}{R_0} = R_N$ and replacing in ***Eqn. 25***:

$$R_N = \alpha e^{-k_1 t} + (1-\alpha) e^{-k_2 t} \quad \textbf{Eqn. 26}$$

For the products:

According to ***Reaction 3 (Eqn.18)*** and ***Reaction 4 (Eqn.19)***, the change in products (*P*) was expressed as:

$$\frac{dP}{dt} = k_1 R_1 + k_2 R_2 \quad \textbf{Eqn. 27}$$

Replacing in ***Eqn. 23*** and ***Eqn. 24***:

$$\frac{dP}{dt} = k_1 R_{1_0} e^{-k_1 t} + k_2 R_{2_0} e^{-k_2 t}$$

Using ***Eqn.18*** and ***Eqn.19*** to express R_{1_0} and R_{2_0} in terms of α:

$$\frac{dP}{dt} = k_1 \alpha R_0 e^{-k_1 t} + k_2 (1-\alpha) R_0 e^{-k_2 t}$$

Dividing both sides by R_0:

$$\frac{d\left(\frac{P}{R_0}\right)}{dt} = k_1 \alpha e^{-k_1 t} + k_2 (1-\alpha) e^{-k_2 t} \quad \textbf{Eqn. 28}$$

Setting the normalized sulfur concentration as: $\frac{P}{R_0} = P_N$ and replacing in ***Eqn. 28***:

$$\frac{dP_N}{dt} = k_1 \alpha e^{-k_1 t} + k_2 (1-\alpha) e^{-k_2 t} \quad \textbf{Eqn. 29}$$

R_1 and R_2 are the more and less reactive residue compounds, respectively, R_0 is the initial residue content, R is the final residue content, all in mass fraction, and P the final products content, all in wt.%. Finally, R_N is the normalized overall residue concentration, which is dimensionless. The initial mass fraction of the residue was 0.525. Then, R_N and P_N were obtained by dividing R and P in 0.525, resulting in a normalized residue fraction of 1.0, and normalized products compositions higher than 1.0 as shown in **Fig. 45**.

In **Table 15** it was reported the estimated kinetic parameters when minimizing the SSE to a minimum value of 0.0285. Accordingly, 52.91% of the components of the residue fraction of the feedstock was readily hydroconverted in lighter hydrocarbons, while the 47.09% were less reactive for HCK during hydro-coprocessing. Supporting the latter, kinetic rate constants for less heavy residue components (α) were about 70 times higher than the rate constants for heavier components in the residue (1- α).

Table 15. Kinetic parameters for HCK during the hydro-coprocessing a vegetable oil and gas oil blend with a sulfided NiO(5.5%)-WO_3(25%)/Al(0.05)-SBA-15 mix2 catalyst.

Rate Constant	T [°C]				Kinetic Parameter			
k_i [h^{-1}]	360	380	400		E_A [kJ mol^{-1}]	A_0 [h^{-1}]	α	$1-\alpha$
k_1	2.2485	4.0203	6.9444		99.903	3.9227×10^8	0.5291	0.4709
k_2	0.0341	0.0606	0.1042		99.030	5.0346×10^6		

On the other hand, as shown in **Fig. 32**, and **Fig. 42** in **Chapter 4**, **Section 4.2.2.3**, and **Chapter 5**, **Section 5.2.2.3**, respectively, one can might say that the less heavy residue compounds correspond to the triglycerides in the *Jatropha curcas* L. oil, and less recalcitrant sulfur compounds in the reaction mixture. This due to in **Fig. 32** only a 4.5% increment in the diesel-like fraction was observed by increasing the metallic load to the highest point in the final NiO(5.5%).WO_3(25%)/Al(0.05)-SBA-15 mix2 sulfided catalyst, which agreed with the magnitude order for the reaction rate constant for heavier residue compounds. For that reason, lighter hydrocarbons yields could be ascribed to hydrotreating reactions (HDO, and HDS) rather than HCK as evidenced in **Fig. 37**, **Chapter 5**, **section 5.2.1.5** for FTIR spectra. Additionally, as shown in **Fig. 42** after 400 °C thermal decomposition in lighter hydrocarbons was evidenced. Therefore, at moderate reaction conditions (360 °C and 380 °C) the slight increase in lighter fractions (Naphtha, Kerosene, Diesel, and Gasoil) could be ascribed to HCK of heavier compounds occurring at low reaction rates as observed in **Table 15** for k_2 values.

6.3. CONCLUSIONS

A kinetic assessment of the hydro-coprocessing of a *Jatropha curcas* L. oil and gas oil blend was carried out for three main reactions: HDS, HDO, and HCK using an improved NiO(5.5%)-WO_3(25%)/Al(0.05)-SBA-15 mix2 sulfided catalyst. Major changes in liquid product distribution (ASTM D2887 procedure) were explained by the hydrotreating reactions (HDS, and HDO) rather than HCK. The latter due to the higher HDO rates of the vegetable oil in the feedstock. The kinetic analysis for HDS and HCK demonstrated that heavier and recalcitrant compounds were more difficult to hydroconvert. Specifically, only a 24.0% of the sulfur compounds and 52.9% of the residue fraction in the feedstock readily reacted on the catalyst surface, increasing HDS, and HCK reactions, while about 96% of the oxygenated compounds in the vegetable oil were fully hydroconverted in hydrocarbons via HDO. The residue fraction included heavy gas oil and the triglycerides of the vegetable oil. Therefore, the diesel-like fraction yield was mainly favored by HCK of such combined residue fraction in the feedstock.

OVERALL CONCLUSIONS AND PERSPECTIVES

- An enhanced NiO(5.5%)-WO_3(25%)/Al(0.05)-SBA-15 catalyst was developed and screened in the hydro-coprocessing of a mixture of a 20 vol.% of vegetable oil (*Jatropha curcas* L.) and gasoil, exhibiting an outstanding performance (25% for HDS, 96% for HDO, and 52.3% for HCK) at low conversion analysis at moderate reaction conditions (360 °C).
- Tailoring intrinsic properties (acidity, metallic character, and porosity) were sequential and systematically carried out. At the first stage, Al/Si molar ratio was varied at 0.1, 0.05, 0.033, and 0.025 fixing metallic content in 2.5 wt.% of NiO and 15 wt.% of WO_3. Accordingly, as ^{27}Al-MAS-NMR showed Ni and W incorporation modified *Al* coordination, increasing octahedral species in comparison with the pristine catalytic supports. At the second stage, fixing Al/Si molar ratio at 0.05, but varying metallic load (NiO+WO_3), the observed effect was enhancing hydrotreating reactions (HDS and HDO), thus, slightly (4.5%) increasing the diesel-like fraction yield or the HCK reaction.
- Major differences in catalytic activity were attributed to the effect of *Al* and *Ni* and *W* incorporation. Specifically, tailoring intrinsic properties (acidity, metallic character, and porosity) promoted the occurrence of both kind of active sites (type I and type II), and the formation of Brønsted-Lowry acid sites, which were the highest for the Al(0.05)-SBA-15 catalytic support as shown in *Pyridine*-FTIR spectra analysis.
- Regarding the operating conditions during the hydro-coprocessing of the mixture vegetable oil and gas oil, the effect of the reaction temperature was elucidated. Higher temperatures than 400 °C produced thermal and non-catalytic effects on liquid product fractions distribution (ASTM D2887 procedure). Therefore, in order to maximize the diesel-like fraction yield it is recommended to operate at 360 °C, which exhibited the highest (49.3%) yield of such fraction at the highest metallic load (30.5%).
- According to a kinetic analysis procedure for HDS, HDO, and HCK in hydro-coprocessing reactions, major changes in the liquid product fraction distribution (ASTM D2887 procedure) were ascribed to HDO and HDS reactions, rather than HCK of heavy components in the gas oil. The latter due to only a 23.3% of sulfur compounds and 52.3% of the residue fraction were readily hydroconverted in lighter hydrocarbons with less sulfur. For that reason, further research should be conducted on the reactivity of model compounds to identify reaction mechanisms in function on intrinsic properties of the NiO(5.5%)-WO_3(25%)/Al(0.05)-SBA-15 sulfided catalyst, and the type of active site, in this case sulfides of Ni and W.

- The catalyst preparation procedure is one of the key points of interest due to the effect it has on catalytic properties of the final sulfided catalyst. In addition, in this research it was reported the occurrence of a $NiWO_4$ oxide phase according to WA-XRD diffraction profiles. The occurrence of such “new” metallic phase and the NiO, and WO_3, enhanced hydro-coprocessing reactions. Therefore, research on the synthesis method should be carried out to enrich the knowledge of materials science in catalytic processes like hydroprocessing.

REFERENCES

1. Manrique C, Guzmán A, Pérez-Pariente J, Márquez-Álvarez C, Echavarría A. Vacuum gas-oil hydrocracking performance of Beta zeolite obtained by hydrothermal synthesis using carbon nanotubes as mesoporous template. Fuel. 2016;182:236-47.
2. El-Sawy MS, Hanafi SA, Ashour F, Aboul-Fotouh TM. Co-hydroprocessing and hydrocracking of alternative feed mixture (vacuum gas oil/waste lubricating oil/waste cooking oil) with the aim of producing high quality fuels. Fuel. 2020;269:117437.
3. Restrepo-Garcia JR, Ramírez GE, Baldovino-Medrano VG. Hydroprocessing of Phenanthrene Over Sulfided Fe–W Supported on Modified SBA-15. Catalysis Letters. 2018;148(2):621-41.
4. Palos R, Kekäläinen T, Duodu F, Gutiérrez A, Arandes JM, Jänis J, *et al.*, Screening hydrotreating catalysts for the valorization of a light cycle oil/scrap tires oil blend based on a detailed product analysis. Applied Catalysis B: Environmental. 2019;256:117863.
5. Brosius R, Kooyman PJ, Fletcher JCQ. Selective Formation of Linear Alkanes from n-Hexadecane Primary Hydrocracking in Shape-Selective MFI Zeolites by Competitive Adsorption of Water. ACS Catalysis. 2016;6(11):7710-5.
6. Al Alwan B, Salley SO, Ng KYS. Hydrocracking of DDGS corn oil over transition metal carbides supported on Al-SBA-15: Effect of fractional sum of metal electronegativities. Applied Catalysis A: General. 2014;485:58-66.
7. Park YK, Lee HW, Jeon JK, Han J, Kim CU, Jeong SY, *et al.*, Hydroconversion of n-dodecane over nanoporous catalysts. Journal of Nanoscience and Nanotechnology. 2013;13(1):714-7.
8. Mendoza-Nieto JA, Vera-Vallejo O, Escobar-Alarcón L, Solís-Casados D, Klimova T. Development of new trimetallic NiMoW catalysts supported on SBA-15 for deep hydrodesulfurization. Fuel. 2013;110(0):268-77.
9. Maity SK, Ancheyta J, Alonso F, Rayo P. Hydrodesulfurization activity of used hydrotreating catalysts. Fuel Processing Technology. 2013;106(0):453-9.
10. Agudelo JL, Mezari B, Hensen EJM, Giraldo SA, Hoyos LJ. On the effect of EDTA treatment on the acidic properties of USY zeolite and its performance in vacuum gas oil hydrocracking. Applied Catalysis A: General. 2014;488(0):219-30.
11. Villasana Y, Ruscio-Vanalesti F, Pfaff C, Méndez FJ, Luis-Luis MÁ, Brito JL. Atomic ratio effect on catalytic performance of FeW-based carbides and nitrides on thiophene hydrodesulfurization. Fuel. 2013;110(0):259-67.

12. Li J, Xia Z, Lai W, Zheng J, Chen B, Yi X, *et al.*, Hydrodemetallation (HDM) of nickel-5,10,15,20-tetraphenylporphyrin (Ni-TPP) over NiMo/γ-Al_2O_3 catalyst prepared by one-pot method with controlled precipitation of the components. Fuel. 2012;97:504-11.

13. Boahene PE, Soni KK, Dalai AK, Adjaye J. Hydroprocessing of heavy gas oils using FeW/SBA-15 catalysts: Experimentals, optimization of metals loading, and kinetics study. Catalysis Today. 2012;207:101-11.

14. Rayo P, Ramírez J, Torres-Mancera P, Marroquín G, Maity SK, Ancheyta J. Hydrodesulfurization and hydrocracking of Maya crude with P-modified NiMo/Al_2O_3 catalysts. Fuel. 2011.

15. Sun X, Fan H, Zhu J. Effect of addition of Y-Al-SBA-15 composite zeolite on catalyst performance in hydrocracking. Shiyou Huagong/Petrochemical Technology. 2013;42(5):518-23.

16. Ben Tayeb K, Lamonier C, Lancelor C, Fournier M, Payen E, Bouduelle A, *et al.*, Study of the active phase of NiW hydrocracking sulfided catalyts obtained from innovative heteopolyanion based preparation. Catalysis Today. 2010;150:207-12.

17. Szczodrowski K, Prélot B, Lantenois S, Douillard J-M, Zajac J. Effect of heteroatom doping on surface acidity and hydrophilicity of Al, Ti, Zr-doped mesoporous SBA-15. Microporous and Mesoporous Materials. 2009;124(1–3):84-93.

18. Olivas A, Zepeda TA. Impact of Al and Ti ions on the dispersion and performance of supported NiMo(W)/SBA-15 catalysts in the HDS and HYD reactions. Catalysis Today. 2009;143(1–2):120-5.

19. Mora-Vergara ID, Hernández Moscoso L, Gaigneaux EM, Giraldo SA, Baldovino-Medrano VG. Hydrodeoxygenation of guaiacol using NiMo and CoMo catalysts supported on alumina modified with potassium. Catalysis Today. 2017.

20. Cao Z, Zhang X, Xu C, Duan A, Guo R, Zhao Z, *et al.*, The Synthesis of Al-SBA-16 Materials with a Novel Method and Their Catalytic Application on Hydrogenation for FCC Diesel. Energy & Fuels. 2017;31(1):805-14.

21. Restrepo-Garcia JR, Baldovino-Medrano VG, Giraldo SA. Improving the selectivity in hydrocracking of phenanthrene over mesoporous Al-SBA-15 based Fe–W catalysts by enhancing mesoporosity and acidity. Applied Catalysis A: General. 2016;510:98-109.

22. Seo M-g, Lee D-W, Lee K-Y, Moon DJ. Pt/Al-SBA-15 catalysts for hydrocracking of C21–C34 n-paraffin mixture into gasoline and diesel fractions. Fuel. 2015;143(0):63-71.

23. Han Y, Gholizadeh M, Tran C-C, Kaliaguine S, Li C-Z, Olarte M, *et al.*, Hydrotreatment of pyrolysis bio-oil: A review. Fuel Processing Technology. 2019;195:106140.

24. Amin A. Review of diesel production from renewable resources: Catalysis, process kinetics and technologies. Ain Shams Engineering Journal. 2019.

25. Templis C, Vonortas A, Sebos I, Papayannakos N. Vegetable oil effect on gasoil HDS in their catalytic co-hydroprocessing. Applied Catalysis B: Environmental. 2011;104(3):324-9.

26. Tan Q, Cao Y, Li J. Prepared multifunctional catalyst Ni_2P/Zr-SBA-15 and catalyzed Jatropha Oil to produce bio-aviation fuel. Renewable Energy. 2020;150:370-81.

27. Jaroszewska K, Fedyna M, Trawczyński J. Hydroisomerization of long-chain n-alkanes over Pt/AlSBA-15+zeolite bimodal catalysts. Applied Catalysis B: Environmental. 2019;255:117756.

28. Vonortas A, Kubička D, Papayannakos N. Catalytic co-hydroprocessing of gasoil–palm oil/AVO mixtures over a NiMo/γ-Al_2O_3 catalyst. Fuel. 2014;116:49-55.

29. Yu F, Zhang C, Geng R, Zhou H, Dong Q, Liu S, *et al.*, Hydrocracking of naphthalene over Beta zeolite coupled with NiMo/γ-Al_2O_3: Investigation of metal and acid balance based on the composition of industrial hydrocracking catalyst. Fuel. 2023;344:128049.

30. Qi L, Peng C, Cheng Z, Zhou Z. Selective hydrocracking of poly-aromatics to mono-aromatics in a catalyst grading system of NiMo/Al_2O_3-HY and NiMo/Beta. Fuel. 2023;351:128941.

31. Ge J-Q, Zhang P, Sun F-M, Xie Z-A, Wu Z-J, Liu B-J. Catalyst grading technology for promoting the diesel hydrocracking to naphtha. Petroleum Science. 2023.

32. Feng W-W, Qian Y-G, Wang T-H, Cui Q-Y, Yue Y-Y, Yuan P, *et al.*, Impacts of support properties on the vacuum residue slurry-phase hydrocracking performance of Mo catalysts. Petroleum Science. 2023;20(4):2575-84.

33. Speight JG. Chapter 11 - Upgrading by Hydrocracking. In: Speight JG, editor. Heavy Oil Recovery and Upgrading: Gulf Professional Publishing; 2019. p. 467-528.

34. Oh S, Lee JH, Choi I-G, Choi JW. Enhancement of bio-oil hydrodeoxygenation activity over Ni-based bimetallic catalysts supported on SBA-15. Renewable Energy. 2020;149:1-10.

35. Gómez-Orozco SY, Huirache-Acuña R, Pawelec B, Fierro JLG, Rivera-Muñoz EM, Lara-Romero J, *et al.*, Characterizations and HDS performances of sulfided NiMoW catalysts supported on mesoporous titania-modified SBA-15. Catalysis Today. 2018;305:152-61.

36. Zhang Z, Cheng J, Zhu Y, Guo H, Yang W. Jet fuel range hydrocarbons production through competitive pathways of hydrocracking and isomerization over HPW-Ni/MCM-41 catalyst. Fuel. 2020;269:117465.

37. Tieuli S, Mäki-Arvela P, Peurla M, Eränen K, Wärnå J, Cruciani G, *et al.*, Hydrodeoxygenation of isoeugenol over Ni-SBA-15: Kinetics and modelling. Applied Catalysis A: General. 2019;580:1-10.

38. Lima RWS, Hewer TLR, Alves RMB, Schmal M. Surface Analyses of adsorbed and deposited species on the Ni-Mo catalysts surfaces after Guaiacol HDO. Influence of the alumina and SBA-15 supports. Molecular Catalysis. 2021;511:111724.

39. Zhang W, Chen Y, Zhuang S, Li R, Hu L. Acid-etched Pt/Al-MCM-41 catalysts for fuel production by one-step hydrotreatment of Jatropha oil. 2021;13(4):679-90.

40. Auersvald M, Shumeiko B, Vrtiška D, Straka P, Staš M, Šimáček P, *et al.,* Hydrotreatment of straw bio-oil from ablative fast pyrolysis to produce suitable refinery intermediates. Fuel. 2019;238:98-110.

41. De Paz Carmona H, Horáček J, Tišler Z, Akhmetzyanova U. Sulfur free supported MoCx and MoNx catalysts for the hydrotreatment of atmospheric gasoil and its blends with rapeseed oil. Fuel. 2019;254:115582.

42. Ibarra Á, Hita I, Azkoiti MJ, Arandes JM, Bilbao J. Catalytic cracking of raw bio-oil under FCC unit conditions over different zeolite-based catalysts. Journal of Industrial and Engineering Chemistry. 2019;78:372-82.

43. Fedyna M, Żak A, Jaroszewska K, Mokrzycki J, Trawczyński J. Composite of Pt/AlSBA-15+zeolite catalyst for the hydroisomerization of n-hexadecane: The effect of platinum precursor. Microporous and Mesoporous Materials. 2020;305:110366.

44. Jaroszewska K, Masalska A, Grzechowiak JR, Grams J. Hydroconversion of 1-methylnaphthalene over Pt/AlSBA-15–Al_2O_3 composite catalysts. Applied Catalysis A: General. 2015;505:116-30.

45. Ochoa-Hernández C, Yang Y, Pizarro P, de la Peña O'Shea VA, Coronado JM, Serrano DP. Hydrocarbons production through hydrotreating of methyl esters over Ni and Co supported on SBA-15 and Al-SBA-15. Catalysis Today. 2013;210:81-8.

46. Rouquerol J, Rouquerol F. 3 - Methodology of Gas Adsorption. In: Rouquerol F, Rouquerol J, Sing KSW, Llewellyn P, Maurin G, editors. Adsorption by Powders and Porous Solids (Second Edition). Oxford: Academic Press; 2014. p. 57-104.

47. Zhao D, Feng J, Huo Q, Melosh N, Fredrickson GH, Chmelka BF, *et al.,* Triblock Copolymer Syntheses of Mesoporous Silica with Periodic 50 to 300 Angstrom Pores. Science. 1998;279(5350):548-52.

48. Bi Y, Zeng S, Nie H, Li M, Yang Q, Xia G, *et al.,* Self-complexation: the nature for high hydrodesulfurization activity of NiWO4 nanoparticles. Catalysis Communications. 2014;57:5-8.

49. Lei Z, Gao L, Shui H, Chen W, Wang Z, Ren S. Hydrotreatment of heavy oil from a direct coal liquefaction process on sulfided Ni–W/SBA-15 catalysts. Fuel Processing Technology. 2011;92(10):2055-60.

50. Baharudin KB, Taufiq-Yap YH, Hunns J, Isaacs M, Wilson K, Derawi D. Mesoporous NiO/Al-SBA-15 catalysts for solvent-free deoxygenation of palm fatty acid distillate. Microporous and Mesoporous Materials. 2019;276:13-22.

51. Li Y, Pan D, Yu C, Fan Y, Bao X. Synthesis and hydrodesulfurization properties of NiW catalyst supported on high-aluminum-content, highly ordered, and hydrothermally stable Al-SBA-15. Journal of Catalysis. 2012;286:124-36.

52. Li D, Li Y, Liu X, Guo Y, Pao C-W, Chen J-L, *et al.*, $NiAl_2O_4$ Spinel Supported Pt Catalyst: High Performance and Origin in Aqueous-Phase Reforming of Methanol. ACS Catalysis. 2019;9(10):9671-82.

53. Blanchard J, Breysse M, Fajerwerg K, Louis C, Hédoire CE, Sampieri A, *et al.*, Acidic zeolites and Al-SBA-15 as supports for sulfide phases: application to hydrotreating reactions. In: J. Čejka NŽ, Nachtigall P, editors. Studies in Surface Science and Catalysis. Volume 158, Part B: Elsevier; 2005. p. 1517-24.

54. Dragoi B, Dumitriu E, Bennici S, Auroux A. Acidic and adsorptive properties of Al modified SBA-15 samples. In: Antoine Gédéon PM, Florence B, editors. Studies in Surface Science and Catalysis. Volume 174, Part B: Elsevier; 2008. p. 953-6.

55. Gómez-Cazalilla M, Infantes-Molina A, Moreno-Tost R, Maireles-Torres PJ, Mérida-Robles J, Rodríguez-Castellón E, *et al.*, Al-SBA-15 as a support of catalysts based on chromium sulfide for sulfur removal. Catalysis Today. 2009;143(1–2):137-44.

56. Thomas R, Kerkhof FPJM, Moulijn JA, Medema J, de Beer VHJ. On the formation of aluminum tungstate and its presence in tungsten oxide on γ-alumina catalysts. Journal of Catalysis. 1980;61(2):559-61.

57. Lima NA, Alencar LDS, Siu-Li M, Feitosa CAC, Mesquita A, M'peko J-C, *et al.*, $NiWO_4$ powders prepared via polymeric precursor method for application as ceramic luminescent pigments. Journal of Advanced Ceramics. 2020;9(1):55-63.

58. Cancino-Trejo F, Santes V, Cardenas JAA, Gallardo M, Maldonado YG, Miranda A L, *et al.*, Active Ni and Fe species on catalysts Ni/Al_2O_3 and $NiFe/Al_2O_3$ for the oxidative dehydrogenation (ODH) of ethane to ethylene assisted by CO2. Chemical Engineering Journal Advances. 2022;12:100404.

59. Scaldaferri CA, Pasa VMD. Production of jet fuel and green diesel range biohydrocarbons by hydroprocessing of soybean oil over niobium phosphate catalyst. Fuel. 2019;245:458-66.

60. Barison A, da Silva CW, Campos FR, Simonelli F, Lenz CA, Ferreira AG. A simple methodology for the determination of fatty acid composition in edible oils through ^{1}H NMR spectroscopy. Magnetic resonance in chemistry : MRC. 2010;48(8):642-50.

61. Siudem P, Zielińska A, Paradowska K. Application of ^{1}H NMR in the study of fatty acids composition of vegetable oils. Journal of Pharmaceutical and Biomedical Analysis. 2022;212:114658.

62. Sepúlveda C, Escalona N, García R, Laurenti D, Vrinat M. Hydrodeoxygenation and hydrodesulfurization co-processing over ReS_2 supported catalysts. Catalysis Today. 2012;195(1):101-5.

63. Infantes-Molina A, Loricera C, Pawelec B, Fierro J, Jiménez-López A, Rodriguez-Castellon E. Effect of Ir and Pt Addition on the HDO Performance of RuS_2/SBA-15 Sulfide Catalysts. Topics in Catalysis. 2015;58.

64. Şenol Oİ, Ryymin EM, Viljava TR, Krause AOI. Effect of hydrogen sulphide on the hydrodeoxygenation of aromatic and aliphatic oxygenates on sulphided catalysts. Journal of Molecular Catalysis A: Chemical. 2007;277(1):107-12.

65. Kagami N, Vogelaar BM, Langeveld ADv, Moulijn JA. Reaction pathways on NiMo/Al_2O_3 catalysts for hydrodesulfurization of diesel fuel. Applied Catalysis A: General. 2005;293:11-23.

66. Malavekar DB, Lokhande VC, Patil DJ, Kale SB, Patil UM, Ji T, *et al.*, Amorphous nickel tungstate films prepared by SILAR method for electrocatalytic oxygen evolution reaction. Journal of Colloid and Interface Science. 2022;609:734-45.

67. Jiang S, Ding S, Jiang Q, Zhou Y, Yuan S, Geng X, *et al.*, Effects of Al introduction methods for Al-SBA-15 on NiMoS active phase morphology and hydrodesulfurization reaction selectivities. Fuel. 2022;330:125493.

68. Hu W, Luo Q, Su Y, Chen L, Yue Y, Ye C, *et al.*, Acid sites in mesoporous Al-SBA-15 material as revealed by solid-state NMR spectroscopy. Microporous and Mesoporous Materials. 2006;92(1):22-30.

69. Dubray F, Paunović V, Ranocchiari M, van Bokhoven JA. Production of jet-fuel-range olefins via catalytic conversion of pentene and hexene over mesoporous Al-SBA-15 catalyst. Journal of Industrial and Engineering Chemistry. 2022;114:409-17.

70. Talebi R. Simple sonochemical synthesis and characterization of nickel tungstate nanoparticles and its photocatalyst application. Journal of Materials Science: Materials in Electronics. 2016;27(4):3565-9.

71. Tirado A, Ancheyta J. Defining appropriate reaction scheme for hydrotreating of vegetable oil through proper calculation of kinetic parameters. Fuel. 2019;242:167-73.

72. Sánchez S, Rodríguez MA, Ancheyta J. Kinetic Model for Moderate Hydrocracking of Heavy Oils. Industrial & Engineering Chemistry Research. 2005;44(25):9409-13.

73. Rodríguez MA, Elizalde I, Ancheyta J. Comparison of kinetic and reactor models to simulate a trickle-bed bench-scale reactor for hydrodesulfurization of VGO. Fuel. 2012;100:91-9.

74. González-Ildelfonso M, Escobar J, Gordillo-Cruz E, del Ángel P, Suárez-Toriello VA, De los Reyes JA. RuS_2-modified NiW/Al_2O_3 catalysts for refractory 4,6-dimethyl-dibenzothiophene hydrodesulfurization. Materials Chemistry and Physics. 2022;278:125568.

75. Chen Z, Wang Y, Wu J, Wang B, Jiang T, Yu J, *et al.*, Composition of sulfur species in deasphalted oils and their molecular-level transformation during the hydrotreating process. Fuel. 2022;328:125335.

76. Alvarez A, Escobar J, Toledo JA, Pérez V, Cortés MA, Pérez M, *et al.*, HDS of straight-run gas oil at various nitrogen contents. Comparison between different reaction systems. Fuel. 2007;86(9):1240-6.

77. Wang W, Tan S, Wu K, Zhu G, Liu Y, Tan L, *et al.*, Hydrodeoxygenation of p-cresol as a model compound for bio-oil on MoS_2: Effects of water and benzothiophene on the activity and structure of catalyst. Fuel. 2018;214:480-8.

78. Philippe M, Richard F, Hudebine D, Brunet S. Inhibiting effect of oxygenated model compounds on the HDS of dibenzothiophenes over $CoMoP/A_{l2}O_3$ catalyst. Applied Catalysis A: General. 2010;383(1):14-23.

79. Viljava TR, Saari ERM, Krause AOI. Simultaneous hydrodesulfurization and hydrodeoxygenation: interactions between mercapto and methoxy groups present in the same or in separate molecules. Applied Catalysis A: General. 2001;209(1):33-43.

APPENDIX 1- Results of kinetic parameters estimation for a five-lumped HCK model

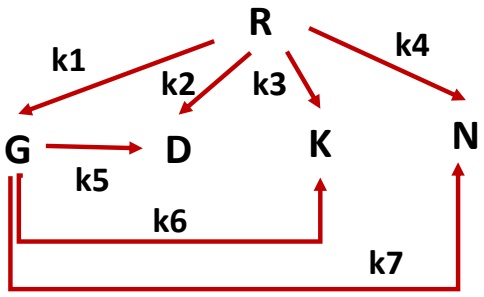

Fig.46. Five-lumped kinetic model for the HCK reaction using the NiO(5.5%)-WO_3(25%)/Al(0.05)-SBA-15 mix2 sulfided catalyst, R=Residue, G=Gasoil, D= Diesel, K=Kerosene, and N= Naphtha.

According to the five-lumped kinetic model shown in **Fig.46** the set of differential equations for each component (lump) is the following:

$$\textbf{\textit{Naphtha:}}\quad \frac{dN}{dt} = k_4 R^a + k_7 G^{\beta}$$

$$\textbf{\textit{Kerosene:}}\quad \frac{dK}{dt} = k_3 R^a + k_6 G^{\beta}$$

$$\textbf{\textit{Diesel:}}\quad \frac{dD}{dt} = k_2 R^a + k_5 G^{\beta}$$

$$\textbf{\textit{Gasoil:}}\quad \frac{dG}{dt} = k_1 R^a - (k_5 + k_6 + k_7) G^{\beta}$$

$$\textbf{\textit{Residue:}}\quad \frac{dR}{dt} = -(k_1 + k_2 + k_3 + k_4) R^a$$

In the previous set of reaction rates, the reaction orders were *a* for the Residue fraction and β for the Gasoil fraction, which were considered the heavier components in the reaction mixture (vegetable oil and gas oil). The SSE for the proposed model was 0.0648 according to ***Eqn. 3*** in Section 6.1.2.

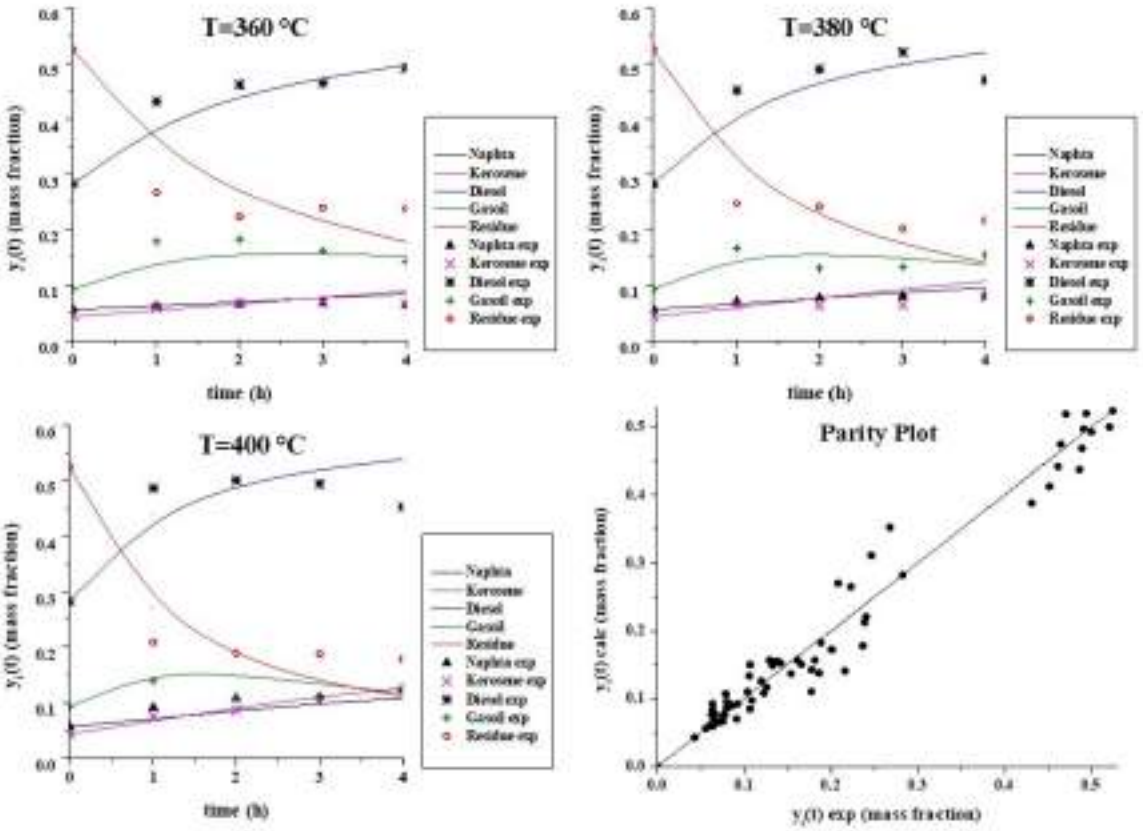

Fig.47. Kinetics and parity chart for the five-lumped HCK model using the NiO(5.5%)-WO_3(25%)/Al(0.05)-SBA-15 mix2 sulfided catalyst at different reaction temperatures (T) and time (h).

Table 16. Kinetic parameters for a five-lumped kinetic model for HCK during the hydro-coprocessing a vegetable oil and gas oil blend with a sulfided NiO(5.5%)-WO_3(25%)/Al(0.05)-SBA-15 mix2 catalyst

Rate Constant	T [°C]			Kinetic Parameter			
k_i [h^{-1}]	360	380	400	E_A [kJmol^{-1}]	A_0 [h^{-1}]	*a*	*β*
k_1	0.3385	0.4768	0.6582	58.93	2.4589×10^4		
k_2	0.5651	0.7881	1.0775	57.18	2.9465×10^4		
k_3	0.0190	0.0279	0.0401	66.31	5.6004×10^3		
k_4	0.0080	0.0118	0.0171	67.50	2.9538×10^3	2.00	1.58
k_5	0.0166	0.0257	0.0387	75.11	2.6050×10^4		
k_6	0.2053	0.2967	0.4195	63.31	3.4270×10^4		
k_7	0.1306	0.1910	0.2731	65.39	3.2373×10^4		